ACS Catalysis

pubs.acs.org/acscatalysis Review

Supported MoO_x and WO_x Solid Acids for Biomass Valorization: Interplay of Coordination Chemistry, Acidity, and Catalysis

Putla Sudarsanam,* Navneet Kumar Gupta, Baithy Mallesham, Nittan Singh, Pavan Narayan Kalbande, Benjaram M. Reddy, and Bert F. Sels

Cite This: *ACS Catal.* 2021, 11, 13603−13648 Read Online

ACCESS | Metrics & More | Article Recommendations

ABSTRACT: Supported molybdenum oxide (MoO_x) and tungsten oxide (WO_x) materials are a vital class of solid acid catalysts for the chemical industry because of their nontoxic nature, strong acidity, remarkable stability in water, hydrogen, and oxygen atmospheres, and excellent reusability performance. These fascinating solid acids play a pivotal role in developing sustainable catalytic routes for renewable biomass processing to produce value-added fuels, chemicals, and platform molecules. The coordination chemistry of MoO_x and WO_x on the support materials (oxides, carbons, or zeolites) controls their acidic strength, active site accessibility, and catalytic activity. Hence, significant efforts have been made toward optimizing the conditions used for catalyst synthesis and biomass processing to tune the coordination chemistry of MoO_x and WO_x with the substrate molecules and, thus, their acid-activity/selectivity performance. This Review provides a comprehensive overview of supported MoO_x and WO_x solid acids for biomass valorization. The importance of the biomass and the role of solid acids for biomass valorization were emphasized, followed by a brief discussion of supported MoO_x and WO_x solid acids. Afterward, the interplay of coordination chemistry, acidic strength, and catalytic activity of supported MoO_x and WO_x solid acids was discussed. Finally, their catalytic applications for the valorization of several biomass substrates and their derivatives were summarized. This Review will provide valuable insights for developing advanced supported WO_x and MoO_x solid acids for catalytic biomass valorization and other challenging acid-catalyzed processes.

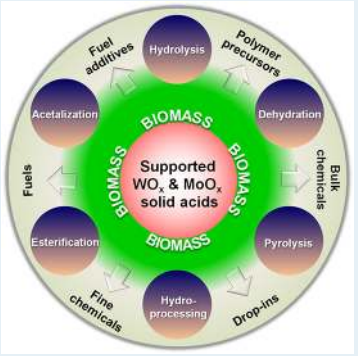

KEYWORDS: *molybdenum oxide, tungsten oxide, biomass valorization, coordination chemistry, acidity, catalysis*

1. INTRODUCTION

1.1. Importance of Biomass. The increases of energy demand and environmental pollution are the biggest challenges humankind is facing this century. To overcome these challenges, the development of alternatives to fossil fuels is considered as a promising solution. Hence, significant attention has been directed to produce energy, fuels, and chemicals from renewable resources, such as wind, solar, biomass, hydropower, and geothermal.[1] The significance of biomass among renewables is realized from its versatile carbon structure that can be converted into most fossil-derived products. Biomass, produced via the photosynthesis process, is available in the form of lignocellulose, starch, oilseed, sugar crops, algae, etc.[2,3] Animal fat (e.g., tallow) can also be used as a biomass source for fuel production (e.g., biodiesel). It was estimated that biomass could contribute ∼9% of fuel share by 2030 in the transport sector.[4,5] Biomass valorization is one of the effective ways to control the net CO_2 emissions since CO_2 release during biomass processing is utilized again in photosynthesis for biomass production. Valorization of biomass to chemicals can also lead to the invention of new routes that maximize the retainment of the original structure of the biomass in the end products. Hence, the focus should be toward maximizing biomass utilization for chemical production, while minimizing carbon emissions that will help balance the carbon cycle as well as meet the increasing energy demand.

1.2. Role of Solid Acid Catalysts in Biomass Valorization. Catalysis is one of the vital routes for the sustainable chemical industry.[6] A tiny amount of the catalyst is enough to achieve higher reaction rates, and its cost is negligible (0.1−1%) compared with that of the total process cost. Hence, more than 90% of chemicals produced in industry involves at least one catalytic step.[7] The chemical reactions are catalyzed by acid, base, or redox materials. Sometimes, bifunctional catalysts (acid−base, acid−redox, or base−redox) are needed, especially for cascade reactions.[4] Among them, acid catalysts (both mono- and bifunctional) cover a wide range of catalytic processes in the chemical industry. Liquid acids, such as HF, HCl, H_3PO_4, and H_2SO_4, are the most widely used acid catalysts in the chemical

Received: July 25, 2021
Revised: October 7, 2021
Published: October 26, 2021

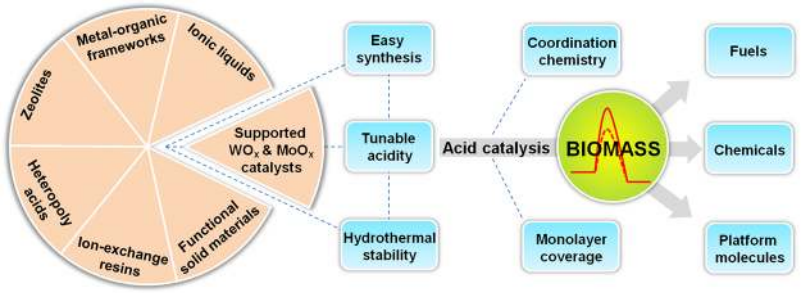

Figure 1. Schematic outline of the Review.

industry because these acids exhibit higher reaction rates and improved product yields in a short reaction time. Inefficient catalyst recovery/reusability and tedious procedures for product isolation/purification are the main drawbacks of these liquid acid catalysts. To overcome these challenges, more attention has been paid to developing efficient solid acid catalysts. Simple separation techniques, such as filtration or centrifugation, can be used to recover these solid acids from the reaction mixture. The recovered solid acid catalysts can be reused directly or after regeneration (e.g., calcination in air or oxygen flow for removing adsorbed organic residues or coke deposits) for the subsequent cycles; hence, waste generation can be prevented during the process.

A variety of solid acid catalysts, such as zeolites, pure metal oxides and supported metal oxides, ion-exchange resins, functionalized silicas, heteropolyacids, immobilized acidic ionic liquids, carbonaceous acids, and metal−organic frameworks have been developed for numerous applications, including biomass valorization.[8−11] When the concentrations of Brønsted and Lewis acid sites are optimized, these solid acids can be efficiently used for several biomass conversion reactions, such as hydrolysis, pyrolysis, dehydration, esterification, acetalization, condensation, hydrogenolysis, hydrodeoxygenation, etc.[12,13] In these reactions, water is a reactant or byproduct and biomass naturally contains higher water content.[14] Here, the poisoning/leaching of the acid sites by water molecules is a key concern, resulting in rapid catalyst deactivation and low catalyst reusability/durability. Hence, the development of hydrothermally stable solid acid catalysts with optimum amounts of Brønsted and Lewis acid sites is crucial for efficient biomass valorization.

1.3. Supported Molybdenum Oxide (MoO_x) and Tungsten Oxide (WO_x) Solid Acids. The pioneering works of Hino and Arata revealed that WO_x dispersed on zirconium oxide (ZrO_2) acts as a "Promising Solid Acid" alternative to hazardous liquid acids, e.g., H_2SO_4.[45] They demonstrated that impregnating zirconium oxyhydroxide with an aqueous solution of tungsten precursor (ammonium metatungstate), followed by calcination at higher temperatures in air, can generate strong acid sites in the WO_x/ZrO_2 catalyst. As a result, the WO_x/ZrO_2 solid acid catalyst is effective in many industrial processes, such as isomerization, alkylation, esterification, and cracking. WO_x/ZrO_2 solid acid exhibits good water resistance ability, but this property also depends on the reaction conditions. It was noticed that the acidic strength of the supported WO_x catalysts originates from well-dispersed WO_x nanoclusters. These WO_x nanoclusters are highly energetic species that will attract the electron density from the support, resulting in the generation of electron-deficient metal-based Lewis acid sites.[16] The hydroxyl groups exist as W−OH−W on the support act as Brønsted acid sites. The acidic strength of these hydroxyl groups highly depend on the structure of W−OH−W (mono-, di-, or polymeric). The hydroxyl groups present on the support can also exhibit a Brønsted acidic nature, but their interaction with the metal sites (W or Mo) will determine the acidic strength. Like WO_x/ZrO_2 solid acid, WO_x species supported on other metal oxides (SiO_2, AI_2O_3, SnO_2, TiO_2, CeO_2, etc.), mixed oxides (TiO_2−ZrO_2, CeO_2−ZrO_2, SiO_2−Al_2O_3, etc.), mesoporous materials (SBA-15), activated carbon, zeolites, etc. are also found to show excellent acidic properties and high catalytic efficiencies.[17−26]

Related solid acid systems, such as supported MoO_x solid acids, have also been studied for many acid-catalyzed reactions because of their excellent acid, hydrothermal stability, and efficient reusability. Hence, supported WO_x and MoO_x solid acids can offer efficient catalytic routes for producing fuels and chemicals from biomass. Metal oxide−support interactions in supported WO_x and MoO_x solid acids can affect the structure, stability, and acidic properties of the active phase, therefore influencing their catalytic performance. These metal oxide−support interactions will be improved by controlling various parameters, such as particle size/morphology, metal composition, preparation method, pretreatment, and the nature of the support. Because of these opportunities, significant efforts have been made to design supported WO_x and MoO_x solid acid catalysts in the last two decades.

1.4. Scope of the Review. Over the last two decades, various review articles on acid catalysis and biomass valorization have been published, summarizing the development of homogeneous and heterogeneous acid catalysts, their physicochemical and acidic properties, and the catalytic applications for the conversion of biomass and its model compounds to fuels and chemicals. In 2002, Corma and García[27] reviewed the role of Lewis acids (both homogeneous and heterogeneous) in catalytic oxidation reactions. In the same year, Okuhara[14] provided a review on developing water-tolerant solid acids (mainly zeolites and heteropolyacids) for the chemical industry. In 2007 and 2009, Busca[28] and Reddy and Patil[29] summarized the catalytic role of various acids for hydrocarbon chemistry and organic synthesis, respectively. In 2014, Rousseau et al.[30] summarized the condensation, dehydration, and dehydrogenation reactions of alcohols over solid catalysts containing cyclic $(MoO_3)_3$ and $(WO_3)_3$ clusters. In 2017, Zhou et al.[15] provided a perspective on the nature and strength of active sites (mainly acidity) in WO_3/ZrO_2 catalyst. Although the above reviews covered acid catalysis, a comprehensive study focusing on the development of supported MoO_x and WO_x solid acids and their catalytic applications for biomass valorization is not reported in the literature until now. Besides, the interplay of coordination chemistry, acidic strength, and catalytic efficiency of these solid acids is not discussed, but it is crucial to develop new solid acids

https://doi.org/10.1021/acscatal.1c03326
ACS Catal. 2021, 11, 13603−13648

for chemical synthesis. Hence, the present Review aims to provide a critical overview of the most notable findings toward developing various supported MoO_x and WO_x solid acids for biomass valorization. The coordination chemistry of MoO_x and WO_x and its role in tuning the acidic strength of the catalysts is critically discussed in this Review. A variety of biomass feedstock and platform molecules, namely, vegetable oils/animal fats, glycerol, lignocellulose, and its components (cellulose, hemicellulose, and lignin) as well as derived compounds of cellulose (cellobiose, glucose, fructose, 5-hydroxymethylfurfural, levulinic acid, etc.), hemicellulose (xylose, furfural, furfuryl alcohol, 2-furancarboxylic acid, etc.), and lignin (guaiacol, cresol, anisole, phenol, eugenol, benzofuran, dibenzofuran, etc.), are covered. The catalyst stability, reusability, poisoning/leaching of the active sites and their regeneration, active site accessibility, and structure−activity correlation of supported MoO_x and WO_x solid acids for various biomass conversion reactions are meticulously discussed in this Review. This comprehensive Review will provide a fundamental understanding and valuable insights toward developing advanced supported WO_x and MoO_x solid acids. The schematic outline of this Review is presented in Figure 1.

2. COORDINATION CHEMISTRY AND ACIDIC STRENGTH OF SUPPORTED MoO_x AND WO_x SOLID ACIDS

The critical aspects of the well-defined MO_x oxides (M = Mo and W) over the oxide supports are based on metal site density and its coordination environment via grafting of metal precursors onto the OH functional groups of support oxides. The density of surface OH groups on supporting oxides is typically controlled by thermal treatment. For example, conventional oxide supports, such as SiO_2 or Al_2O_3, exhibited an OH density of around 0.8 OH per nm^2; however, it is higher for ZrO_2 (6.2−9.4 OH per nm^2).[31] The concentration of OH groups on metal oxides can be varied by the partial dehydration method.[32,33] The nature and density of these reactive OH groups are beneficial for grafting metal precursors for isolated active metal site generation. The OH groups on ZrO_2 are typically assigned as terminal OH and OH bonded to the several Zr atoms (bridged, tribridged or multicoordinated).[32−36] Terminal OH groups are directly bonded to a single cation of oxide framework. However, multicoordinated OH groups are situated at low-index faces. Grafting usually occurs by the protonolysis of anionic ligands of metal precursors to form metal sites over the support by the formation of M−O bonds. When metal is anchored by monocoordination on the support, the resulting metal sites are well-defined within the coordination spheres and display better catalytic activity, selectivity, and stability than their molecular analogs. Moreover, these surface coordinated metals can be transformed to the crystalline metal oxide nanoparticles (NPs) or the other structures distinct from molecular analogy. Another possibility includes the low coordination of metallic sites that form isolated unsaturated sites on oxide supports and are often considered as the most active sites in supported metal oxide catalysts.[37,38] Oxygen atoms on the surface of the oxide supports usually terminate in the form of oxide (−O−) or hydroxyl (−OH and $-(OH)_2$) linkages.[39,40] Thermal treatment of the oxide support can remove the surface −OH groups in the form of water, resulting in the formation of a more stable −O− group and a lower amount of total surface OH groups.[41−43] The lower number of surface OH groups can lead to the formation of isolated and well-defined sites with metal precursors, and their electronic environment can be modified by post-treatment.[44] In this section, we describe the formation of well-defined MoO_x and WO_x complexes grafted on oxide supports. The post-treatment strategies will be discussed, which are essential to tune the nature of coordination in grafted species and, in turn, the change in surface structure and generation of new active sites. The preparation of controlled surface species and the structure of metallic sites allow unique binding with substrates for the rational design of next-generation heterogeneous catalysts derived from the structural-activity relationship.

2.1. Coordination Models of Supported MoO_x and WO_x Solid Acids. Supported MoO_x and WO_x are an important class of solid acid catalysts, whose acidity is stronger than conventional sulfuric acid due to the unique coordination and formation of reactive metallic sites.[15] Most outstanding catalytic examples include low-temperature isomerization of alkanes, such as butane and *n*-pentane.[45] Besides, these catalysts are used for several biomass transformations, such as glycerol to acrolein,[46,47] glucose or fructose dehydration to 5-hydroxymethylfurfural (HMF),[48,49] cellulose to hexanedione,[50] and levulinic esters synthesis.[51] The nature and strength of the acid sites of the supported metal oxides are crucial for catalytic applications. The surface stabilized MoO_x and WO_x species act similarly on various oxide supports like Al_2O_3, TiO_2, ZrO_2, Nb_2O_5, and MgO as surface density (3−4.6 M sites per nm^2) is quite close up to monolayer loading.[52] The monolayer is basically described as a maximum dispersion of active metal sites (closely packed atoms of a single layer) on the oxide support. The structure of the MoO_x and WO_x species on the oxide support depends on the coverage. At low surface coverage, highly tetrahedral distorted and isolated structures are formed. With the increase of the Mo and W loading up to the monolayer coverage, polymetalate species of highly distorted octahedral mono-oxo structures could be formed on the oxide surface. Depending on the preparation methods and surface coverage, different types of (isolated and crystalline) MoO_x and WO_x species are formed on SiO_2. In the case of Mo, isolated mono-oxo $O{=}MoO_4$ and dioxo $(O{=})_2MoO_2$ species on SiO_2, especially dioxo $(O{=})_2MoO_2$ species, are dominant (Figure 2).[53−56] Over monolayer saturation, the crystalline MoO_3 NPs

Figure 2. Proposed structures of the MO_x species on the SiO_2 surface (M = Mo or W). Dioxo $(O{=})_2MO_2$, mono-oxo $O{=}MO_4$, and species coexist with crystalline MO_3.

are formed. Silanol groups are consumed by the formation of a Mo−O−Si bond, which provides a strong interaction of surface oxides.[57] Similarly, in the case of WO_x grafted on SiO_2, the coexistence of mono-oxo $O{=}WO_4$ and dioxo $(O{=})_2WO_2$ species on the surface with a majority of dioxo species is possible. However, interestingly, monomeric and oligomeric species may coexist at a low loading of WO_x on SiO_2, and the crystalline WO_3 NP formation typically occurs even below 1 W per nm^2.[57−59] Analogous structures of both oxidized metals

https://doi.org/10.1021/acscatal.1c03326
ACS Catal. 2021, 11, 13603−13648

(MoO_x and WO_x) over silica support show similar inorganic coordination chemistry.

When MoO_x or WO_x is grafted on the Al_2O_3 surface, isolated dioxo $(O{=})_2MO_2$ species and mono-oxo $(O{=})MO_4$ species are formed at low surface coverage (up to monolayer) with dominating dioxo $(O{=})_2MO_2$ species[60−66] (Figure 3). At high

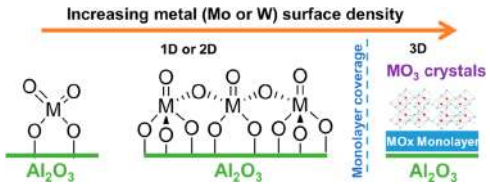

Figure 3. Proposed structures of MO_x species on the Al_2O_3 surface (M = Mo or W). Dioxo $(O{=})_2MO_2$, oligomeric mono-oxo $(O{=})MO_4$, and crystalline MO_3 growth on the monolayer of MoO_x.

surface coverage, dioxo $(O{=})_2MO_2$ and oligomeric mono-oxo $(O{=})MO_4$ species are formed. After an increase in the metal loading above the monolayer (ca., >4.6 Mo atoms per nm^2 and >4.5 W atoms per nm^2), crystalline MO_3 formation also occurs above the MO_x surfaces as hydroxyl groups, responsible for the grafting, are no longer available.

Under the oxidizing conditions, a similar type of oligomeric WO_x species formation below the monolayer (<4.5 W atoms per nm^2) on the TiO_2 species has also been reported.[67] Below 1 W per nm^2, the isolated WO_x surface sites are dominant without the formation of the W−O−W bond; however, oligomeric sites containing the W−O−W bond are formed at a surface coverage of ∼1−4.5 W per nm^2.

MoO_x and WO_x supported on ZrO_2 are another class of interesting materials for acid-catalyzed reactions.[68] Usually, MO_x/ZrO_2 materials (M = Mo or W), synthesized by taking amorphous ZrO_x support, are more active than the crystalline ZrO_2 support, suggesting the critical role of amorphous ZrO_2 in the formation of the most active catalytic sites.[69−71] Due to the unique catalysis over MO_x/ZrO_2 synthesized using amorphous ZrO_x support, many research groups investigated the role of Zr in the generation of highly active sites.[69,70] Similar to the other oxide supports, below monolayer coverage, isolated mono-oxo and dioxo metal sites are formed with a thickness of atomic layers (Figure 4). Above the monolayer coverage, 3D crystalline MO_3 NPs are formed on the surface of ZrO_2.

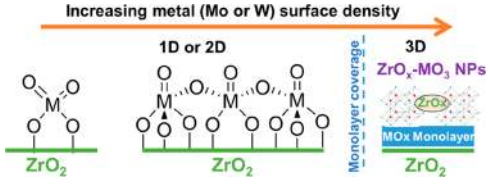

Figure 4. Proposed structures of MO_x species on the ZrO_2 surface (M = Mo or W). Dioxo $(O{=})_2MO_2$, oligomeric mono-oxo $(O{=})MO_4$, and crystalline $ZrO_x{-}MO_3$ growth on the monolayer of MoO_x.

The Raman spectroscopic study on MoO_x supported on ZrO_2 showed the Mo interaction with the surface hydroxyl group of ZrO_2 and formation of Mo−O−Mo and O=Mo bonds in the poly-MoO_x octahedral structure at monolayer coverage (∼5 Mo/nm^2).[69] By thermal treatment at 700 °C, isolated tetragonal-pyramidal $O{=}MoO_4$ species were formed due to the dissociation of the Mo−O−Mo bonds. In MoO_3/ZrO_2 material with Mo surface density above 5 Mo/nm^2, the formation of MoO_3 and $Zr(MoO_4)_2$ species was confirmed by Raman spectroscopy. Basically, thermal treatment at 450 °C led to the formation of MoO_3 as the major species; however, higher temperature treatment results in the formation of distorted tetrahedral coordinated $Zr(MoO_4)_2$ clusters. The formation of Mo−O−Zr species was crucial for strong acidity.[72] A similar phenomenon was observed for WO_3/ZrO_2 material. The Wachs's research group reported a well-accepted and the latest coordination model for WO_3/ZrO_2 material.[73,74] They proposed the formation of a composite Zr-WO_x disordered structure of ∼0.8−1.0 nm of size on the oxide surface, which is basically formed above the monolayer (>4.5 W per nm^2). When amorphous ZrO_x is used, the Zr^{4+} can be easily extracted to the WO_x cluster above the Hüttig temperature of ZrO_2; however, the possibilities of the mobility of Zr^{4+} are less for the crystalline ZrO_2 oxide. Although the existence of surface mono-, di-, and polymetalate species was proven by the Raman spectroscopic study, the coordination metal sites (appeared as brighter spots in Figure 5A,B) were clearly identified by the electron microscopic

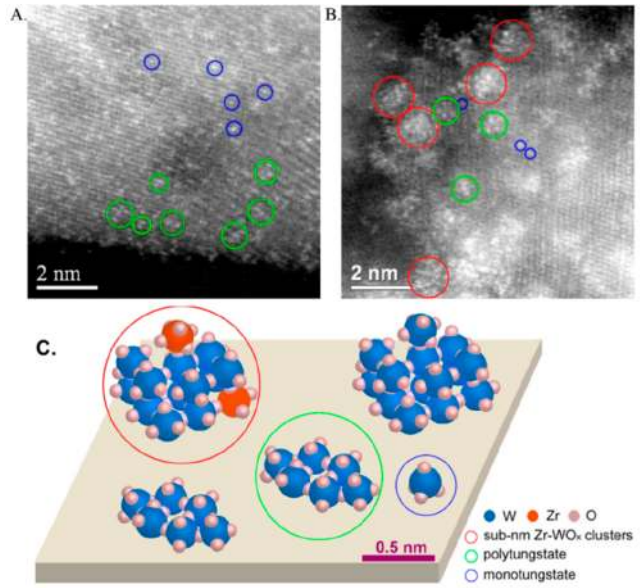

Figure 5. STEM-HAADF images of the supported WO_x/ZrO_x catalysts (A, below the WO_x coverage; B, above the monolayer coverage of WO_x) and schematic representation of surface metal coordination (C). STEM-HAADF: scanning transmission electron microscopy−high angle annular dark-field. Panels A and B: Reproduced with permission from ref 74. Copyright 2009 Nature. Panel C: Reproduced with permission from ref 76. Copyright 2012 Elsevier.

technique.[74] Below the monolayer, only mono- and dimetalate species are formed on a single layer (Figure 5A). However, above the monolayer, the disordered Zr-WO_x mixed oxide clusters together with mono- and polytungstates were noticed particularly in the range of 0.8−1 nm (Figure 5B). The incorporation of ZrO_x into the WO_x species has been confirmed by several spectroscopic techniques.[75] The schematic representations of the mono-, di-, and polytungstates are shown in Figure 5C.[76]

MoO_x and WO_x stabilized on metal oxides can act cooperatively with noble metal nanoparticles (NM NPs) anchored on the same metal oxide surface. The strong acidity, induced by the interactions of MoO_x (WO_x) with the supports or NM NPs, shows a favorable effect in activating reactant/

https://doi.org/10.1021/acscatal.1c03326
ACS Catal. 2021, 11, 13603−13648

intermediates for further transformation over NM NPs or both sites involving different cascade reactions. Aihara et al.[77] studied a correlation between the structural features of WO_x on the Pt/WO_3/Al_2O_3 catalyst for glycerol hydrogenolysis to 1,3-propanediol. Two different kinds of WO_x species over the monolayer surface below 20 wt % were evidenced by the H_2-TPR study (Figure 6). The catalytic activity of Pt/WO_3/Al_2O_3 showed a

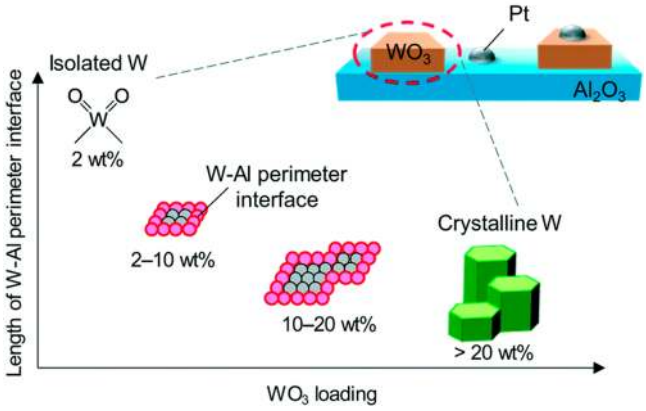

Figure 6. Models of W species on Pt/WO_3/Al_2O_3 catalysts. Reproduced with permission from ref 77. Copyright 2019 Royal Society of Chemistry.

positive correlation between the W−Al perimeter interface and 1,3-propanediol yield; however, catalytic activity drops at higher WO_x loading where highly crystalline WO_x is formed over Al_2O_3 support. This indicates that the W−(OH)−Al located at the WO_x−Al_2O_3 perimeter interface is essential for glycerol hydrogenolysis. The other model reaction hydrodeoxygenation (HDO) of dibenzofuran to biphenyl was studied over the Pt/MoO_x/MgO catalyst by Zhang et al.,[78] and the effect of MoO_x species was investigated in detail. The addition of MoO_x enhances the HDO activity significantly by 26 times, and the HDO rate over Pt/MgO was only 0.04 μmol s^{-1} g^{-1}; however, Pt/7MoO_x/MgO showed 1.06 μmol s^{-1} g^{-1}. The highest product yield was obtained by using the Pt/7MoO_x/MgO catalyst, where monolayer coverage of MoO_x was mainly evidenced. The catalytic activity was improved until <2.27 Mo per nm^2 surface Mo coverage, where MoO_x species were in the dispersed form. A further increase in the loading of >6.19 Mo per nm^2 suppresses the reaction rate, meaning that crystalline MoO_x species reduce the availability of active MoO_x species for the reaction. Over the Pt/MgO catalyst, the etheric bond was adsorbed on Pt and successively converted to the *o*-phenylphenol and biphenyl. However, in the case of the Pt/MoO_x/MgO catalyst, the presence of unsaturated MoO_x sites involved in the adsorption of etheric oxygen of dibenzofuran and cleavage of the C−O bond take place by the neighboring H−Pt species, leading to the efficient formation of the biphenyl compound.

Summarizing this section, we conclude that MoO_x and WO_x show similar coordination modes with different oxide supports. At low surface coverage, isolated tetrahedrally coordinated dioxo species are formed; however, at high surface coverage, octahedrally coordinated distorted polymetalate species of different nature are realized. The degree of polymerization and polymetalate species' formation depends on the coverage and oxide supports' properties (Hüttig temperature and surface hydroxyl group density). Silica-supported MO_x (M = Mo and W) catalysts mainly contain MO_3 crystalline NPs due to the low density and poor reactivity of the silica hydroxyl groups with MO_x species. In the case of Al_2O_3 support, the crystalline poly-MO_x formation is favored up to the monolayer and the MO_3 formation is observed above the monolayer coverage. Interestingly, the ZrO_2 support shows a unique coordination behavior above the monolayer because of the lability of the Zr cation above the Hüttig temperature of its oxide. Hence, the Zr-incorporated polymetalate cluster is formed, resulting in the formation of Zr−O−M bonds. This type of bond formation has a unique stabilization of Brønsted acid sites for several organic transformations. It was important to note that the formation of MO_3 crystalline NPs has occurred at a very low loading (1 metal atom per nm^2) of MO_x on silica versus ∼4.5 metal atoms per nm^2 over other supports like Al_2O_3, TiO_2, and ZrO_2.

2.2. Role of Coordination Chemistry on the Acidic Strength of Supported MoO_x and WO_x Solid Acids. WO_x and MoO_x supported on SiO_2 tend to form isolated surface oxide species.[79] Acid catalysis of the SiO_2 supported material is mainly associated with the surface-bounded WO_x and MoO_x species. The Fourier-transform infrared spectroscopy (FTIR) measurement of lutidine adsorbed WO_x showed that WO_x/SiO_2 has only Brønsted acidity, corresponding to the protonated lutidine.[80] It was found that, with an increase in the W density, the Brønsted acidity increased up to 1.3 W per nm^2 and plateaued for higher loading. In contrast, the bare SiO_2 support evidenced neither Brønsted acidity nor Lewis acidity when FTIR was performed after desorption of the sample at 150 °C. Hahn et al.[81] studied the MoO_x formation over various supports, such as SiO_2 and SiO_2−Al_2O_3 of different Brønsted and Lewis acidities. For low Mo-loaded material, they suggested the formation of Brønsted acid sites on the boundaries between MoO_x and support (Mo−O(H)−Si(Al)).[82,83] However, with an increase in the Mo loading, the formation of an additional Mo−O(H)−Mo bond is favored. The formation of poly-MoO_x species blocked the surface Lewis acidity. With an increase in the Mo loading, the subsequent drop of support Lewis acidity was also demonstrated. Moreover, the degree of surface poly-MoO_x species highly depends on the surface Lewis acidic character.

The most exciting material in this family is ZrO_2 supported WO_x and MoO_x due to the unique structural features and surface acidity. Depending on the loading of WO_x and MoO_x on ZrO_2 material, both Brønsted and Lewis acid sites can be obtained, while the nature and location of the active sites are actively debated in the literature. At low loading, surface coordinatively unsaturated Zr^{4+} atoms are available as Lewis acid sites as they exhibit electron-deficient character. The loading of WO_x and MoO_x coordinated to the OH groups of support and formed surface species can be further stabilized by coordinating to the surface Lewis acid sites, generating the Brønsted acid sites on the MO_x species.[84] Several models are presented to explain the nature and location of Brønsted acid sites on WO_x and MoO_x supported on the ZrO_2 catalyst.[15]

Iglesia and co-workers reported the formation of Brønsted acid sites by the replacement of high-valence with low-valence cations (for example, $W^{6+} \rightarrow H^{\delta+}(WO_3)_n^{\delta+}$).[85,86] From the XANES (X-ray absorption near edge structure) experiment over the WO_x density from 3 to 15 W per nm^2, it was shown that the WO_6 units are present over the complete range of WO_x density. Since W^{6+} is reducible, it was considered for the Brønsted acid sites over the WO_x domains. However, this model was inconsistent for the known loading (∼4.5−5 W per nm^2) of WO_x on ZrO_2.[87,88] Knözinger and co-workers[87,88] performed low-temperature FT-IR spectroscopy analysis with adsorbed

https://doi.org/10.1021/acscatal.1c03326
ACS Catal. 2021, 11, 13603−13648

CO as a probe molecule over 3.6 to 23.9 wt % of WO_x on ZrO_2. Above the monolayer loading of WO_x on ZrO_2, the Zr^{4+}−CO stretching band was observed, meaning that the Zr cation was still available for coordination with a gaseous CO molecule. Therefore, they proposed that the pseudoheteropolytungstates containing Zr^{4+} are responsible for the active site generation above the monolayer. A trace amount of Zr cation incorporation led to a surface negative charge compensated by proton as a Brønsted acid site. This model lacks the explanation of the local structure of the Zr−WO_x cluster because, in the proposed pseudoheteropolytungstates structure, Zr is present at the center of poly-WO_x and still available for CO interaction. Furthermore, the formation of Lewis acidity together with Brønsted acidity above monolayer was evidenced on the Zr−WO_x cluster.[89]

Most recently, Lai and Wachs[67] employed several advanced characterization techniques, such as in situ Raman, in situ UV−vis DRS, XPS, and STEM-HAADF, to understand the position of Zr atoms and surface acidity. In situ Raman and UV−vis DRS showed the formation of crystalline WO_3 NPs above 4.5 W per nm^2. The formation of bulk WO_3 crystal was dominant on the crystalline ZrO_2 compared to the amorphous $Zr(OH)_x$ support. Above the monolayer coverage, Zr stabilized disordered WO_x species with the three-dimensional structure are formed on the support. To understand more in-depth about the structure of the Zr−WO_x cluster, a density functional theory (DFT) calculation was performed on the model structure of the WO_x clusters (isolated monomeric, dimeric, and trimeric) as well as the well-defined 3D Zr-substituted Keggin structure ($H_3PW_{12}O_{40}$), where Zr is present on the center by substituting P atoms, the substitution of W addenda atoms, and ZrO_x cluster grafted on the $H_3PW_{12}O_{40}$ cluster. The DFT calculation showed the increasing Brønsted acidity (decreasing deprotonation energy) of WO_x clusters from monomeric to trimeric species. Further, the incorporation of the Zr atom in the Keggin 3D structure drops the deprotonation energy by 22−118 kJ/mol and subsequently enhances the Brønsted acidity. This means the substitution of the Zr cation delocalizes the charge on the neighboring oxygen atom compensated by the proton, which is responsible for improving the strength of the surface Brønsted acidity of the metal clusters. This confirmed the higher acidity of Zr−O(H)−W sites than W−OH sites. The highest Brønsted acidity was obtained for ZrO_x grafted on the Keggin structure and further improved by increasing the number of ZrO_x clusters on the external surface. To obtain high catalytic activity for the particular reaction, the formation of the Zr−WO_x cluster on the support can be controlled by the catalyst's synthesis and post-treatment procedure.[90,91] Although Lai and Wachs were able to explain the nature of the surface sites by combining the experimental findings with the DFT calculations using a simple Keggin model structure, the more complex size-selected structural model is required to explain the Zr location on the WO_x cluster.

In addition to pyridine-adsorbed FTIR analysis, solid-state nuclear magnetic resonance (ssNMR) analysis is considered a powerful technique to estimate both qualitative and quantitative measurements of the acid sites, along with their local structure and coordination models in solid acids by selecting a suitable probe containing nuclei having a spin (e.g., ^1H, ^{13}C, ^{15}N, and ^{31}P).[92] In general, the ^1H ssNMR technique of pyridine-d_5 adsorption is used for probing acid hydroxyls in solid materials. The ^1H resonance arises in the range of 2−10 ppm by the pyridine-d_5 adsorption over Si−OH and Al−OH functional groups,[93,94] characterized by nonacidic and weakly acidic groups, respectively. However, the pyridine-d_5 adsorbed on Brønsted acid sites forming a pyridinium ion can give a ^1H signal at 12−20 ppm.[95] The spatial proximity between proton and active species on the Mo/ZSM-5 catalyst can also be estimated by double resonance ssNMR spectroscopy.[96] Subramaniam and co-workers[97] found that the air-regenerated catalyst (mesoporous silica-supported WZr oxide) after the ethanol dehydration reaction exhibits improved Brønsted acidic strength as estimated by ss-NMR analysis. The combustion (i.e., air regeneration) of adsorbed hydrocarbon species on the catalyst surface can generate surface water and free radicals, which induced the formation of heteropolytungstate species with additional Brønsted acid sites. The existence of both Brønsted and Lewis acid sites in supported WO_x solid acids can be effectively estimated using the ^{15}N ssNMR analysis of pyridine-d_5 (Figure 7). It was demonstrated that the bridged −OH

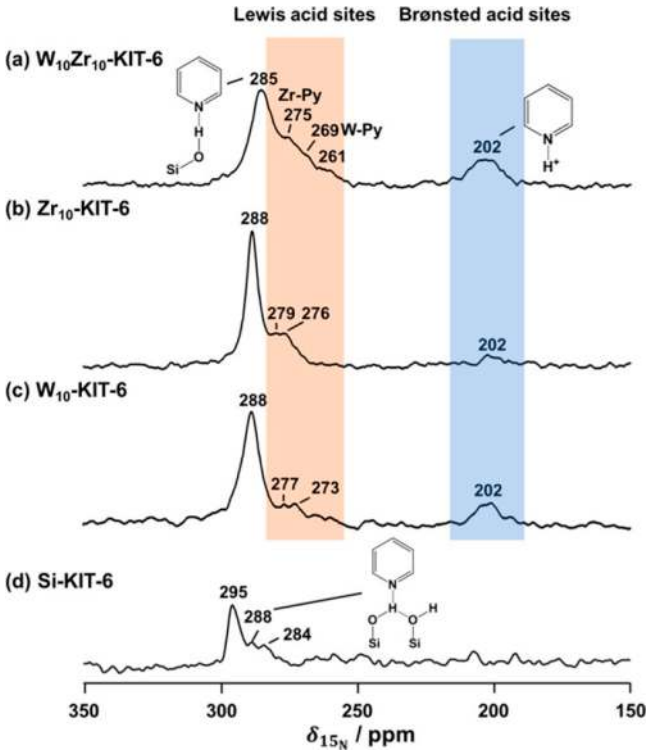

Figure 7. Acidity analysis of WZr-KIT-6 using the ^{15}N ssNMR technique with a pyridine-d_5 probe. Reproduced from ref 97. Copyright 2018 American Chemical Society.

groups, existing as W−OH−W, in surface tungsten dimers or multimers of a supported WO_x catalyst exhibit strong Brønsted acidic character, while the weak acidity was due to terminal W−OH and Si−OH sites.[98] Furthermore, the nature of these acid sites was confirmed by quantum chemistry calculations.

The strength of the acid sites (particularly Brønsted acid sites) in solid acids can also be studied by ^{13}C ssNMR using 2-^{13}C-acetone as the probe.[99] Although ^1H and ^{13}C ssNMR methods are helpful for analyzing acid sites and their strength, their application is limited due to the narrow chemical shift (^1H ssNMR) and low natural abundance and high experimental cost in the case of ^{13}C ssNMR.[92] Recently, ^{31}P ssNMR has been recognized as the most preferable and sensitive method for identifying Brønsted and Lewis acid sites in solid acids. Therefore, probe molecules, such as trimethylphosphine (TMP) and trimethylphosphine oxide (TMPO), are extensively

https://doi.org/10.1021/acscatal.1c03326
ACS Catal. 2021, 11, 13603−13648

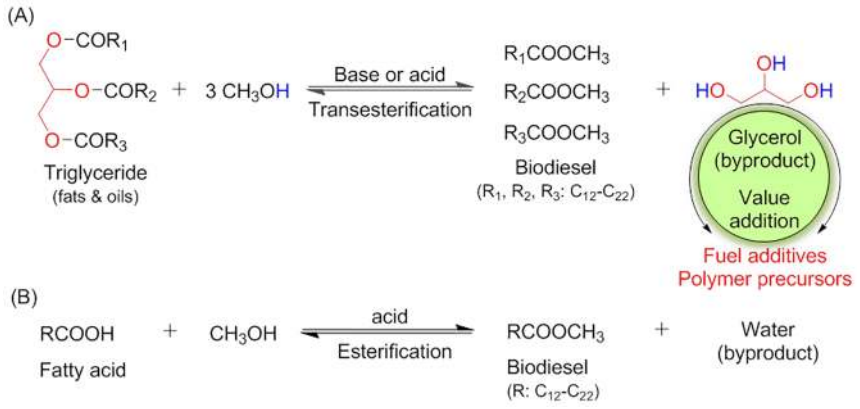

Figure 8. (A) Biodiesel synthesis by the transesterification of triglycerides with methanol over acid or base catalysts. (B) Biodiesel synthesis by esterification of fatty acids with methanol over acid catalysts. R is a fatty acid alkyl group.

used to analyze acid sites in solid catalysts.[92,100,101] The ^{13}P chemical shift for TMP adsorbed on Brønsted acid sites led to the resonance band in a narrow range from −2 to −5 ppm, whereas the Lewis acid adsorbed TMP gives signals in the range of −20 to −60 ppm. TMPO is the most frequently used probe molecule for acidity analysis due to the broader range of resonance signals for the TMPO adsorbed acidic catalyst.[102,103] Fan and co-workers analyzed the acidity of the WO_x−ZrO_2 catalyst using ^{31}P-ssNMR with TMPO as a probe molecule.[101] A broad signal from 40 to 90 ppm containing three parts was analyzed as physisorbed TMPO and TMPO adsorbed on Lewis and Brønsted acid sites. The chemical shift above 57 ppm was characterized as surface Brønsted acid sites.

3. CATALYTIC APPLICATIONS OF SUPPORTED MoO_x AND WO_x SOLID ACIDS FOR BIOMASS VALORIZATION

3.1. Valorization of Oil and Fat Biomass for Biodiesel Synthesis.

Biodiesel (fatty acid methyl ester, FAME) is a clean, sustainable, and biodegradable fuel. It is produced from triglycerides (oils and fats) and fatty acids via transesterification and esterification, respectively (Figure 8).[104−106] Biodiesel is considered the most promising substitute to diesel fuel for automobile vehicles.[4,107] Owing to the enormous benefits, global biodiesel production and consumption are increasing significantly, and its production is predicted to increase from 22.7 million tons in 2012 to 36.9 million tons in 2021.[108] In the transesterification reaction, glycerol is a byproduct (Figure 8A). Longer chain alcohols can be used in transesterification and esterification, but their high cost and difficulty in the separation/purification of the resulting heavier products limit their use for biodiesel synthesis.

3.1.1. Biodiesel Synthesis by Transesterification of Triglycerides. Liquid-phase bases (e.g., NaOH, KOH, or $NaOCH_3$) are the commonly used catalysts for the transesterification of triglycerides to biodiesel, but these catalysts are highly sensitive to moisture and free fatty acid (FFA), leading to soap formation, along with biodiesel formation during the transesterification process. In this case, additional steps are needed to separate and purify biodiesel, increasing the production cost. Although using refined vegetable oils (with less than 0.5 wt % FFAs) is recommended for biodiesel synthesis using alkali catalysts, the refined oils are costly, increasing the overall production cost. Alternatively, using hydrothermally stable catalysts, especially MoO_x- and WO_x-based solid acids, for biodiesel synthesis has received significant attention in recent years. They exhibit high water-tolerant capacity and can prevent saponification, resulting in high purity biodiesel production at economically viable conditions.

A variety of supported MoO_x and WO_x solid acid catalysts have been studied for biodiesel synthesis. For instance, Xie and Yang[109] found that the $AlPO_4$ supported WO_3 and MoO_3 solid acids show the best catalytic performance in soybean oil transesterification with methanol than the bare WO_3 and MoO_3 catalysts. Among them, the $WO_3/AlPO_4$ solid acid provided higher biodiesel yield, attributed to its strong acidic strength. The obtained conversions of soybean oil were 32.8%, 29.6%, 34.5%, 56.3%, and 72.5% over WO_3, MoO_3, $AlPO_4$, $MoO_3/AlPO_4$, and $WO_3/AlPO_4$, respectively. The WO_3 loading (30 wt %) and calcination temperature (800 °C) of $WO_3/AlPO_4$ solid acid were optimized for biodiesel synthesis. There was no effect of FFA and water on the catalytic performance of $WO_3/AlPO_4$ solid acid for biodiesel synthesis. After the catalyst was separated from the reaction mixture, the liquid sample was analyzed by the ICP technique, and only 1.8 ppm of tungsten was found, indicating that the tungsten species are tentatively stable under the reaction conditions. Hence, the 30 wt % $WO_3/AlPO_4$ solid acid showed good reusability for up to 4 cycles for biodiesel synthesis. Another work also demonstrated higher catalytic activity of supported WO_3 solid acids compared with supported MoO_3 solid acids for biodiesel production.[110] The deposition of WO_3 on the SnO_2 support led to improved acidity and good structural stability. This is due to the formation of $(WO)_x$ clusters on the SnO_2 support, resulting in the delocalization of the negative charge across the extended W−O network, which can accommodate protons responsible for the strong acidic nature of the WO_3/SnO_2 catalyst. As a result, there were considerable yields of biodiesel (79.2% from soybean oil). Good catalyst reusability was achieved for up to four cycles (about 72% biodiesel yield), and then, there was a sudden decrease in biodiesel yield (57.8%) for the fifth recycle of WO_3/SnO_2 solid acid. This is due to the continuous blockage of the surface active sites by reaction intermediates and products with the repeated use of the catalyst. The lack of a synergistic metal−support interaction and strong acid sites could be the reasons for achieving lower biodiesel yields in the case of supported MoO_3 solid acids. For biodiesel production, the Mo leaching was significantly inhibited after depositing MoO_3 on Al_2O_3, due to the presence of strong MoO_3−Al_2O_3 interactions that induced the creation of new strong acidic centers, although a low specific

https://doi.org/10.1021/acscatal.1c03326
ACS Catal. 2021, 11, 13603−13648

surface area was found.[111] So, the support plays a crucial role in improving the catalyst's acidity by optimizing the interactions of MoO_3 and WO_3 with the supports.

The significance of WO_x/ZrO_2 solid acid over a sulfated zirconia solid acid for transesterification of triglycerides and esterification of carboxylic acids was noticed by López's group.[112] Although the sulfated zirconia showed higher catalytic activity, a significant sulfur loss was noticed during both transesterification and esterification reactions, resulting in a rapid decrease in catalytic activity during a long period reaction. In contrast, the regeneration of the catalytic activity of tungstated zirconia was achieved by simply recalcining it in air and was found to be the most suitable catalyst for biodiesel synthesis. No leaching of the active W species was noticed, as evidenced by the reusability studies. The WO_3/ZrO_2 solid acid catalyst also effectively converted *S. obliquus* lipids to biodiesel (94.6% yield).[113] Although this catalyst showed appreciable stability, there is a continuous decrease in biodiesel yield (73% after the sixth cycle) due to the leaching of the catalyst's active sites during the reaction and washing steps. The activity of this WO_3/ZrO_2 catalyst is much higher than an enzyme catalyst and comparable to a liquid-phase H_2SO_4 acid catalyst. It confirms the importance of WO_x-based solid acid for biodiesel synthesis. The addition of Al_2O_3 to WO_x/ZrO_2 solid acid enabled it to use in continuous-flow transesterification of soybean oil to biodiesel at 200−300 °C in a fixed bed reactor.[114] About 90% conversion was achieved over 100 h of the time-on-stream period at 250 °C. The comparison of the activity studies revealed the high catalytic performance of $WO_x/Al_2O_3-ZrO_2$ solid acid over two solid superacids, namely, SO_4^{2-}/SnO_2 and SO_4^{2-}/ZrO_2. This superior activity might be due to the improved properties achieved by the strong interaction of WO_x with $Al_2O_3-ZrO_2$ mixed oxide.

The porosity of the support (e.g., mesoporous SiO_2) plays a vital role in improving the mass transport properties during the processing of bulky molecules like triglycerides.[115,116] For instance, the presence of intra- and interparticle pores in the silica support allowed efficient transportation of reactants and products during transesterification of *Croton megalocarpus* oil, giving 96% biodiesel yield over a 2 wt % WO_3-loaded catalyst.[107] Some of the WO_3 particles are found to partially block the mesopores of the support. So, optimization of WO_3 loading is crucial to achieve a higher accessibility of the active sites. The doping of zirconium into MCM-41 mesoporous silica and its consequent effect on the catalytic efficiency of WO_x solid acids were studied for the transesterification of sunflower oil with methanol at 200 °C.[117] The 15 wt % WO_3-loaded solid acid gave about 80% biodiesel yield after 2.5 h of reaction time. Biomass contains a considerable amount of water, which can adsorb on the acid sites, forming a layer around protons and, thus, inhibiting the accessibility of the acid sites to the reactant molecules. To understand this, the catalyst's stability was studied by adding 5 wt % water to the reaction mixture. Interestingly, the catalyst's activity was maintained (82% biodiesel yield), indicating good catalyst stability under hydrothermal conditions. Hence, this catalyst was efficiently reused for three cycles without applying any post-treatment. The promoting role of CaO in mesoporous silica (SBI-15) supported MoO_3 solid acid was noticed for biodiesel production. The solid catalyst with 40% $CaO-MoO_3$ loading and calcination at 550 °C showed the best performance, giving 83.2% oil conversion after 50 h of reaction.[118] The FFAs and water present in the feedstock have not demonstrated any detrimental effect on the activity of the $CaO-MoO_3-SBA-15$ catalyst, indicating its excellent hydrothermal stability. A slight decrease in biodiesel yield from 83.2% (1st cycle) to 77.2% (5th cycle) was found, revealing good reusability of the catalyst. The synergistic interaction between the CaO, MoO_3, and SBA-15 silica is responsible for enhancing the catalyst activity and stability. Owing to highly dispersed Mo active species and the strong interaction between the Mo oxide species and mesoporous Na-Beta support, 7 wt % Mo/Na-Beta catalyst showed improved transesterification activity.[119] Although an 18% decrease in biodiesel yield was found after the first recycle, there is not much change for the subsequent three cycles. This study revealed that proper washing treatment using an organic solvent is needed to remove the adsorbed species (from the catalyst surface) that blocked the pore channels and active sites.

The production cost of biodiesel can be reduced by using waste cooking oil as feedstock, but waste cooking oil contains a considerable concentration of FFAs. As pointed out, saponification occurs via a base-catalyzed transesterification if the feedstock contains free fatty acids.[120] In this case, the use of supported MoO_x and WO_x solid acids is preferred as they simultaneously catalyze both transesterification of waste cooking oil and esterification of FFAs. For instance, biodiesel synthesis from waste cooking oil, containing a high concentration of FFAs, was carried out using the Fe−Mn-doped tungstated molybdena catalyst. The biodiesel yield was found to be 92.3%, and the catalyst reduced the content of FFAs to about 0.62%, indicating the dual role of the catalyst. The catalyst was stable for up to 6 cycles, and then, a considerable loss in biodiesel yield was found for the seventh cycle, which was due to the mass loss of the catalyst during the recovery and washing of the catalyst. Among MoO_3/SiO_2, WO_3/ZrO_2, MoO_3/ZrO_2, and $WO_3/ZrO_2-Al_2O_3$ solid acids, MoO_3/SiO_2 (5 wt % Mo) showed the best performance in transesterification of waste oil, giving 79% biodiesel yield at 200 °C, 1:6 molar ratio of oil to alcohol, and 3% w/w catalyst.[121] The high efficacy of the MoO_3/SiO_2 catalyst can be ascribed to its superior BET surface area (265 m^2/g); thus, more surface active sites are readily available for the reaction. As noticed by Komintarachat and Chuepeng,[122] the catalytic activity of the WO_x solid acids in transesterification of used cooking oil (15% FFA content) is highly dependent on the support: $Al_2O_3 > SiO_2 > SnO_2 > ZnO$. This is due to the large pore volume (0.95 cm^3/g) and high specific surface area (260 m^2/g) of the Al_2O_3 compared to the other supports. The large pores of Al_2O_3 can enhance the mass transport properties of bulky molecules, resulting in higher reaction rates and improved product yields. As a result, the WO_x/Al_2O_3 catalyst was reused efficiently for three recycles, but a significant decrease in product yield was found in the fourth and fifth recycles. The particle shape (flower) of the $W/TiO_2/SiO_2$ catalyst played a key role in the transesterification of waste oil with ethanol.[123] More than 98% yield of fatty acid ethyl ester was obtained. Only <5 ppm of total metal content was found in the biodiesel after the fourth recycling test, indicating the stability of the catalyst.

3.1.2. Biodiesel Synthesis by Esterification of Fatty Acids. Fatty acids are long-chain organic acids and produced via hydrolysis of triglycerides with glycerol as a byproduct. The acid-catalyzed esterification of fatty acids with alcohols is an effective strategy for biodiesel synthesis. The MoO_3/ZrO_2-TiO_2 solid acid shows a 36% conversion of oleic acid to yield biodiesel, while WO_3/ZrO_2-TiO_2 solid acid shows a negligible performance compared with the blank test.[124] Highly dispersed MoO_3 species present on the surface of the ZrO_2-TiO_2 exhibit

https://doi.org/10.1021/acscatal.1c03326
ACS Catal. 2021, 11, 13603−13648

excellent acidic strength without any significant decrease of the specific surface area compared to ZrO_2−TiO_2 that showed a negligible conversion of fatty acid. Park et al.[125] developed a pellet-type WO_3/ZrO_2 solid acid, which showed steady-state conversion of oleic acid (70%) to biodiesel even after 140 h of reaction time. The oxidation state of tungsten controlled the acidity and activity of the WO_3/ZrO_2 solid acid. The molybdenum-containing silica solid acid catalyst, used for the esterification of fatty acids (lauric acid and oleic acid) with methanol and ethanol, was highly resistant in terms of leaching, attributed to the encapsulation of Mo sites in the silica network, indicating high stability of the catalyst.[126] About 95% conversion of fatty acids was achieved, and kinetic studies revealed that the activity of the solid acid decreases with the decreasing concentration of acid sites. The calcination temperature and W surface density strongly affected the catalytic efficiency of WO_x/ZrO_2 solid acids in palmitic acid esterification.[127] The polymeric tungsten species on tetragonal ZrO_2 support are essential to creating Brønsted acid sites. The 15 wt % WO_x/ZrO_2 solid acid was resistant to leaching, recovered easily, and reused efficiently without significant activity loss by simply calcining the catalyst.

Several studies pointed out the importance of W loading in controlling acidity and catalytic activity of supported WO_3-based solid acids. Rao et al.[128] found that the 13.8 and 25.1 wt % tungsten-loaded solid acids exhibit much lower performance in palmitic acid esterification in methanol, although they contain more acid sites than their lower loading counterparts. This is due to the formation of undesirable species, such as lacunary or dimeric Keggin ions on the support surface and/or blockage of the support pores at higher W loadings, which prevented the accessibility of bulky fatty acid molecules to reach acid sites on the catalyst inner surface. Since pyridine is a smaller molecule, it can diffuse effectively through the pores of the catalyst; thus, more acid sites were estimated by pyridine-adsorbed FT-IR analysis of higher tungsten-loaded catalysts. Notably, the 7.8 wt % tungsten-loaded solid acid showed the best esterification activity. This solid acid is resistant to leaching (as investigated by the hot-filtration test), easily recovered, and efficiently reused without much loss in the catalytic activity. In contrast, a higher tungsten-loaded catalyst exhibits lower acidity due to the formation of WO_3 crystals.[129] However, the application of calcination temperature led to improved dispersion of WO_x species on the surface of Zr-SBA-15. These WO_x species act as strong acid sites, which catalyzed the esterification of palmitic acid with cetyl alcohol. The X-ray fluorescence results revealed the significant leaching of WO_3 species during the reaction due to the lack of strong interaction between WO_3 and Zr-SBA-15. Another work also highlighted the significance of the high dispersion of $(WO)_x/ZrO_2$ NPs on MCM-41 support in achieving improved esterification of oleic acid with methanol.[130] Thus, the 15−20 wt % WO_3-loaded catalysts after calcination at 700 °C showed the best catalytic performance with oleic acid conversion close to 100%. The 15 wt % WO_3-loaded solid acid catalyst is active at high reaction temperatures (200 °C). Additionally, the stability of catalyst is confirmed by the analysis of the reaction solution and recyclability for up to four cycles.

The significance of mesoporosity of Ti−Mo[131] and Al−Mo[132] mixed oxide catalysts was realized in the esterification of FFAs in *Euphorbia lathyris* crude oil and *Jatropha curcas* crude oil with methanol, respectively. Owing to the porous structure, which allows easy diffusion of the reactants and products, improved conversions of the fatty acids and excellent catalyst reusability were noticed over both mesoporous catalysts. In the case of Mo-rich catalysts, crystalline MoO_3 species were formed on the catalyst surface, which blocked the pores of the catalyst.[131] Therefore, optimum Mo loading is important in order to maintain structural features and catalytic activity. It has been shown that the lower concentration of acid sites and the lower number of accessible acid sites were found in the Ti_5Mo_5 catalyst, showing lower esterification activity compared with the Ti_7Mo_3 catalyst. The best Ti_7Mo_3 catalyst showed good reusability with 87.3% and 82.3% in the first and fifth recycles, respectively. Zhang et al.[107] investigated oleic acid esterification with methanol over modified porous Mo−Zr solid acids. Several monofunctional carboxylic acids, such as lauric acid, myristic acid, stearic acid, and palmitic acid, were used as modifiers during solid acid synthesis. It was shown that the modified solid acids contain grainy structures and loose honeycombed surfaces. As a result, the modified porous Mo−Zr solid acids exhibited higher acid strength and larger specific surface area. Among the catalysts tested, the highest esterification activity was found over the stearic acid-modified Zr−Mo oxide, giving a 94.2% conversion of oleic acid, which is slightly decreased to 84.2% after the sixth recycling of the catalyst. Two reasons were speculatively proposed for this slight decrease: mass loss of the catalyst during recovery/reuse and active sites blockage by the adsorbed carbon residues. Sarkar et al.[133] evidenced a comparable activity of mesoporous SnO_2/WO_3 solid acid to liquid acid H_2SO_4 in oleic acid esterification with ethanol. The mesoporous SnO_2/WO_3 solid acid with a specific surface area of 130 m^2/g exhibits up to 90% oleic acid conversion at 80 °C for a 2 h reaction time. Kinetic studies reveal the first-order dependency of the reaction on the concentration of oleic acid and solid acid. The conversion of oleic acid is dependent on the reaction temperature and the nature of the alcohols used. The FTIR analysis of the spent catalyst indicated the presence of C−H and C═O bonds on the catalyst surface, corresponding to the intermediate and/or reactant/product. So, catalyst regeneration, i.e., removing these adsorbed species, has been done by simply calcining the sample at 400 °C for 3 h, which was confirmed by FT-IR analysis of the regenerated catalyst. No leaching of the active tungsten species was found during the reaction, revealing the high catalyst stability. The catalytic efficiency of WO_3 (Lewis acid) combined with a microporous zeolite (USY, Brønsted acid) was tested for oleic acid esterification with methyl acetate.[120,134] WO_3 species partially blocked the Brønsted acid sites of USY by blocking micropores that control the accessibility of the reactants to mesoporous cavities. Compared with a conventional wet-impregnation method, the ultrasonic-assisted activation improved the catalyst's performance, giving about 79 and 80 wt % conversions over 10% and 20% WO_3/USY catalysts.

3.2. Valorization of Glycerol. Glycerol, one of the top 12 platform chemicals, can be converted into several high-value chemicals using various catalytic routes. Glycerol is synthesized from fossil fuel-derived chemicals (e.g., propylene) and obtained as a byproduct in the biodiesel synthesis process via trans-esterification of triacylglycerides with alcohols. About 1 kg of glycerol is obtained for every 10 kg of biodiesel production in the transesterification process. To replace diesel fuel in the transport industry, many countries have increased biodiesel production, causing an oversupply of glycerol. In Europe alone, more than 1 billion liters of glycerol are produced every year. Glycerol contains three −OH groups, which can undergo various transformations mainly via acid and oxidation routes. Hence,

https://doi.org/10.1021/acscatal.1c03326
ACS Catal. 2021, 11, 13603−13648

the conversion of glycerol into value-added chemicals is highly beneficial for the sustainable biodiesel industry. The acidic property of the catalysts plays a pivotal role in glycerol conversion routes, such as esterification, acetalization, dehydration, and hydrogenolysis (Figure 9). For these reactions, supported MoO_x and WO_x solid acids are found to be the most promising catalysts because of their remarkable structural and acidic properties.

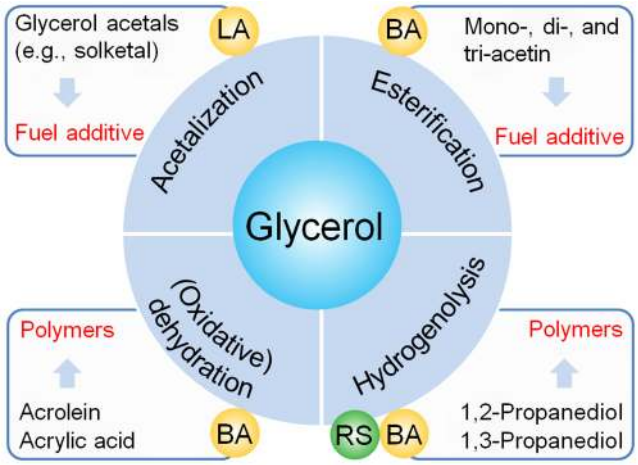

Figure 9. Acid-catalyzed reactions of glycerol: acetalization, esterification, (oxidative) dehydration, and hydrogenolysis. BA: Brønsted acid sites; LA: Lewis acid sites; RS: redox sites.

3.2.1. Esterification. Glycerol esterification is a vital reaction because the resulting products can be used as fuel additives for diesel and biodiesel.[135] Acetic acid and acetic anhydride are widely acetylating agents in glycerol esterification. Acetic acid is widely studied because of its low price compared with acetic anhydride. The products of glycerol esterification with acetic acid are known as acetins (monoacetin, diacetin, and triacetin).[26] Acetins are important chemicals for the food, cosmetic, and pharmaceutical industries. They are key ingredients in the manufacturing of plasticizers and can be used as emulsifying and softening agents. Monoacetin and diacetin are crucial chemicals for producing biodegradable polyesters. Diacetin and triacetin can be used as fuel additives because they can effectively improve fuel properties (e.g., cold, viscosity, octane rating, and cloud point),[135,136] but monoacetin is not preferable as a fuel additive because of its relatively high solubility in water.

The acidic nature of the catalysts determines the reaction pathway of glycerol esterification. In the case of Brønsted acid catalyst, acetic acid is protonated by Brønsted acid sites, followed by nucleophilic attack of oxygen from the −OH of glycerol on the sp^2 carbon of the protonated acetic acid. Then, elimination of water gives an acetin product. In contrast, the Lewis acid site (a metal cation) activates the carbonyl oxygen of acetic acid, forming a carbocation intermediate. The remaining process is the same as in a Brønsted acid-catalyzed reaction mechanism. Supported MoO_x- and WO_x-based solid acids contain both Brønsted and Lewis acid sites. Hence, both reaction mechanisms are possible in glycerol esterification. The control of product selectivity is vital to obtain high yields of a particular acetin.[135] The formation of mono- and diacetin is highly relevant to the steric hindrance of three hydroxyl groups of glycerol. Thus, the produced mono- and diacetin typically represent isomer forms. The selectivity of mono-, di-, and triacetin also depends on the catalysts' properties (acidity and stability) and reaction parameters (glycerol/acetic acid molar ratio, catalyst amount, reaction temperature, and reaction time).

Reddy et al.[26] systematically investigated glycerol esterification with acetic acid using $WO_3/TiO_2{-}ZrO_2$ and $MoO_3/TiO_2{-}ZrO_2$ solid acids. The high dispersion of MoO_3 species on the surface of $TiO_2{-}ZrO_2$ results in a high concentration of acid sites induced by synergistic metal−support interactions. As a result, complete glycerol conversion with 80% triacetin selectivity was obtained over $MoO_3/TiO_2{-}ZrO_2$ solid acid, although it has a lower BET surface area and low concentration of acid sites compared with the $WO_3/TiO_2{-}ZrO_2$ catalyst. Raman spectroscopy analysis revealed the presence of geometrically different WO_x sites in the $WO_3/TiO_2{-}ZrO_2$ catalyst, which can block the surface active sites, a key reason for the low catalytic efficacy of $WO_3/TiO_2{-}ZrO_2$ solid acid in glycerol esterification. The $MoO_3/TiO_2{-}ZrO_2$ solid acid showed stable activity with no noticeable change in the conversion and selectivity of up to five cycles. Another work also reported higher catalytic efficacy of a supported MoO_3 solid acid (MoO_3/SnO_2) than a WO_3/SnO_2 solid acid for glycerol esterification.[21] Both MoO_3/SnO_2 and WO_3/SnO_2 solid acids exhibited more Brønsted acid sites than the Lewis acid sites. The improved esterification activity of MoO_3/SnO_2 solid acid was attributed to a high concentration of acid sites associated with strong acid strength. The WO_3 loading in WO_3/polypyrrole solid acid determines the glycerol conversion and triacetin selectivity.[137] About 82% glycerol conversion with 32%, 50%, and 18% selectivity to monoacetin, diacetin, and triacetin, respectively, was obtained over 5% WO_3-loaded nanocomposite catalyst, while in the case of 20% WO_3/polypyrrole nanocomposite, 98% glycerol conversion and 70% triacetin selectivity were achieved. The addition of polypyrrole enhances the dispersion of WO_3 particles and the catalyst's acidity. Also, the nanocomposites exhibit good thermal stability because polypyrrole has a more compact structure after the addition of WO_3. Hence, the improved catalytic performance of WO_3−polypyrrole was achieved in glycerol esterification with acetic acid.

3.2.2. Acetalization and Ketalization. Glycerol condensation with aldehydes (acetalization) and ketones (ketalization) provides valuable chemicals for polymer, petrochemical, and pharmaceutical industries.[25] For example, the ketalization of glycerol with acetone gives solketal, which is a promising fuel additive. Glycerol acetals and ketals improve biodiesel properties. The addition of these oxygenated compounds to diesel may significantly reduce auto exhaust emissions. Benzaldehyde and furfural are widely used in glycerol acetalization. The resulting cyclic products are promising precursors for the synthesis of 1,3-dihydroxyacetone and 1,3-propanediol.[23]

The condensation of glycerol with ketones or aldehydes follows different reaction pathways, depending on the nature of the acid sites. In the Lewis acid-catalyzed reaction, a carbocation is formed by the interaction of the carbonyl oxygen of acetone with the Lewis acid sites. Then, one of the hydroxyl groups of glycerol attacks this carbocation, followed by a dehydration step to give solketal or a six-membered cyclic product. In the case of a Brønsted acid-catalyzed reaction, a two-step mechanism was proposed.[25] First, the Brønsted acid sites promote the formation of tertiary alcohol by enhancing the interaction between the glycerol's terminal −OH group and the acetone's carbonyl group. Then, the dehydration of the alcohol gives a carbenium ion, which is attacked by the secondary or terminal −OH group

https://doi.org/10.1021/acscatal.1c03326
ACS Catal. 2021, 11, 13603−13648

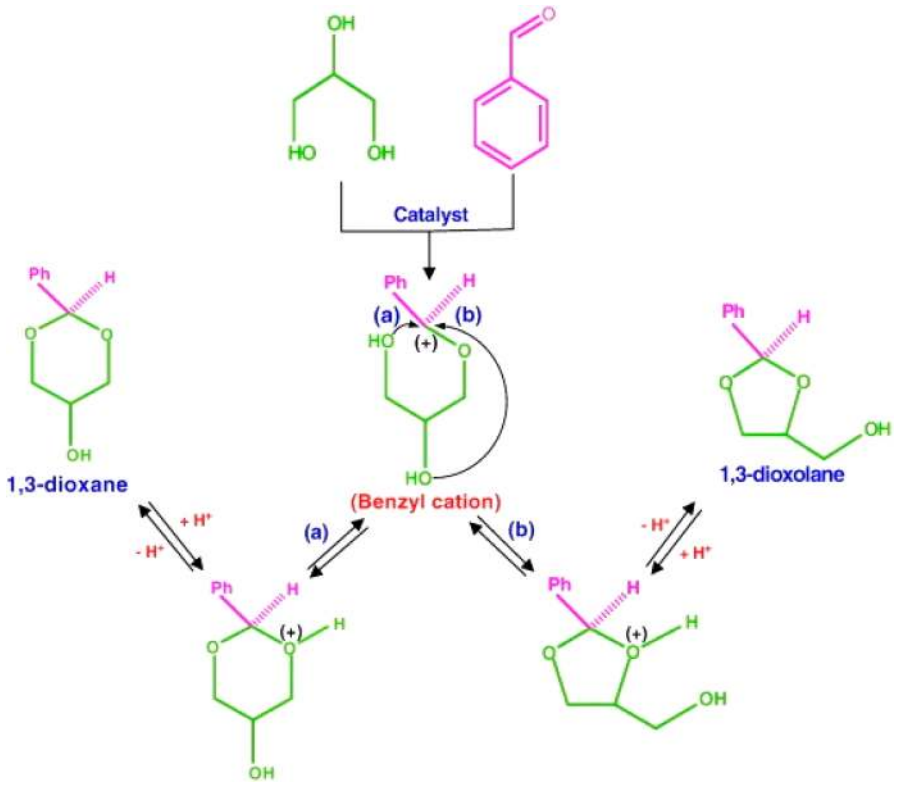

Figure 10. Formation of (a) 1,3-dioxane and (b) 1,3-dioxolane products via acetalization of glycerol with benzaldehyde using solid acid catalysts. Reproduced with permission from ref 23. Copyright 2013 Elsevier.

of glycerol, providing solketal or a six-membered cyclic product, respectively. A similar reaction pathway can occur when the aldehydes (e.g., benzaldehyde and furfural) are used in the glycerol acetalization reaction.

The selectivity of the cyclic products in glycerol acetalization/ketalization is dependent on the carbonyl compound.[138] Two structural isomers, such as solketal and 2,2-dimethyl-1,3-dioxan-5-ol, are formed in glycerol ketalization with acetone. However, this reaction mainly gives a solketal product (more than 95%). The reason is that the methyl groups at the axial position of the six-membered product induce strong steric repulsions. Hence, solketal is thermodynamically more stable than the six-membered cyclic product. In contrast, a negligible difference in the selectivity of products is noted in glycerol acetalization with aldehydes.[23] Two isomeric acetals, i.e., (a) 1,3-dioxane and (b) 1,3-dioxolane, are formed with almost 50% of each product (Figure 10).

The Reddy group developed nanocrystalline MoO_3/SnO_2 and WO_3/SnO_2 solid acids for glycerol acetalization.[25] These catalysts are found to be active at room temperature. The MoO_3/SnO_2 solid acid exhibited the highest glycerol conversion and product selectivity, attributed to a high concentration of acid sites, larger specific surface area, and enhanced structural defects. Especially, the MoO_3/SnO_2 solid acid has more lattice defects (i.e., oxygen vacancies) as revealed by Raman spectroscopy analysis. This is due to the incorporation of Mo^{6+} (ionic radius: 0.62 Å) into the SnO_2 lattice (Sn^{4+} = 0.71 Å). Since the ionic size of Mo^{6+} is higher than that of W^{6+} (0.56 Å), enriched lattice strain was found when Mo^{6+} replaced Sn^{4+} in the SnO_2 lattice; hence, more lattice defects are generated in the case of MoO_3/SnO_2 material. Moreover, the MoO_3/SnO_2 solid acid has smaller-sized crystallites, indicating a strong metal−support interaction, which is beneficial for catalytic reactions. Reddy et al.[22] also investigated the glycerol ketalization over WO_x/ZrO_2 and MoO_x/ZrO_2 solid acids, along with the SO_4^{2-}/ZrO_2 solid acid. Results revealed that the integration of WO_x or MoO_x with ZrO_2 led to strong surface acidity, giving higher glycerol conversion and solketal selectivity. Among these catalysts, better results were achieved with MoO_x/ZrO_2 solid acid, attributed to higher BET surface area and more acid sites. Despite the catalysts tested, an excellent selectivity of ∼97% toward solketal was obtained at all reaction conditions. In another work, they found that the integration of MoO_3 with the mixed oxide supports (TiO_2−ZrO_2) results in enhanced acidic properties due to the synergistic metal−support interactions. The MoO_x/TiO_2−ZrO_2 catalyst showed about 74% glycerol conversion with 51% 1,3-dioxane selectivity.[23] Glycerol conversion is dependent on the reaction temperature, but the solvent's effect was negligible. Low glycerol conversion was found in the case of substituted benzaldehydes, because of the steric hindrance of the substituents.

The mesoporosity of the solid acids assisted in achieving higher reaction rates in glycerol acetalization because of the improved diffusion of bulky molecules like glycerol through the porous channels during the reaction.[139] The mesoporous W−Zr−O solid acids, containing both Lewis and Brønsted acid sites, showed efficient reusability for the glycerol acetalization without the need for any post-thermal/chemical treatments. Higher yields of bioadditives were achieved over these mesoporous solid acids than the conventional catalysts due to the presence of a greater number of accessible active sites in mesoporous solid acids. Sol−gel synthesized mesoporous MoO_3/SiO_2 solid acids (1−20 mol % MoO_3 loadings) were tested for glycerol acetalization with various aldehydes.[140] Microscopic images showed highly dispersed MoO_3 NPs (20 mol % MoO_3) on an amorphous silica support, resulting in enhanced acid and

https://doi.org/10.1021/acscatal.1c03326
ACS Catal. 2021, 11, 13603−13648

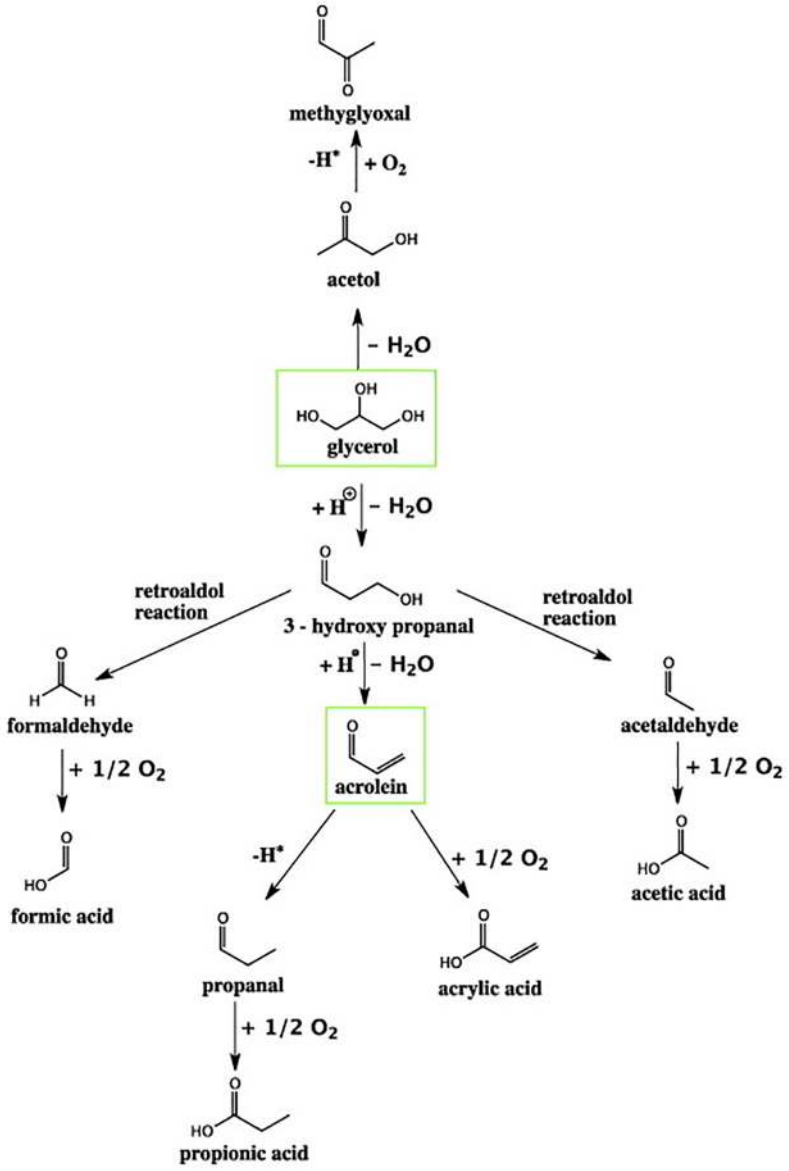

Figure 11. Formation of various products during glycerol dehydration in the presence of a solid acid catalyst. Reproduced with permission from ref 144. Copyright 2015 Elsevier.

catalytic properties for glycerol acetalization. About 72% benzaldehyde conversion with 60% selectivity to the six-membered acetal was obtained over 20% MoO_3/SiO_2 solid acid in an 8 h reaction time at 100 °C reaction temperature. The mesoporous structure enabled improved accessibility of the active sites to the reactants as well as the faster diffusion of the intermediates and the products that favored glycerol acetalization toward the formation of six-membered acetal. In the case of substituted benzaldehydes, conversion was decreased with increased selectivity of the six-membered acetal. The co-incorporation of Zr and Mo in an ordered mesoporous silicate KIT-6 was achieved by a one-pot hydrothermal method.[141] The resulting catalyst showed optimal catalytic performance in solketal synthesis with a 97.8% selectivity. Excellent catalyst reusability was noticed for up to five cycles. After each cycle, the regeneration of the catalyst was done by calcination at 500 °C for 2 h to remove the adsorbed organic species from the catalyst's active sites. No metal species were found in the liquid sample of the reaction as analyzed by the leaching test.

3.2.3. Dehydration and Oxidative Dehydration. Dehydration is one of the promising glycerol valorization routes, giving acrolein, a key chemical for producing glutaraldehyde, DL-methionine, pentaerythritol, quinoline, 1,2,6-hexanetriol, and cycloaliphatic epoxy resins.[108,142,143] Moreover, acrolein is used to synthesize acrylic acid, an important intermediate used for producing polyacrylate polymers. Acrolein is produced mainly through propylene oxidation in the gas phase using bismuth molybdate catalysts. Although complete propene conversion is achieved with more than 85% acrolein selectivity, this process and propene production by the steam cracking reaction both use fossil fuel-derived precursors and reagents.[142,143] Therefore, using glycerol for acrolein production is undoubtedly a sustainable strategy.

In addition to acrolein, various other products are also possible during glycerol dehydration, depending on the catalyst's acidity and the reaction parameters (Figure 11). Acrolein formation is favored on the Brønsted acid sites. The first step in glycerol dehydration is the formation of 3-

https://doi.org/10.1021/acscatal.1c03326
ACS Catal. 2021, 11, 13603−13648

hydroxypropanal or acetol by eliminating water as a by-product.[144] Further dehydration of 3-hydroxypropanal gives acrolein. The retroaldol reaction of 3-hydroxypropanal gives acetaldehyde and formaldehyde from which acetic acid and formic acid can be formed, respectively. Acrolein and propanal are the sources for acrylic acid and propionic acid under the oxygen atmosphere conditions (called oxidative dehydration), respectively.

Significant attention has been paid toward developing potential supported WO_x and MoO_x solid acids for the glycerol dehydration reaction in continuous-flow conditions because the acidic properties of these catalysts can be efficiently optimized to achieve higher yields of acrolein. Ulgen and Hoelderich[142] developed a WO_3/TiO_2 solid acid for the dehydration of glycerol in the gas phase. About 85% selectivity to acrolein was obtained at complete glycerol conversion. The use of oxygen increased the glycerol conversion; however, acrolein selectivity was decreased slightly. The titania carriers (sulfate amount) and specific surface area were found to be critical factors for the activity of WO_3/TiO_2 solid acid. The ZrO_2 precursor ($ZrO(OH)_2$ hydrogel and its derived alcogel) used to synthesize WO_3/ZrO_2 solid acid showed a significant effect on its catalytic efficacy in glycerol dehydration.[145] The WO_3/ZrO_2 solid acid synthesized using $ZrO(OH)_2$ hydrogel-derived alcogel showed a high acrolein yield (62−68%) at >93% glycerol conversion for more than 30 h of reaction time. The effects of H_2 or O_2 cofeeding, partial pressures of glycerol/water, reaction temperature, and the addition of transition metals (Ni, Pt, Pd, and Rh) or metal ions (Na^+, K^+, and Mg^{2+}) were investigated. The increase of the molar ratio of glycerol/H_2O resulted in low acrolein selectivity and catalyst deactivation. The catalyst deactivation rate was reduced remarkably after adding 4−8 kPa O_2 to the reaction feed, but the acrolein selectivity was slightly decreased. In contrast, adding 4 kPa H_2 to the reaction feed does not affect the glycerol conversion and product selectivity. Only Pt or Pd modifiers show a favorable effect in the reaction. Over the 15 wt % WO_3/ZrO_2 catalyst, complete glycerol conversion and 65% acrolein selectivity were achieved, which was attributed to the presence of a high concentration of Brønsted acid sites.[146] The WO_3/ZrO_2 solid acid showed better catalytic efficacy than the Nb_2O_5/ZrO_2 solid acid in glycerol dehydration at the complete conversion of glycerol,[143] but no synergetic catalytic effect was found when the reaction was performed using a mixed W−Nb catalyst. The addition of O_2 to the reaction feed does not affect the acrolein yield but prevents the catalyst deactivation rate. The structure−activity relationship shows that the active surface structure of the catalyst for glycerol dehydration is polymeric oxide exposing W@O species and Brønsted acidic groups, but W−Nb−O mixed oxides, prepared by a hydrothermal method, showed excellent catalytic performance in the gas-phase dehydration of glycerol.[147] The textural and acidic properties of the mixed oxide were improved by controlling the metal composition in the catalyst, resulting in higher yields of acrolein from the glycerol dehydration reaction. No leaching of the active sites of the W−Nb oxide catalyst was found after three cycles, indicating its high catalytic stability under aqueous reaction conditions. Cecilia et al.[148] found that the phosphoric acid treatment enhanced the catalytic performance of WO_3/Zr-SBA-15 solid acid toward acrolein for a short period, but it caused the catalyst deactivation due to the poisoning of the textural and acidic properties of the catalyst, which led to decreased available acid sites for the reaction. About 97% glycerol conversion and 41% acrolein yield were achieved over a 20 wt % W-loaded catalyst at 325 °C after 2 h of reaction time, and this activity was maintained up to 8 h. Thermogravimetric analysis of the spent catalyst revealed the presence of various types of carbonaceous species on the catalyst surface. Hence, a regeneration step was suggested by thermally treating the catalyst at 550 °C under oxygen flow, thus removing the adsorbed carbonaceous species from the catalyst.

Interestingly, the acrolein selectivity increases with an increase in coke formation over WO_3/TiO_2 solid acid during the vapor-phase glycerol dehydration.[144] The catalyst regenerated by partial oxidation of coke was found to improve the acrolein selectivity from 10% to 25% within 15 min of reaction time. Compared to a multitubular fixed bed reactor, improved catalyst regeneration was achieved on a fluidized-bed reactor because it minimizes hot spots, allowing the homogeneous distribution of carbon particles on the catalyst surface. The catalytic performance of hypothetical monolayer loadings of WO_3 supported on Al_2O_3, SiO_2, and TiO_2 was investigated for glycerol dehydration.[149] Better metal dispersion and hydrated tungstate species were found in WO_3/TiO_2 and WO_3/Al_2O_3, while WO_3/SiO_2 solid acid contains crystalline WO_3 particles. The addition of oxygen to the reaction feed improved the catalyst's stability. Among the solid acids tested, the WO_3/TiO_2 catalyst shows the highest acrolein selectivity (80%) at the increased conversion of glycerol. This is due to the inhibition of the formation of unidentified products, including carbon precursors, by adding oxygen to the reaction, thus enhancing acrolein selectivity. A correlation between the catalyst's Brønsted acidity and acrolein selectivity was found. Owing to the mesoporous structure of Al_2O_3, the WO_3/Al_2O_3 solid acid showed higher catalytic activity and durability in glycerol-to-acrolein dehydration than the other supported WO_3 catalysts and zeolites, especially with 20 wt % WO_3 loading.[150] The reason is that Brønsted acid sites inside the mesopores of 20 wt % WO_3/Al_2O_3 solid acid are readily accessible for glycerol molecules during the reaction. There is no noticeable change in the Brønsted acidity and mesoporosity of the catalyst after the reaction, indicating the catalyst's stability against coke formation. The WO_3 loading and O_2 flow have a significant effect on the catalyst's durability. The addition of SiO_2 to WO_3/ZrO_2 results in the formation of larger mesopores and reduced basicity, which prevented byproduct formation during the glycerol dehydration, resulting in enhanced product selectivity and catalyst stability at 300 °C.[151] Besides, larger pores can improve the accessibility of the active sites to the glycerol molecules, thus achieving improved reaction rates. The catalysts prepared by incorporating siliceous species into the $ZrO_x(OH)_{4-2x}$ and the subsequent anionic exchange with peroxotungstate showed 78% acrolein selectivity at complete glycerol conversion. About 82% glycerol conversion was maintained after 177 h of reaction.

The catalytic behavior of a multicomponent WO_x/H_3PO_4-activated montmorillonite (W/Mt-P) catalyst was tested for glycerol dehydration in the gas phase.[152] The acid activation of montmorillonite and the subsequent addition of WO_x affected the catalyst's acidity, metal leaching, and the WO_x type ($2.7 \leq x \leq 3$). The strength of the weak and medium acid sites was enhanced, while the strong acid sites were weakened in 12 wt % W-loaded Mt-P catalyst. As a result, an excellent selectivity (81.8%) to acrolein at 89.6% glycerol conversion was achieved over the 12% W/Mt-P catalyst at a 320 °C reaction temperature. This study showed that strong acid sites induce coke formation, resulting in rapid catalyst deactivation. Akizuki et al.[153] studied

https://doi.org/10.1021/acscatal.1c03326
ACS Catal. 2021, 11, 13603−13648

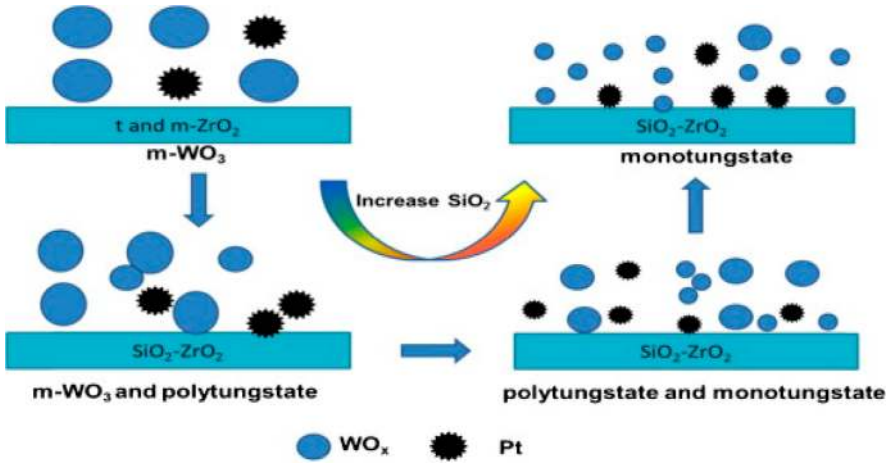

Figure 12. Structure evolution of the PtW/Zr catalysts containing different amounts of SiO_2. Reproduced with permission from ref 161. Copyright 2014 Elsevier.

the catalytic stability of WO_x/TiO_2 solid acid in glycerol dehydration under supercritical water conditions (400 °C) by changing the reaction pressure (250 and 330 bar). At 330 bar pressure, coke formation was prevented because of the enhanced diffusion of the coke precursors through the catalyst pores than at 250 bar pressure, but high metal leaching (especially WO_x species) from WO_x/TiO_2 solid acid was found at 330 bar reaction pressure due to high ionic products of water; i.e., sub- and supercritical water exhibits both acid and base properties. The WO_x species are unstable under alkaline conditions. They also investigated the kinetics of glycerol dehydration on WO_3/TiO_2 solid acid in supercritical water at 400 °C and 330 bar pressure.[154] The reaction pathway of glycerol dehydration was proposed on the basis of the product distribution. Acrolein degradation to acetaldehyde was noticed under supercritical water conditions. The increase in the WO_3 content of the WO_3/TiO_2 solid acid led to a higher reaction rate for glycerol-to-acrolein dehydration because of improved BET surface area and strong acidity. The effect of the coke formation in governing the catalyst acid strength and product selectivity in glycerol dehydration was also studied using WO_3/TiO_2 solid acid.[155] Interestingly, although coke was accumulated on the catalyst surface, about 73% acrolein selectivity at 100% glycerol conversion was achieved over WO_3/TiO_2 solid acid after 6 h of reaction time. The reason is that coke particles cover the active sites of the catalysts, responsible for the side reactions; hence, the acrolein selectivity was increased with time-on-stream. As a result, the selectivity of acetone and propanal was higher at the conditions where a lower amount of coke formed. The concentration of Lewis/Brønsted acid sites was decreased with reaction time, as confirmed by FT-IR pyridine analysis. In contrast, there is not much change in the number of strong acid sites after 14 h of reaction time. Two reasons were reported: (1) molecular oxygen used in the feed can promote catalyst regeneration and (2) there is preferential adsorption of coke on basic- or medium-strength acid sites compared to strong acid sites.

Acrylic acid (AA) is a high-value chemical for the polymer industry. The widely used AA-based polymer products are superabsorbents (diapers), textiles, and paper additives. AA is also used in adhesives, coating materials, and polyelectrolytes. Acrylic acid is produced through an energy-intensive two-step gas-phase oxidation process, wherein propylene (a derivative of crude oil) is oxidized to acrolein and further oxidation gives AA. AA production from biomass-based compounds like glycerol is sustainable and needs both acid and redox catalytic active sites. Hence, there is a huge demand to develop efficient bifunctional catalysts for AA production from glycerol. The gas-phase dehydration of glycerol was studied over the Ni-, Co-, and Cu-promoted Mo catalysts supported on the Al_2O_3 spheres.[156] Interestingly, acrolein was obtained as the main product instead of acrylic acid for all the catalysts. The Cu-promoted Mo/Al_2O_3 showed a higher glycerol conversion due to the synergistic effect of Cu^{1+}/Cu^0 and Mo^{5+}/Mo^{4+} redox species. Moreover, the addition of Cu has a significant effect on the partial reduction of MoO_x, which prevents acetol production. Exciting results were found in pure and mixed MoV oxide catalyzed oxidative dehydration of glycerol.[157] Catalyst deactivation was noticed over the MoO_x/Al_2O_3 catalyst, which showed a higher selectivity to acrolein. The addition of vanadium oxide prevents the deactivation of MoO_x/Al_2O_3 solid acid by promoting coke oxidation with its labile lattice oxygen via the Mars-van Krevelen mechanism. In contrast, acrylic acid is the primary product obtained over an MoV mixed oxide catalyst supported on a microporous ZSM-5 zeolite.[158] So, the support and the respective metal−support interaction play a key role in tuning product selectivity in oxidehydration of glycerol over MoV mixed oxide catalyst. Only a 6% decrease in the efficacy of the MoV_2O_8/ZSM-5 catalyst was found during the 8 h reaction time, while almost 31% and 20% decreases in the efficiencies of zeolite support and the bulk mixed oxide were found, respectively. Two factors contributed to the high stability of the MoV_2O_8/ZSM-5 catalyst: (1) strong metal−metal and metal−support interaction, which inhibited the phase transition of MoV_2O_8 to the less active $Mo_4V_6O_{25}$ phase and (2) synergistic effect of acid-redox active sites that promoted the removal of coke residues via oxidation route.

3.2.4. Hydrogenolysis. Glycerol hydrogenolysis is a multistep reaction, involving dehydration followed by hydrogenation to produce valuable chemicals, such as 1,2-propanediol (1,2-PDO) and 1,3-propanediol (1,3-PDO).[159] Other byproducts (e.g., 1-propanol, 2-propanol, ethylene glycol, ethanol, etc.) are also possible from this reaction due to side reactions involving C−O and C−C bond cleavages in glycerol (methanol, ethane, and methane). 1,3-PDO is a valuable chemical and used as a monomer for synthesizing polypropylene terephthalate resins.

https://doi.org/10.1021/acscatal.1c03326
ACS Catal. 2021, 11, 13603−13648

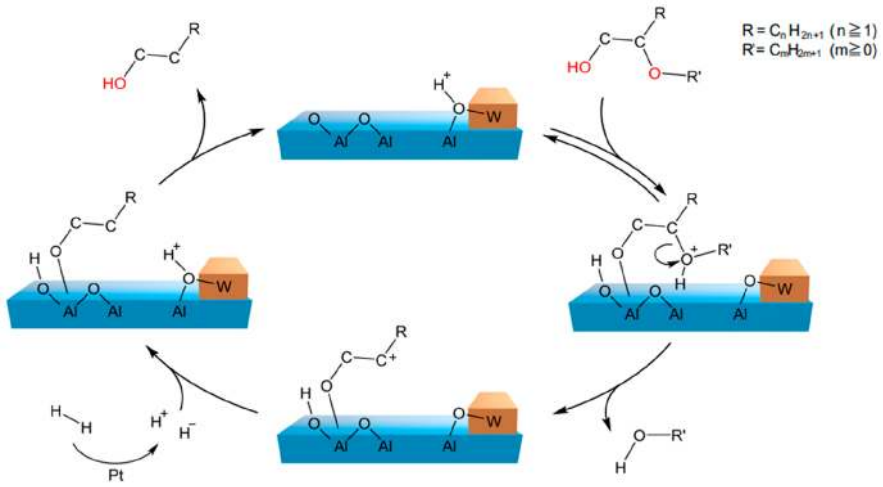

Figure 13. Dissociation mechanism of a C−O bond at a secondary carbon over a $Pt/WO_3/Al_2O_3$ catalyst. Reproduced with permission from ref 166. Copyright 2020 Elsevier.

1,2-PDO is used as antifreeze liquids and additives in liquid detergent.[160] Both two-step and three-step mechanisms are proposed for glycerol hydrogenolysis that depend on the catalyst's properties and process conditions. The two-step mechanism involves a dehydration step to obtain acetol or 3-hydroxypropoanal (acid sites) and then a hydrogenation step over redox sites (metal) to obtain 1,2-PDO or 1,3-PDO. The three-step mechanism involves dehydrogenation, dehydration, and hydrogenation that require acid and base as well as redox sites to achieve higher glycerol conversion and product selectivity.

Since both acid and redox sites are needed for glycerol hydrogenolysis, various multicomponent catalysts are developed, consisting of supported WO_3 and MoO_3 (acid sites) coupled with the noble metals (redox sites). Mainly, the combination of Pt and WO_3 was found to have a remarkable effect on the glycerol hydrogenolysis reaction. The addition of an appropriate amount of SiO_2 to $Pt/WO_x/ZrO_2$ catalyst remarkably improved the WO_x dispersion as well as induced the formation of active polytungstate species with improved acidity, while surplus SiO_2 addition converts polytungstate to monotungstate species (Figure 12).[161] The 5 wt % SiO_2-loaded $Pt\text{-}WO_x/ZrO_2$ catalyst showed superior activity with 52% selectivity of 1,3-PDO. The platinum metal and polytungstate were found to be the active species, and a two-step dehydration−hydrogenation mechanism was proposed for the reaction. Kurosaka et al.[162] investigated hydrogenolysis of glycerol to 1,3-PDO using WO_3/ZrO_2 catalysts doped with 2 wt % Pt. An approximate 24% yield was obtained over the $Pt/WO_3/ZrO_2$ catalyst. Both glycerol conversion and 1,3-PDO selectivity were significantly affected by the nature of the support, noble metal, and the catalyst synthesis method. More Brønsted acid sites and high dispersion of smaller-sized Pt particles were found when Pt and WO_3 dispersed on tetragonal (t-ZrO_2) compared with monoclinic (m-ZrO_2).[163] As a result, the $Pt-WO_x/t\text{-}ZrO_2$ catalyst showed higher activity in glycerol hydrogenolysis, giving about 49% yield of 1,3-PDO. The catalyst maintained good recyclability of up to five cycles with only an ∼0.54% decrease in the yield of liquid products per cycle, which was more likely due to the mass loss of the catalyst during its recovery/reuse.

Higher yields of 1-propanol (28%) and 2-propanol (15%) with 14% and 18% yields of 1,3-PDO and 1,2-PDO, respectively, in glycerol hydrogenolysis over the $Pt/WO_3/Al_2O_3$ catalyst in a gas−solid fluidized bed reactor were obtained.[164] Mechanistic studies revealed that the reaction occurs via multiple steps, involving glycerol dehydration to acrolein over acid sites (WO_3), followed by its rehydration to hydroxypropanal and finally a metal-promoted hydrogenation step to give 1,3-PDO. An excellent yield (38.5%) of 1,3-PDO was obtained from the $Pt/WO_x/Al_2O_3$ catalyzed glycerol hydrogenolysis at 90 bar of H_2 pressure after 4 h of reaction time.[165] The presence of more hydrogen favors the formation of 1,3-PDO. Spectroscopic studies revealed the multiple roles of WO_x for glycerol hydrogenolysis: (i) a strong adsorption site for glycerol, (ii) a proton donor, and (iii) a stabilizing agent for the secondary carbocation. Particularly, the W−(OH)−Al species at the W−Al perimeter interface provide Brønsted acid sites, which protonate the O atom of the secondary carbon and then cleave the C−O bond to give a secondary carbocation during the hydrogenolysis of various biomass-based alcohols and ethers, including glycerol (Figure 13).[166] The demonstrated correlation between the length of the W−Al perimeter interface and 1,3-PDO yield supports the above mechanism.[167]

Improved catalytic results were found in glycerol hydrogenolysis (77.5% conversion) to 1,3-PDO (54.8% selectivity) when Au (0.1 wt %) was added to the $2Pt/7.5W/Al_2O_3$ catalyst.[168] In this catalyst structure, Au is dispersed as single atoms and Pt NPs (∼2 nm) are decorated with $Au-WO_x$ at the periphery. The improved H-spillover at the interface between Pt and WO_x generates Brønsted acid sites, which cleave the secondary C−O bond of glycerol, giving excellent results from the glycerol hydrogenolysis reaction (Figure 14). Here, Au enriches the exposed Pt surface for achieving H-spillover capacity by weakening the $Pt-WO_x$ interaction, attributed to electron transfer from W to Au as confirmed by chemisorption and XPS studies. The glycerol conversion was slightly decreased from 41.4% (first cycle) to 35.7% (fourth cycle), while there was no noticeable variation in the 1,3-PDO selectivity (∼57%). The aggregation of Pt particles and coke deposition were found to be the reasons for decreased glycerol conversion. Darbha and co-workers[169] demonstrated that ^1H NMR spectroscopy analysis could efficiently quantify the products from glycerol hydrogenolysis instead of gas chromatography.

A mesoporous Pt/WO_3 catalyst was developed to produce 1,3-PDO from glycerol hydrogenolysis.[170] Compared with commercial WO_3, the mesoporous WO_3 has a larger BET

https://doi.org/10.1021/acscatal.1c03326
ACS Catal. 2021, 11, 13603−13648

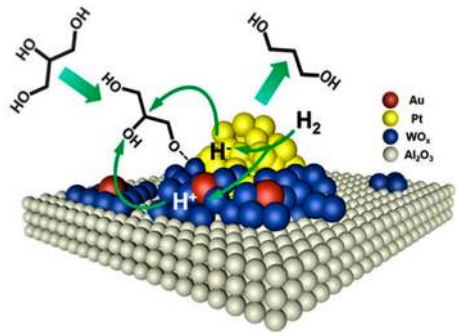

Figure 14. Proposed mechanism of glycerol hydrogenolysis over the 0.1Au-2Pt/7.5W/Al catalyst. Reproduced from ref 168. Copyright 2021 American Chemical Society.

surface area and better reducibility, resulting in a high dispersion of Pt particles on the mesoporous WO_3. About 39% 1,3-PDO selectivity at 18% glycerol conversion was obtained at 180 °C and 55 bar H_2 pressure for a 12 h reaction time. Higher selectivity (50.5%) to 1,3-PDO was achieved from glycerol hydrogenolysis over a multicomponent $Pt/WO_3/TiO_2/SiO_2$ catalyst in a slurry batch reactor.[171] The effects of solvent, H_2 pressure, and reaction time/temperature on the product yields were systematically investigated. It was shown that the weak Brønsted acid sites of WO_3 play a vital role in the formation of 1,3-PDO. It is evident from the above studies that 1,3-PDO is the primary product in glycerol hydrogenolysis catalyzed by supported $Pt-WO_x$ catalysts. In contrast, the combination of Rh with the MoO_x/SiO_2 catalyst (Mo/Rh = 0.13) shows a higher selectivity to 1,2-PDO (41%) with a 9.6% selectivity to 1,3-PDO in glycerol hydrogenolysis at 80 bar hydrogen pressure and 120 °C reaction temperature.[172] The reason is that the catalyst preferentially cleaves the C−O bond in $-O-C-C-CH_2OH$ than that in $-O-C-CH_2OH$ of glycerol, but the formation of 1,2-PDO in glycerol hydrogenolysis seems to be due to the presence of MoO_x in the catalyst.[173] For instance, about 45% selectivity to 1,3-PDO was found over the $Pt-W/ZrO_2$ catalyst, while 1,2-PDO (49% selectivity) is the main product over the $Pt-Mo/ZrO_2$ catalyst. The variation in the product formation with W- and Mo-based catalysts can be explained by changes in their acid and redox properties induced by Pt addition. The glycerol conversion was significantly decreased from 35% to 15% after the second run, which was maintained in the third run. The catalyst deactivation was more likely due to the leaching of the active sites under hydrothermal conditions.

Over Pd-containing MoO_3/Al_2O_3 catalysts, prepared by the wetness impregnation method, very high selectivity (>90%) to 1-propanol and 2-propanol was achieved in glycerol hydrogenolysis.[174] The synergetic $Pd-MoO_3$ interaction and the presence of weak to moderate acid sites on the catalyst were responsible for the activity of the $Pd-MoO_3/Al_2O_3$ catalyst. The reusability studies, after activating the spent catalyst at 500 °C in air flow for 2 h, revealed that glycerol conversion and product selectivity remain the same up to 6 h, and then, a significant decrease in the product selectivity was found. The catalyst deactivation after 6 h is due to the agglomeration of the catalyst particles and/or coke deposits. Satisfactory results (12.7% glycerol conversion and 32.3% 1,3-PDO selectivity) from the hydrogenolysis of glycerol were achieved over noble-metal free $Cu-WO_x-TiO_2$ catalysts.[175] More Brønsted acid sites were found in the catalyst prepared by a modified evaporation-induced self-assembly method (EISAM) than the impregnated catalyst. This is due to the formation of the homogeneous dispersion of tetrahedrally WO_x species, giving more W^{5+} species in the EISAM catalyst. The catalyst showed good reusability with 12% glycerol conversion and 30.8% 1,3-PDO selectivity after the fifth recycle. Allyl alcohol (23.3% selectivity) was the main product with glycerol conversion of 97.1% over $MoFe/CeO_2$ catalysts.[176] The particle size and crystalline degree of CeO_2 support (nanoparticle contains better properties compared to the nanocube) play a crucial role in improving metal−support interaction, acidity, and reducibility of the catalysts. Hence, the catalyst's activity and stability were enhanced toward allyl alcohol synthesis. Shozi et al.[160] investigated glycerol hydrogenolysis using γ-Al_2O_3 and SiO_2 supported MoO_3 and WO_3 catalysts without using any redox metal. Low-carbon alcohols are the primary products: 1-propanol, 2-propanol, ethanol, and methanol with the selectivities of 70.6%, 64.8%, 54.6%, and 34.6% were achieved over W/Al_2O_3, Mo/SiO_2, W/SiO_2, and Mo/Al_2O_3 catalysts, respectively. When the H_2 amount of the glycerol was doubled, the total selectivity of the lower alcohols was significantly increased to 85.3%, 73.6%, 72.8%, and 66% over W/Al_2O_3, Mo/Al_2O_3, Mo/SiO_2, and W/SiO_2 catalysts, respectively. The presence of improved Brønsted acidity, higher BET surface area, and superior reducibility were the reasons for the higher activity of alumina-supported catalysts, which are more pronounced in the WO_3/Al_2O_3 catalyst. Consequently, the WO_3/Al_2O_3 catalyst showed higher activity in glycerol hydrogenolysis.

3.2.5. Other Methods for Glycerol Valorization. Hydrogen production via glycerol steam reforming was studied on molybdena−alumina catalysts. Two methods, such as sol−gel and gel combustion, were used to synthesize the catalyst.[177] Molybdena loading determines glycerol conversion and H_2 selectivity with improved productivities over the 2% MoO_3 catalyst. Glycerol carbonate is a potential chemical for the synthesis of advanced polycarbonates and polyurethanes. Besides, it can be converted into epichlorohydrin and used as a green solvent for many applications, which was attributed to its unique properties, including high flash point, high boiling point, and low volatility. Mallesham et al.[24] found that the combination of MoO_3 and SnO_2 provides a sufficient concentration of acid sites (~81.45 μmol g^{-1}). As a result, about 67% yield of glycerol carbonate was achieved over MoO_3/SnO_2 solid acid at a 150 °C reaction temperature with excellent catalyst reusability. In contrast, only 27% and 57% yields of glycerol carbonate were obtained over SnO_2 (46.47 μmol g^{-1}) and WO_3/SnO_2 solid acids (61.81 μmol g^{-1}) as they contain a lower concentration of acid sites. As shown in Figure 15, the catalyst's acid sites are essential to activate the carbonyl oxygen of urea, and it reacts with glycerol toward glycerol carbonate formation.

3.3. Valorization of Lignocellulose Biomass. Lignocellulose biomass is abundantly available in nature as a renewable organic carbon feedstock.[178] It has a complex structure composed of various functional molecules that can be used to produce a wide range of platform molecules, drop-in chemicals, biofuels, and fuel additives. Hence, it has the potential to replace fossil fuels for chemical production in the chemical industry. In nature, lignocellulose is synthesized by photosynthesis using atmospheric CO_2, H_2O, and solar light. Lignocellulose tissues form the structure of the plant, and it contains three main polymers, namely, cellulose, hemicellulose, and lignin. Cellulose (30−50% of total dry lignocellulose) is a crystalline polymer of glucose consisting of stable hydrogen-bonded chains of 1−4-β

https://doi.org/10.1021/acscatal.1c03326
ACS Catal. 2021, 11, 13603−13648

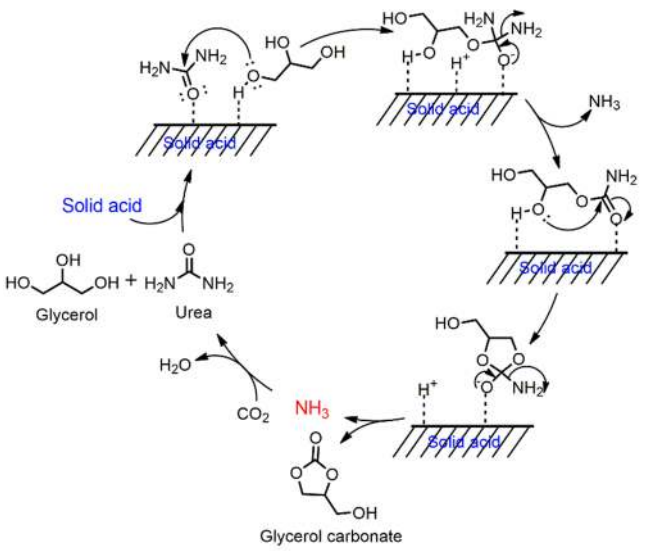

Figure 15. Proposed reaction mechanism for glycerol carbonylation with urea over MoO_3/SnO_2-based solid acids. Here, the activation of carbonyl oxygen of urea by the acid sites (Lewis) of the catalyst is critical to achieving improved yields of glycerol carbonate. Reproduced with permission from ref 24. Copyright 2020 Springer Nature.

linked glucose molecules. Hemicellulose (20−40%) is an amorphous organic polymer composed of several C5 and C6 carbohydrates.[178] Because of strong H-bonding in cellulose, it exhibits higher thermal and chemical stability than hemicellulose. Lignin (15−25%) is a complex aromatic polymer consisting of several p-substituted aromatic units. Lignin gives structural strength to every part of the plant by strongly enclosing both cellulose and hemicellulose. The rigidity and hydrophobic characteristics of the plants are also due to the presence of lignin.

3.3.1. Catalytic Fast Pyrolysis of Lignocellulose. Currently, three processes are found to be efficient in directly transforming lignocellulosic biomass into valuable hydrocarbons:[179,180] (1) gasification to produce synthesis gas (CO and H_2), a key feedstock to obtain liquid fuels via Fischer−Tropsch synthesis; (2) pyrolysis or liquefaction to bio-oil and the subsequent upgrading using catalytic approaches to give hydrocarbon fuels; (3) pretreatment−hydrolysis route to sugars and their processing under catalytic conditions or fermentation to produce fuel-grade hydrocarbons. Raw lignocellulosic biomass can be used in the first two routes, but only its components, i.e., cellulose and hemicellulose, can be processed via the third route. Among them, pyrolysis is of great interest because the resulting bio-oils are considered the cheapest liquid fuels. Pyrolysis involves thermal treatment of lignocellulose (400−700 °C) under inert atmosphere conditions, and then, rapid condensation gives liquid bio-oil products. There are two types of pyrolysis processes, namely, slow pyrolysis and fast pyrolysis.[180] In slow pyrolysis, biochar is the main product due to the application of low temperatures and long residence times. In contrast, the fast pyrolysis of lignocellulose using moderate temperatures and short vapor residence times will maximize bio-oil yields at the expense of biochar. The obtained bio-oil can be directly used in a burner for power generation or in engines and turbines. Moreover, transportation fuels and drop-in chemicals can be produced by further upgrading bio-oil (i.e., oxygen removal). The main drawback is that the fast pyrolysis gives more than 200 oxygenated compounds due to the additional successive reactions, such as depolymerization, dehydration, and C−C bond cleavage.[178] It contains mainly a mixture of aromatics and aliphatic oxygenated products, including alcohols, aldehydes, ketones, phenolics, carbohydrates, and carboxylic acids. Pyrolysis bio-oil is acidic with a pH of ∼2−3 and corrosive; hence, it is not stable at room temperature and can experience condensation/polymerization reactions, resulting in drastically increased viscosity and meager combustion properties.[181] Therefore, the conversion of lignocellulose directly into stable transportation hydrocarbon fuels with low oxygen content is a great challenge.

To tackle the above concerns, the catalytic fast pyrolysis (CFP) of lignocellulose, integrating the fast pyrolysis step with catalytic upgrading, has attracted much attention to produce a high-quality bio-oil with low oxygen content that will make the resulting bio-oil to use in the current technologies (Figure 16).[182,183] CFP is a one-pot process wherein the pyrolysis vapors

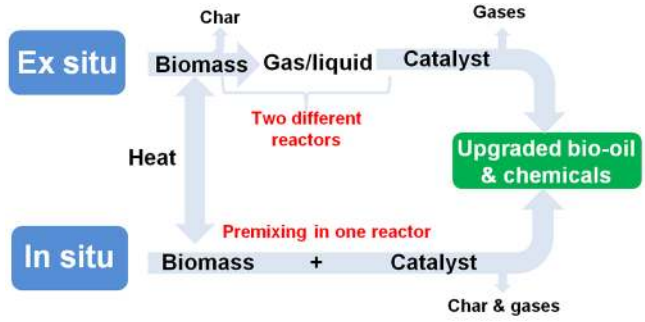

Figure 16. Schematic representation of ex situ and in situ catalytic fast pyrolysis processes.

are in contact with a catalytic bed before condensation and eventually avoids the unwanted condensation and re-evaporation steps.[184] In ex situ CFP, pyrolysis and upgrading processes will be done separately, meaning that biomass is not mixed with the catalyst. In contrast, biomass is added to the catalyst before heating during the in situ CFP process. Compared with a noncatalytic route, the above routes can produce high-quality bio-oil. However, during the in situ CFP process, the catalyst experiences deactivation due to the formation of char and ash because of strong intimate biomass−catalyst contact. Compared with the in situ process, the commercialization risks can be minimized via the ex situ CFP process, evidenced by the techno-economic and uncertainty estimations.

Several CFP processes have been developed for producing higher quality bio-oils from lignocellulose without using extensive pretreatment. Solid acid catalysts, particularly Mo-oxide-containing catalysts, show excellent performance in catalytic fast pyrolysis of lignocellulose. For instance, as reported by Murugappan et al.,[184] the MoO_3 catalysts supported on TiO_2 and ZrO_2 are significantly effective for the CFP of pine lignocellulose at 500 °C and ≤0.75 bar H_2, but different levels of deoxygenation were found, which is strongly dependent on the mass ratio of biomass to MoO_3. A higher percentage of aromatic and olefinic compounds are obtained for <1.5 mass ratios of biomass to MoO_3. On the other hand, partially deoxygenated compounds, such as phenols and furans, are obtained with decreased selectivity of aromatic and olefinic compounds for ≥1.5 mass ratios of biomass to MoO_3. For ≥5 mass ratio of biomass to MoO_3, the catalyst deactivation was noticed, which is

https://doi.org/10.1021/acscatal.1c03326
ACS Catal. 2021, 11, 13603−13648

due to the coke adsorption on the catalyst's surface. In the case of mesoporous silica (KIT-5) supported MoO_x catalysts, a high selectivity to furans (valuable jet/diesel fuel precursors) was obtained in the CFP of the biomass.[185] It was found that the 2.5 and 3.7 wt % Mo/KIT-5 catalysts show a better performance than the 1.5 wt % Mo-loaded catalyst. This is due to the effective control of the agglomeration or sintering of Mo sites during the synthesis or the reaction by mesoporous silica, providing more accessible active sites to the pyrolysis vapors. The catalyst deactivation was due to the formation of coke by the lignin fraction.

The presence of atmospheric pressure H_2 improves the quality and yield of bio-oil while minimizing the production of char and coke in the CFP of biomass using W- and Mo-based catalysts.[186] The catalytic performance of Al_2O_3- and Fe-based catalysts as well as a commercial hydrotreating catalyst was also investigated in this work. The Mo-based catalyst is effective in biomass pyrolysis, giving a higher yield of hydrocarbon-rich bio-oil, which contains mainly aromatic and aliphatic compounds with <10 wt % oxygen content. Under the CH_4 atmosphere, a good yield (39%) of aromatic hydrocarbons was achieved in the CFP of raw switchgrass over the MoZn/HZSM-5 catalyst at 700 °C.[187] Compared with monometallic catalysts (MoO_3/HZSM-5), the bimetallic catalysts showed a higher catalytic performance because of their ability to activate both CH_4 and pyrolysis bio-oil. Aromatic chemicals were obtained at higher reaction temperatures under both helium and methane atmospheres. The torrefaction of switchgrass before pyrolysis gave low yields of aromatic chemicals due to cellulose and lignin loss during torrefaction. The shape selectivity of microporous HZSM-5 zeolite toward a particular product cannot be ruled out in this study. A similar kind of catalyst (MoO_3/HZSM-5) is also tested for the pyrolysis of lignocellulose components under both helium and methane atmospheres.[180] The lignin-derived aromatics yield was increased to 15.13% (from 12.8%) when the pyrolysis was switched from helium to methane. However, methane was ineffective in improving the yields of aromatics from the carbohydrates fraction over the MoO_3/HZSM-5 catalysts. The Mo-based active sites promoted deoxygenation of lignin-derived phenolic compounds, while inhibiting the formation of polyaromatics and coke.

Nolte et al.[188] carried out the ex situ HDO of bio-oil produced from the pyrolysis of cellulose, lignin, and corn stover using a bare MoO_3 catalyst at 1.8 bar total pressure of H_2. The MoO_3 catalyst is effective toward hydrocarbons formation. When an initial induction period was applied, the catalyst's efficiency was improved to remove the oxygen species of the pyrolysis vapors. The product mixture contains mainly C1 to C6 linear alkanes as well as aromatics with ∼75−90 C% total yield of hydrocarbons from the volatile pyrolysis products (apart from char). The HDO efficiency of MoO_3/TiO_2 (MoO_3: 10 wt %) catalyst for producing fuel-grade molecules from the fast pyrolysis vapors (wheat straw) was compared to an industrial MoO_3/Al_2O_3 catalyst.[189] The oxygen content of the bio-oil was significantly reduced overall at 50 vol % H_2, and coke formation was effectively controlled by the TiO_2 supported catalysts. It indicates that, by using suitable catalysts, bio-oil quality can be improved at low hydrogen pressures. Much progress needs to be made to improve the purity and yield of biocrude by developing appropriate catalysts, cofeeding of H_2 or a hydrogen-rich feedstock, and optimizing the reactor design.

3.3.2. Other Processing Methods. In addition to the catalytic pyrolysis method, hydrolysis and hydroprocessing of lignocellulosic biomass using solid acid catalysts were also investigated to fully valorize it into useful chemicals and fuel grade molecules. Bhaumik and Dhepe[190] developed an effective methodology for the direct hydrolysis of crop waste (wheat straw, rice husk, and bagasse) into furfural using a sol−gel synthesized WO_3/SiO_2 solid acid. The WO_3/SiO_2 solid acid showed an excellent catalytic performance with a maximum of 87% furfural yield using a water/toluene (1:2 v/v) system at 170 °C after 8 h of reaction time. The WO_3/SiO_2 catalyst contains silicotungstic-type acid species, which are essential for efficient one-pot hydrolysis of crop waste. The WO_3/SiO_2 solid acid is stable and effectively reused after washing with water without any decline in the catalyst's activity for up to eight cycles. The synthesis of C5 and C6 sugar alcohols via hydrolytic hydrogenation of raw *Pennisetum* lignocellulose was done using a WO_3/ZrO_2 solid acid combined with a Ru/C catalyst.[70] A 36.8% biomass conversion and 11.6% and 8.3% yields of C6 and C5 sugar alcohols, respectively, were obtained with WO_3/ZrO_2 solid acid, while only 16.8% biomass conversion and 3.3% and 9.6% yields of C6 and C5 sugar alcohols, respectively, were achieved with bare ZrO_2 support. Although a lower activity and higher concentration of undesired liquid products were found from the HDO of solvolysed lignocellulosic biomass over a bare MoO_2 catalyst, its eco-friendly character and easy preparation method compared to sulfide containing catalysts made it a suitable catalyst for the HDO of lignocellulose.[191] A simultaneous process involving hydrolysis, dehydration, aldol-condensation, and hydrogenation was developed for converting lignocellulosic-biomass (corncobs) and biomass-derived carbohydrates (tapioca flour) using WO_3-ZrO_2 and Pd/WO_3-ZrO_2 catalysts along with other metal oxide-based catalysts.[192] The WO_3-ZrO_2 solid acid is effective for the hydrolysis/dehydration reaction of corncob and tapioca flour into furans, i.e., HMF and furfural. On the other hand, the impregnation of the WO_3-ZrO_2 solid acid with Pd led to improved activity toward the formation of C5−C15 organics from the aldol-condensation/hydrogenation of the furans. Higher yields of C5/C8/C13 compounds were obtained from corncob because it contains a higher percentage of hemicellulose, while tapioca flour gave more C6/C9/C15 compounds. Liquid alkanes with high cetane numbers can be obtained from these water-soluble organic compounds, which are considered promising alternatives to diesel fuel in the transportation industry. This study proved the successful application of WO_3-ZrO_2 solid acid in the aqueous-phase conversion of lignocellulose, but the catalyst reusability and leaching tests will provide more information about the catalyst stability.

3.4. Valorization of Cellulose and Its Derived Compounds. Cellulose is a major component of lignocellulosic biomass, constructing cell walls of plants together with hemicellulose and lignin.[193,194] Cellulose is a long-chain polysaccharide composed of the linear chains of glucan linked together by β-1,4-glycosidic bonds with glucose as the repeating units at different degrees of polymerization. The ability of these chains to form inter- and intramolecular hydrogen bonding provides a unique property of high chemical stability and mechanical strength and the formation of a robust crystal structure. Cellulose, a carbon-rich abundant renewable resource, has attracted considerable attention as a potential raw material for producing sustainable chemicals and fuels. A notable process is the hydrolysis of β-1,4-glycosidic bonds to obtain glucose from cellulose. Glucose can be used to synthesize numerous industrially essential chemicals, such as fructose, 1,6-anhydro-

https://doi.org/10.1021/acscatal.1c03326
ACS Catal. 2021, 11, 13603−13648

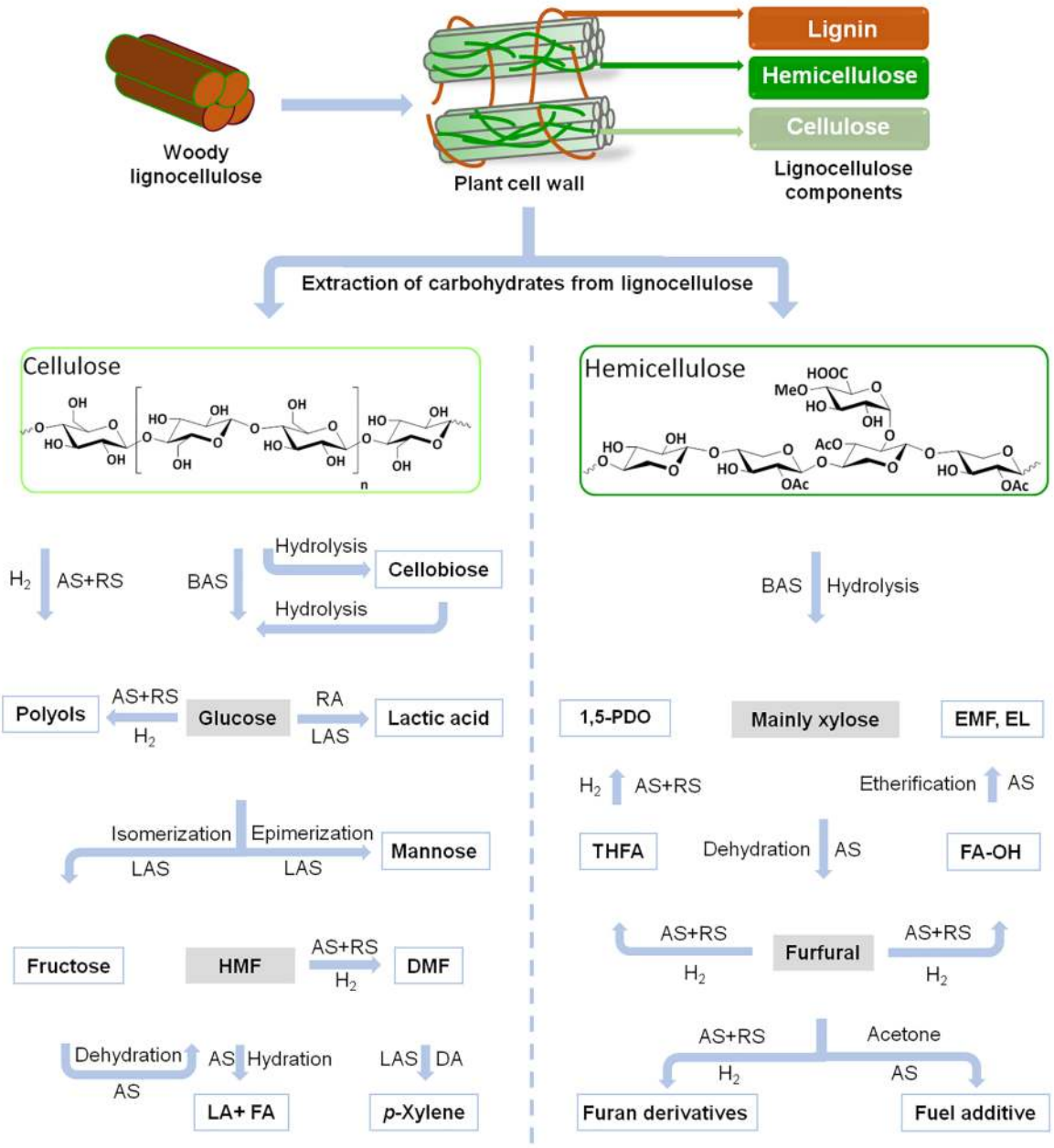

Figure 17. Various acid site-catalyzed steps in cellulose and hemicellulose upgrading. BAS: Brønsted acid sites; LAS: Lewis acid sites; AS: acid sites; RS: redox sites; RA: retro-aldol; HMF: 5-hydroxymethylfurfural; DMF: dimethylformamide; DA: Diels–Alder reaction; LA: levulinic acid; FA: formic acid; THFA: tetrahydrofurfuryl alcohol; 1,5-PDO: 1,5-pentanediol; FA–OH: furfuryl alcohol; EMF: 5-ethoxymethylfurfural; EL: ethyl levulinate.

glucose, 5-hydroxymethylfurfural (HMF), and organic acids over bifunctional redox catalysts. Figure 17 shows various acid site-catalyzed steps (e.g., hydrolysis, dehydration, hydration, isomerization, aldol condensation, etherification, hydroprocessing, etc.) in cellulose and hemicellulose upgrading. Therefore, various structurally different Mo- and W-based solid acid catalysts have been developed for cellulose valorization.

3.4.1. Hydrolysis. Cellulose can be catalytically depolymerized to the monomeric glucose by either enzymes or catalysts. Higher yields of glucose from cellulose in the presence of enzymes can be achieved at ambient temperature and pressure, but it requires longer reaction times. On the other hand, enzymes are quite expensive and possess recyclability problems. Liquid acids are often applied for faster cellulose hydrolysis compared to enzymatic reactions, but liquid catalyst requires harsh reaction conditions and causes reactor corrosion and poor catalyst reusability. Therefore, when one considers the sustainability point of view, heterogeneous solid catalysts are advantageous because of their good recyclability and high product selectivity. The poor interaction of solid catalyst with solid cellulose is a key concern to achieve higher results from the hydrolysis reaction. To overcome this, the addition of minute amounts of a liquid acid, i.e., HCl, is suggested to initiate the hydrolysis to solubilize the cellulose into the reaction mixture and then maintain the hydrolysis with the heterogeneous solid catalyst.[195] Among various heterogeneous catalysts, carbon materials have received much attention for cellulose hydrolysis because of their wide availability. The ease of carbon synthesis processes, especially from biomass, make it exceptionally attractive for industrial applications. In general, acidic groups

https://doi.org/10.1021/acscatal.1c03326
ACS Catal. 2021, 11, 13603–13648

such as sulfonic and carboxylic functionalities located at the surface of carbon materials are important for cellulose hydrolysis. Although sulfonic acid groups on carbon are highly active, the hydrothermal stability is quite disappointing. In addition, the preparation of activated carbon material includes oxidation of the carbon surface in the presence of strong acids, which tends to produce a large amount of hazardous waste in the form of gypsum. Thus, efforts to develop noncarbonaceous materials led to understanding the hydrolysis catalysis of WO_3 supported catalysts. Chambon et al.[196] investigated the catalytic performance of WO_3/ZrO_2 and WO_3/Al_2O_3 for the cellulose hydrolysis in water at 190 °C, and the activity was compared with classical strong Brønsted and Lewis acid catalysts, i.e., $Cs_2HPW_{12}O_{40}$, $Cs_{2.5}H_{0.5}PW_{12}O_{40}$, HY zeolite, and sulfated zirconia. The WO_3/ZrO_2 and WO_3/Al_2O_3 solid acids exhibited a promoting effect on the cellulose depolymerization to achieve around 45% conversion, while the formation of oligosaccharides and polymers was suppressed. After the cellulose hydrolysis, glucose is synthesized and further transformed to HMF and lactic acid. Using WO_3/ZrO_2 and WO_3/Al_2O_3, lactic acid yields of about 27% and 18.5% were obtained, respectively. This efficiency was attributed to water autoprotolysis to form soluble intermediates and the subsequent conversion to lactic acid over the Lewis acid sites. Moreover, good catalysts' stability and efficient recyclability are the additional benefits of the tungsten-based catalysts for cellulose depolymerization. A negligible amount of W (1.5 wt % of total W from WO_3/Al_2O_3 and 2.3 wt % of total W from WO_3/ZrO_2) was found in the liquid sample of the reaction, but the role of these leached species on the reaction rate can not be ruled out. In contrast, strong Brønsted solid acids $Cs_{2.5}H_{0.5}PW_{12}O_{40}$, $Cs_2HPW_{12}O_{40}$, and HY zeolite affect cellulose depolymerization under similar reaction conditions. Leaching of the active species is noticed in the case of sulfated zirconia. Moreover, a range of different products was obtained with the above strong Brønsted acids due to the further transformation of glucose and HMF to acid substrates (levulinic and formic acids).

Pt addition to WO_3/Al_2O_3 solid acid led to enhanced cellulose depolymerization at 190 °C under H_2 pressure conditions, providing about 40% total yields of acetol and propylene glycol through the intermediate formation of pyruvaldehyde.[197] The presence of Lewis acid sites in the WO_3/Al_2O_3 catalyst is responsible for the pyruvaldehyde formation, which is further transformed into lactic acid over WO_3/Al_2O_3. The presence of Pt on WO_3/Al_2O_3 accelerates the formation of acetol and propylene glycol. The leaching of Pt and W was negligible after the catalyst usage, indicating the high stability of the catalyst. They also studied the influence of the H_2/He atmosphere on the hydrothermal conversion of cellulose using WO_3/ZrO_2 solid acid in hot water conditions at 190 °C.[50] 2,5-Hexanedione is the main product from the cellulose over WO_3/ZrO_2 solid acid in the H_2 atmosphere, while lactic acid is obtained in the presence of He. The structure−activity properties revealed that Brønsted acid sites formed by the interaction of hydrogen with the WO_3/ZrO_2 solid acid promote the fast hydride transfer steps, resulting in high yields of 2,5-hexanedione. The Brønsted acid sites were considered for the initial cellulose depolymerization, while the interaction between soluble species to Lewis acid sites resulted in lactic acid in the absence of H_2. The activity of a solid acid based on TiO_2 anchored with MoO_3 was compared with the SO_4^{2-}/TiO_2 catalyst for the hydrolysis of cellulose at 190 °C.[198] The dispersion of MoO_3 on TiO_2 led to improved catalyst acidity, resulting in the increased conversion of cellulose in the range of 27−35%. The glucose yield was low due to the further transformation of glucose into other products induced by isomerization, epimerization dehydration, and hydration. Among others, lactic acid and 1,6-anhydroglucose were also observed over MoO_3/TiO_2 catalyst due to higher acidic strength, whereas these products were not detected in the presence of TiO_2 and H_2SO_4 catalysts.

3.4.2. Hydrogenolysis. Ethylene glycol (EG) is an essential precursor for producing polyester fibers and can be used for antifreeze purposes. Hydrolysis of ethylene oxide, obtained via selective oxidation of fossil-based ethylene, is the primary process for EG production. The selective conversion of cellulose to EG is possible under optimized hydroprocessing conditions, but the challenge is to develop efficient bifunctional catalysts with optimized acid-redox sites.[199] Doping transition metals (Nb and Ti) into bulk WO_3 led to improved hydrolysis of cellulose to glucose because of strong Brønsted acidity, but there is not much improvement in EG yield because the strong acid sites promote unwanted humins formation. In contrast, a slightly improved selectivity of EG (57%) was found when the mesoporous WO_3 was doped with Nb. Further improvement in EG selectivity was noticed when these materials were impregnated with a Ru/carbon catalyst, indicating the importance of acid-redox sites for the cellulose-to-EG process. A similar effect (improved EG selectivity) was noticed when Ru was added to a mesoporous WO_3/ZrO_2 solid acid.[200] The mesoporous WO_3/ZrO_2 solid acid exhibited remarkable hydrothermal stability at 220 °C and 65 bar H_2 pressure, which might be due to the strong WO_3−ZrO_2 interaction enabled by the mesoporous structure. This WO_3/ZrO_2 solid acid may find potential applications for the aqueous-phase reactions. Baek et al.[201] investigated the effect of non-noble metals addition (Ni, Cu, Fe, and CO) on the activity of W/SiO_2−Al_2O_3 catalysts for the hydrogenolysis of cellulose into different polyols. The correlation between the surface acidity of the catalyst and the polyol yields was demonstrated in this work. The Ni promoted W/SiO_2−Al_2O_3 catalyst provided higher polyols yields with good reusability when the catalyst contained Al/(Al + Si) of 0.6. In other catalysts, more metal leaching was found, a key reason for their low recyclability, but Ni loading should be optimized in Ni−W/SBA-15 catalyst for efficient hydrogenolysis of cellulose carried out at 50 bar H_2 pressure, 245 °C, and 2 h.[202] The catalyst with 10% Ni and 20% W loadings and prepared at pH = 1 gave higher yields of low carbon polyols (65% of EG, 6.5% of 1,2-propylene glycol, and 3% of glycerol), but EG yield decreases rapidly during two recycles, which is more likely due to the leaching of Ni species under hydrothermal conditions.

Xiao et al.[203] investigated the effect of hydrogen donors on the activity of M-W/SBA-15 (M = Ni, Cu, Zn, and Pd) catalysts for the selective hydrogenolysis of cellulose. It was important to note that only 20 bar of extra pure H_2 is required for the high yield (42.2%) of EG production at 230 °C in 5 h. The isopropanol was found to be an efficient hydrogen donor for the reaction, partially converted to acetone, and provided indigenous pressure in the reaction system. An XRD study showed the formation of metal alloys that played a favorable role in achieving improved yields of targeted products due to a synergistic metal−metal interaction. Hydrochar is obtained from cellulose hydrogenolysis at 215 °C under 65 bar H_2 when the reaction was carried out with only activated carbon (AC) due to the hydrothermal carbonization of cellulose.[204] The combination of W and Ni with AC, prepared by a two-step

https://doi.org/10.1021/acscatal.1c03326
ACS Catal. 2021, 11, 13603−13648

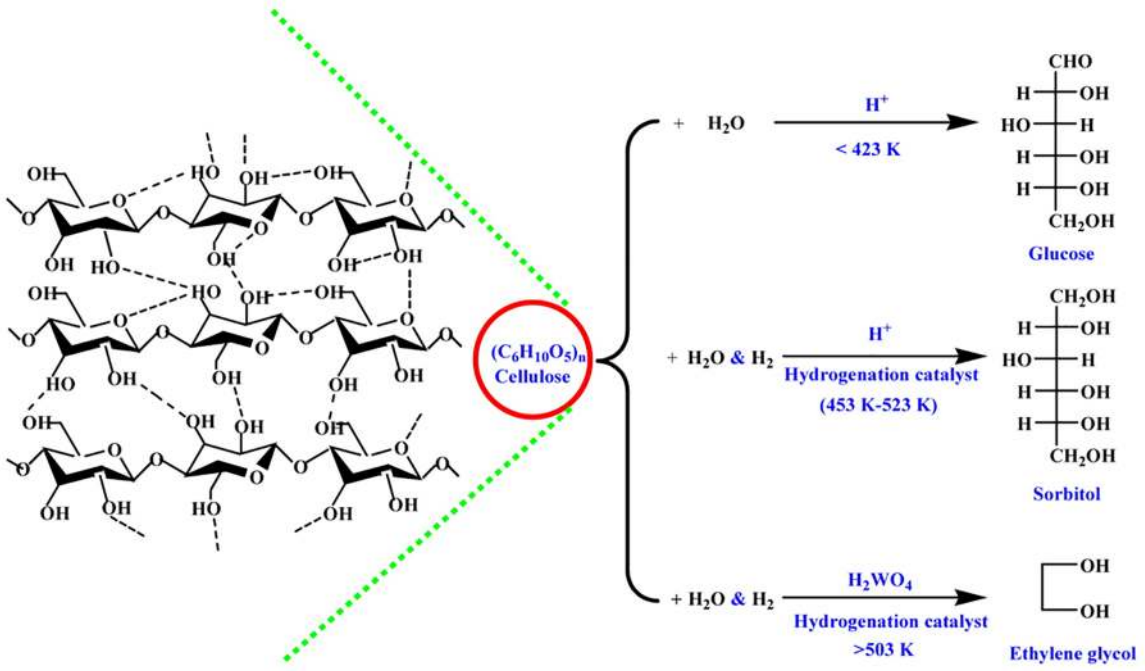

Figure 18. Conversion of cellulose to glucose, sorbitol, and ethylene glycol by varying the catalyst and reaction conditions. Reproduced from ref 206. Copyright 2013 American Chemical Society.

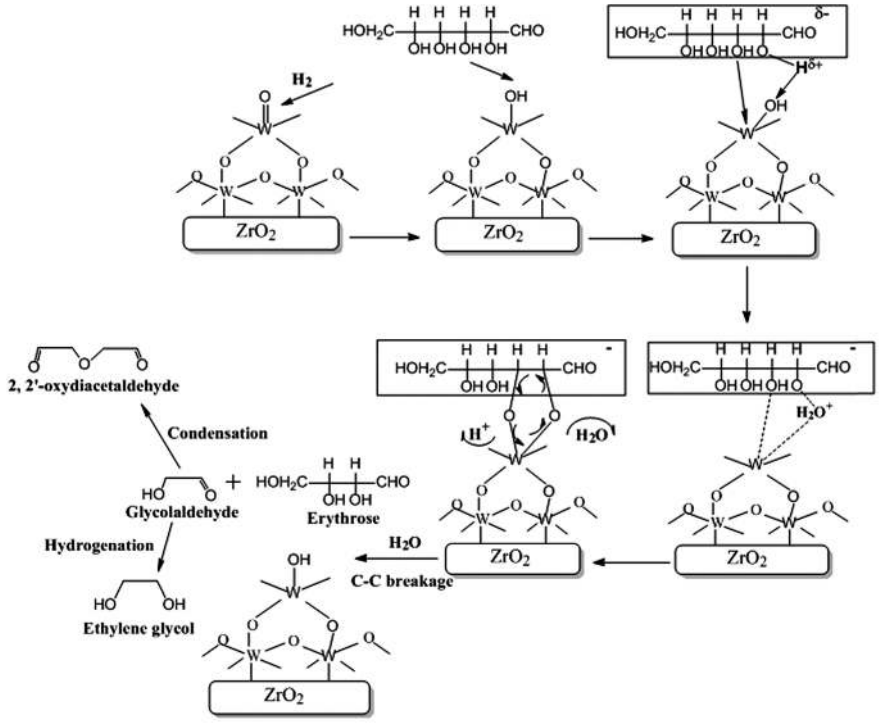

Figure 19. Proposed reaction mechanism for selectively breaking the glucose C−C bond. Reproduced with permission from ref 207. Copyright 2017 Royal Society of Chemistry.

incipient wetness method, demonstrated the highest catalytic performance with 88.4% cellulose conversion, 78.4% carbon efficiency, and 43.7% yield of EG. In contrast, meager yields of EG and decreased carbon efficiency were obtained over the coimpregnated catalyst and physically mixed Ni/AC + W/AC catalyst. Metal leaching and the formation of inactive $NiWO_4$ species were observed during the multiple uses of the Ni/W/AC catalyst, resulting in decreased polyol yield. The formation of polyols like EG, which act as a chelating component because of its ability to bind strongly with metal sites, was the primary reason for metal leaching and structural changes in the catalyst. Zhang's[205,206] group has made significant efforts in producing EG from cellulose using tungsten-based multifunctional catalysts. A higher yield (61%) of EG was achieved after adding

https://doi.org/10.1021/acscatal.1c03326
ACS Catal. 2021, 11, 13603−13648

a small amount of Ni (2 wt %) to the tungsten catalyst, indicating the synergistic effect of the bimetallic catalyst. When the reaction was conducted at above 503 K temperature, the formation of sorbitol was inhibited, giving only EG (Figure 18).[206] It indicates that the W−Ni-based catalyst played a key role not only in cellulose hydrolysis but also in C−C cleavage toward EG formation. The catalyst showed good reusability with negligible loss in EG yield over three recycles. No metal leaching was found as estimated by ICP elemental analysis. Catalyst oxidation by the reaction medium was suggested to be a factor for the observed decrease in EG yield after the third cycle.

Chai et al.[207] studied the hydrogenolysis of cellulose to EG over WO_3−ZrO_2 solid acids combined with Ru/C. The EG yield was found to be improved with the higher tungsten surface density. This is explained by the formation of isolated W^{5+}−OH species as the active sites for glucose to glycolaldehyde, followed by its hydrogenation to EG over Ru/C catalyst (Figure 19). Liu et al.[208] noticed the dual role of WO_3 as a solid acid for the hydrolysis of cellulose to glucose and as a promoter in the selective cleavage of the C−C bonds in the sugar intermediates during cellulose hydrogenolysis, giving considerable yields of EG and propylene glycol over a Ru/C catalyst. Cellulose conversion and polyol distribution were maintained for five cycles, and no leaching of WO_3 and modifications in the catalyst structure were found, indicating excellent stability of the catalysts. Like EG, propylene glycol is also an essential chemical for synthesizing antifreeze, fine chemicals, and polyesters.[209] Graphene nanocomposite supported Ru−$W_{18}O_{49}$ catalyst, prepared by solvothermolysis, showed nearly unit conversion of cellulose to 62.5% yield of EG at 245 °C after a 1 h reaction time.[210] Material characterization presented the ∼7 and ∼5 nm average size of Ru NPs and $W_{18}O_{49}$ nanowires, respectively, over graphene nanosheets. This catalyst can be reused three times, and the EG yields were obtained in the range of 48.7−62.5%. However, leaching of the tungsten species into the aqueous medium was noticed with catalyst recycling; thus, the EG yields were decreased continuously during three cycles. Cellulosic ethanol production with a 43.2% yield was also reported using a multifunctional Mo/Pt/WO_x catalyst.[211] The cascade type of the reaction occurred on the catalyst surface by converting cellulose to EG and then to ethanol. This catalyst contained isolated MoO_x sites directly bonded to metallic Pt particles via the MoO_x−Pt−WO_x interfacial structure on the support surface. Owing to the presence of abundant active sites, this energetic interface promoted the rate-determining step, i.e., hydrogenolysis of EG to ethanol. The liquid sample of the reaction contains about 40.8 ppm W, which was found to be active for converting cellulose to glycolaldehyde but not active for EG hydrogenolysis to ethanol. Hydrodeoxygenation (HDO) of cellulose to simple hydrocarbons was studied using a MoO_3 catalyst under low H_2 pressure conditions.[188] The yields of *n*-butane and *n*-pentane from the HDO of cellulose were ∼10−14 and ∼2−5 times greater than iso-butane and iso-pentane yields, respectively. High selectivity to alkanes was observed at higher MoO_3 loadings (≥20:1 catalyst/cellulose), whereas alkenes selectivity was increased at lower MoO_3 loadings (≤10:1 catalyst/cellulose).[212] Except for levoglucosan, a similar trend was found with the cellulose-derived compounds, namely, methylglyoxal, glycolaldehyde, furfural, and HMF.

3.4.3. Dehydration and Catalytic Fast Pyrolysis. 5-Hydroxymethylfurfural (HMF) is a promising platform molecule for synthesizing a variety of fuel-grade molecules, plastic monomers, and other industrial chemicals.[213−216] It is synthesized from cellulose-derived glucose by isomerization and dehydration steps. Li et al.[217] prepared MoO_3−ZrO_2 solid acid modified by stearic acid for the catalytic dehydration of cellulose to HMF along with other carbohydrates. About 11% yield of HMF was obtained at 160 °C in 200 min, when cellulose was used as the feedstock. The solid catalysts with strong acid sites showed good reusability for seven cycles without much loss in catalytic activity. Compared to water, which generally causes the leaching of the active sites, ionic liquid (1-butyl-3-methylimidazolium chloride) as a solvent effectively converts cellulose to glucose, fructose, and HMF over WO_x- and MoO_x-based polyoxometalates.[218] The reaction follows cellulose conversion to glucose, epimerization of glucose to mannose, and then dehydration to HMF with an overall product yield of 28.6%. The results were not influenced by decreasing the cellulose loading. However, water addition led to significantly decreased product yields, which obviously indicates the role of water in poisoning and/or leaching of the active sites. The catalytic fast pyrolysis of cellulose using Mo/KIT-5 catalysts with different Mo loadings was studied.[185] The 1 g Mo- and 2 g Mo-loaded catalysts showed better performance than the 0.25 g Mo-loaded catalyst for the transformation of cellulose into furans. Mo addition to Ni/SiO_2−Al_2O_3 catalyst inhibits Ni agglomeration during the hydrotreatment of pyrolytic sugars from pine conducted at 180 °C and 120 bar H_2 in a batch reactor.[219] Thus, the bio-oil produced by the bimetallic Ni−Mo catalyst contains a higher H/C ratio and a lower molecular weight than the Cu- and Pd-promoted Ni catalysts. Catalyst deactivation was found particularly for monometallic catalysts due to the metal agglomeration. In the case of bimetallic catalyst, Mo prevented Ni from sintering via a strong Mo−Ni interaction, and thus, the catalyst deactivation was very low.

3.4.4. Valorization of Cellulose-Derived Compounds. The depolymerization/hydrolysis of cellulose gives various platform molecules and high-value chemicals that can be upgraded to industrially useful fuels and chemicals.[220] The commonly obtained compounds from cellulose are cellobiose, glucose, fructose, HMF, levulinic acid, etc. In the following sections, valorization of these compounds using MoO_x- and WO_x-based solid acids was discussed.

3.4.4.1. Cellobiose. Cellobiose is the subunit of cellulose consisting of two glucose units, and it is obtained through the partial hydrolysis of cellulose. So, the hydrolysis of cellobiose gives glucose over WO_3/ZrO_2 solid acids synthesized with various WO_3 loadings (1−20 wt %).[221] An increased concentration of Brønsted acid sites was found in WO_3/ZrO_2 solid acids with the increase of WO_3 loading. Hence, better catalytic results of cellobiose hydrolysis to glucose (the main product) were obtained in the case of higher WO_3-loaded catalysts. A significant metal loss (3 wt % of W) was found from 15.2 wt % WO_3-loaded catalyst after a 32 h reaction time at 97 °C; hence, the reaction rate of cellobiose was decreased significantly. Wang et al.[222] noticed that ZrO_2 doping exhibits a significant effect in modifying the acid and catalytic properties of WO_x/SBA-15 solid acids for cellobiose hydrolysis. Doping the WO_3/SBA-15 catalyst with 5 wt % ZrO_2 led to a strong ZrO_x−WO_x interaction, stabilizing the polytungstate species (Brønsted acid sites) and improving the BET surface area of the catalyst. About 75% cellobiose conversion with 32% and 20.6% yields of glucose and mannose, respectively, was found over a 5 wt % ZrO_2-loaded WO_3/SBA-15 catalyst, outperforming a conventional impregnated WO_3/ZrO_2 solid acid. This is due to the improved accessibility of the uniformly dispersed active

https://doi.org/10.1021/acscatal.1c03326
ACS Catal. 2021, 11, 13603−13648

species in the mesoporous framework of the SBA-15 support for the bulky reactant molecules, like cellobiose. Here, the isomerization of glucose over WO_x species gives mannose. In addition, minor yields of HMF, formic acid, levulinic acid, erythrose, and glycoaldehyde were also achieved. The presence of an excessive ZrO_2 amount (>10%) induced the transformation of polytungstate sites to isolated monotungstate sites, which can migrate and block the pores, resulting in low BET surface area and a lower number of accessible strong acid sites. Both cellobiose conversion and glucose/mannose selectivity were decreased drastically during the second run, which was due to the significant leaching of the W species (35% of W). In the subsequent runs, the leaching was prevented, and about 52% W loss was found after the fourth run. This is due to the weak interactions of the WO_x species with the ZrO_2, which were leached during the second run. The strongly bounded WO_x species were leached slowly in the subsequent runs. The significance of mesoporosity of the active phase (Ta_xW_{10-x} and x = 0 to 10) was also realized for the hydrolysis of cellobiose, conducted at 100 °C using 5 mL of water.[223] W addition led to increased acidic strength and the reaction rate, reaching the optimum results for Ta_3W_7 oxide. As a result, this solid acid gave the highest turnover frequency rate (0.75 h^{-1}) for the cellobiose-to-glucose reaction compared to other solid acids, namely, niobic acid, zeolites, ion-exchange resins, and a liquid acid (H_2SO_4). High specific surface area, strong Brønsted acid sites, enhanced accessibility of acid sites to the reactant molecules, and faster diffusion rates, achieved due to the mesoporous structure of the catalyst, are the key reasons for the high catalytic performance of mesoporous Ta_3W_7 solid acid in cellobiose hydrolysis. Considerable yields of glucose, along with HMF and humins, were achieved from cellobiose hydrolysis catalyzed by W−TiO_2 solid acid.[224] A much faster reaction rate was found for xylan hydrolysis over this catalyst, giving good yields of xylose and furfural, with a lower amount of humins formation.

3.4.4.2. Glucose. The complete hydrolysis of cellulose gives glucose, which can be converted to fructose, platform chemicals (HMF and levulinic acid), fuel grade molecules (ethanol), and high-value chemicals (EG and 1,2-propanediol).[225,226] In glucose-to-high value chemical transformation, glucose valorization to HMF is a crucial step, which needs both Lewis (for glucose-to-fructose isomerization) and Brønsted acid sites (dehydration of fructose to HMF). Since glucose-to-HMF is a cascade reaction, the formation of HMF depends on the rate of the glucose isomerization to fructose (Lewis acid site promoted step), which is an equilibrium-limited reaction. The rate of glucose isomerization will be improved when fructose is continuously converted to HMF, which is highly dependent on the Brønsted acidic strength of the catalyst. Hence, the optimum ratio of Brønsted acid sites to Lewis acid sites is beneficial to achieve improved glucose conversion and HMF selectivity.

The metal composition in an ordered mesoporous $Nb_xW_{(8-x)}$ oxide effectively controlled the amount of Brønsted and Lewis acid sites.[225] As expected, the Lewis acid sites catalyzed the glucose-to-fructose isomerization, and the subsequent synthesis of HMF via fructose dehydration was catalyzed by Brønsted acid sites. The mesoporous network of the catalyst helps to better access the active sites with faster diffusion rates of reactants and products. The Nb_4W_4 oxide solid acid showed the best catalytic performance (90.2 kJ/mol apparent activation energy) and good stability in the aqueous medium even after four recycles, attributed to its remarkable mesoporosity and optimized Brønsted/Lewis acid sites, but for every recycling test, the Nb_4W_4 catalyst was thermally treated at 400 °C for 4 h to remove the adsorbed organic residues. Pure WO_3 mainly contains the Lewis acid sites. To introduce Brønsted acid sites in WO_3, two strategies were applied: a facile nontemplated sol−gel method and doping with transition metals.[227] Thus, the modified WO_3 catalyst showed promising activity in the glucose-to-HMF process in an H_2O/THF solvent system. No leaching of active W^{5+} sites was found after four cycles; thus, a good yield (about 55%) of HMF was obtained.

The MoO_3−ZrO_2 solid acid, modified by stearic acid, gave a 26.6% yield of HMF at 150 °C in a 3 h reaction time.[217] The presence of balanced Lewis/Brønsted acid sites (ZrMo-mixed oxides) and basic sites (ZrO_2 moieties) are the critical factors for the catalytic performance of the MoO_3−ZrO_2 solid acid in the glucose-to-HMF route. Han et al.[228] used reduced graphene oxide as a support because of its catalytically favorable properties, such as strong stability and high specific surface area, for preparing a WO_3 solid acid for HMF synthesis. An improved yield (36%) of HMF (about 58% glucose conversion) was obtained at 120 °C in 2 h, attributed to optimum amounts of acid sites in the catalyst.

A solid-state-catalyst mediated hydrothermal flow reactor system was designed for glucose conversion over a bare WO_3 solid acid, which showed a notable catalytic activity toward HMF synthesis under relatively mild conditions in aqueous solutions at 120 °C.[229] The WO_3−TiO_2 solid acid catalyst synthesized by a microwave-assisted hydrothermal method contains a higher concentration of surface acid sites than that of the solution combustion synthesis-based catalyst.[230] Since glucose-to-HMF conversion is dependent on the catalyst's acidic properties, improved yields of HMF were achieved over the WO_3−TiO_2 catalyst. The addition of Al_2O_3 to the WO_3−TiO_2 catalyst enabled the formation of basic sites along with innate acid sites. Note that the first step, i.e., glucose-to-fructose, can also be catalyzed by basic sites.[231] Hence, the best yield of HMF was achieved when the catalyst contained a molar ratio of acidic−basic sites of around 2.35. A higher percentage of Brønsted to Lewis acid sites is favorable for achieving higher sugar conversion and HMF selectivity, as noticed over mesoporous Ta−W oxides.[232] The reason is that the second step, i.e., dehydration of fructose to HMF, is strongly catalyzed by Brønsted acid sites. So, the consumption of fructose will induce the isomerization step. Another interesting result is that 2-butanol addition leads to increased sugar conversion and HMF selectivity. The reusability studies revealed that the activity of the Ta_7W_3 oxide catalyst was considerably decreased when the reaction was conducted in an aqueous medium. In contrast, using the 2-butanol/H_2O system, negligible loss in the glucose conversion and HMF selectivity was found over the repeated use of the catalyst. Here, 2-butanol plays a dual role, i.e., inhibiting the formation of humins and/or removing humins adsorbed on the catalyst's surface, thus regenerating the active sites for the subsequent catalytic cycles.

The hydrogenolysis of glucose to selectively produce polyols requires both acid and redox sites in solid catalysts.[233] For this, WO_x was added to a redox Pd/Al_2O_3 catalyst, and the effect of WO_x content was studied. With an increase in the W density, the surface area of the Pd metal is decreased, but the concentration of acid sites is increased. Isolated WO_4 and oligomeric WO_x species are responsible for the Lewis acidity of the catalyst, while polymeric WO_x species act as Brønsted acid sites. Fructose obtained via the Lewis acid site-catalyzed glucose isomerization

https://doi.org/10.1021/acscatal.1c03326
ACS Catal. 2021, 11, 13603−13648

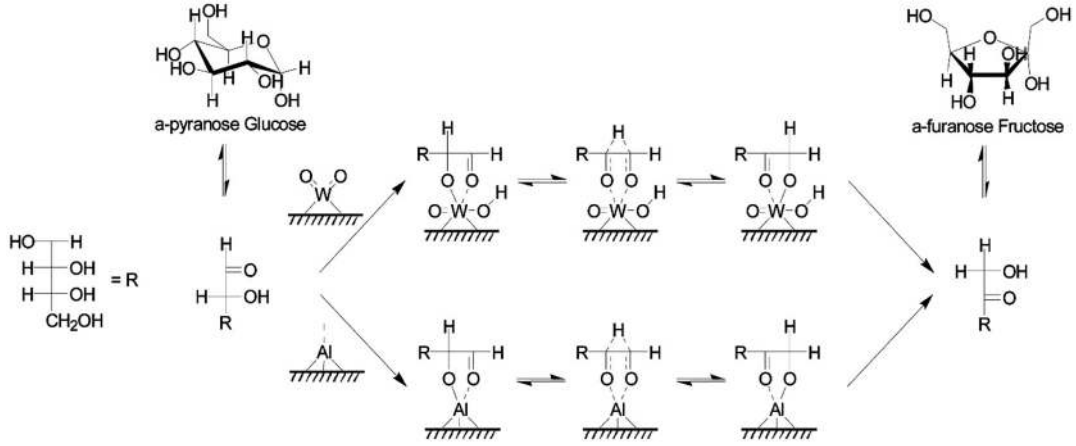

Figure 20. Mechanism of isomerization of glucose to fructose on isolated WO_4 or AlO_4 species of the Pd−WO_x/Al_2O_3 catalyst. Reproduced from ref 233. Copyright 2015 American Chemical Society.

(Figure 20) can undergo hydrogenolysis over the redox sites to give 1,2-PDO. Hence, both Lewis acid and Pd metal sites are needed to achieve a high selectivity of 1,2-PDO. In contrast, there is no role of Brønsted acid sites for the 1,2-PDO formation. Among the catalysts tested, the Pd−WO_x(5%)/Al_2O_3 catalyst showed about 60% selectivity to 1,2-PDO at 92% glucose conversion due to the balanced concentration of Lewis acid and redox sites. This catalyst showed good stability during the 200 h reaction time with no leaching of Pd, but a traceable amount of W species was found in the liquid sample of the reaction. The synergy between Ru metal sites and WO_x acid sites in supported Ru−W catalysts was found toward the selective formation of lower diols (EG, 1,2-PDO, and butanediol (BDO)) from the glucose hydrogenolysis in the liquid phase.[234] Among mesoporous SiO_2, carbon nanofibers, and activated carbon supports used, abundant acid and redox sites were found in the Ru−W/SiO_2 catalyst that played a crucial role in selectively cleaving the glucose C−C bonds toward lower diols formation. As a result, high selectivity to diols (87.3%) at the complete conversion of glucose was found at 205 °C and 40 bar H_2 over a 50 h reaction. This is due to the presence of highly dispersed active metal sites and a strong metal−support interaction that inhibited the leaching or sintering of the active sites; thus, the catalytic activity was maintained over 50 h time-on-stream study. Interestingly, a higher yield of EG products (55.9%) was achieved in the case of the Ru/WO_3 catalyst, although it has a lower BET surface area because of greater numbers of higher oxidation W^{5+} species. The surface modification of the Ru−W/SiO_2 bifunctional catalyst by polyethylene glycol led to improved yields (91.7%) of lower diols (EG, PG, and BDO) in the continuous-flow hydrogenolysis of glucose.[235] This is due to the high dispersion of smaller-sized WO_x clusters/particles with more surface-exposed acid sites and strong Ru−WO_x interface sites that efficiently catalyzed the C−C bond cleavage and hydrogenation steps to yield diols, respectively.

The solid acids, mainly supported MoO_3 catalysts, are found to be active for the epimerization of glucose to mannose in an aqueous medium.[236] A high selectivity (94.5%) to mannose at the near-equilibrium glucose conversion (29.2%) was obtained over a MoO_x/AC catalyst, which showed good stability and higher activity than a bare MoO_3 catalyst. This indicates the importance of the support and its interaction with MoO_3 for achieving improved results in biomass conversion. However, some amount of Mo species was leached with the repeated use of the catalyst. The MoO_x NPs immobilized on an activated carbon showed excellent activity for glucose epimerization to mannose.[237] The MoO_x NPs (3.05 nm) were synthesized by oxidizing metal Mo using H_2O_2. Owing to the strong MoO_x−glucose interaction, this catalyst outperformed several reported catalysts and can be used for 16 days under 24 V with stable catalytic activity, and a negligible amount of Mo (3.2% of total Mo) was leached into the reaction medium. Lactic acid (LA) and its derivatives are essential chemicals for pharmaceutical and chemical industries. LA is mainly used for the production of polymers.[238] Retro-aldol of glucose in methanol gives methyl lactate (MLA). For this reaction, various metal oxides are used as cocatalysts with Sn-Beta-P catalyst. Among them, an improved yield of MLA from 25% to 52% was achieved from glucose over the combination of Sn-Beta-P and WO_3 catalysts. The reason is that the WO_3 species adsorbed on the zeolite surface cover its silanol defects, thus promoting the retro-aldol reaction of fructose toward MLA formation. There was no obvious decrease in MLA yield after the second cycle, but it decreased rapidly in the third cycle. However, the activity of the catalyst was regained by calcination of the recovered catalyst (after the third cycle) at 550 °C for 1 h, which was due to the removal of adsorbed carbon species from the catalyst surface.

3.4.4.3. Fructose. The isomerization of glucose gives fructose (fruit sugar), and it is catalyzed by acids, bases, or enzymes. The dehydration of fructose provides HMF, which is an acid-catalyzed reaction, mainly with Brønsted acid sites. Compared with glucose, fructose is the preferred precursor for HMF production because the six-membered ring of glucose is more stable than the five-membered fructose.[239] To have more Brønsted acid sites in pure WO_3, a hydrated WO_3 material was synthesized by a hydrothermal method.[240] The density of Brønsted acid sites in WO_3·nH_2O was optimized by adjusting the lattice water content. The optimized catalyst afforded 73% yield of HMF with good reusability activity (up to 5 cycles) and 50% higher HMF selectivity compared to an anhydrous WO_3 catalyst. Although a significant increase of fructose conversion was noticed over a conventional WO_3/ZrO_2 solid acid, lower yields of HMF (<10%) were achieved.[239] Improved yields of HMF were obtained when the dehydration of fructose was conducted under microwave treatment conditions.[241] The WO_x/ZrO_2 solid acid showed 67% fructose conversion and

https://doi.org/10.1021/acscatal.1c03326
ACS Catal. 2021, 11, 13603−13648

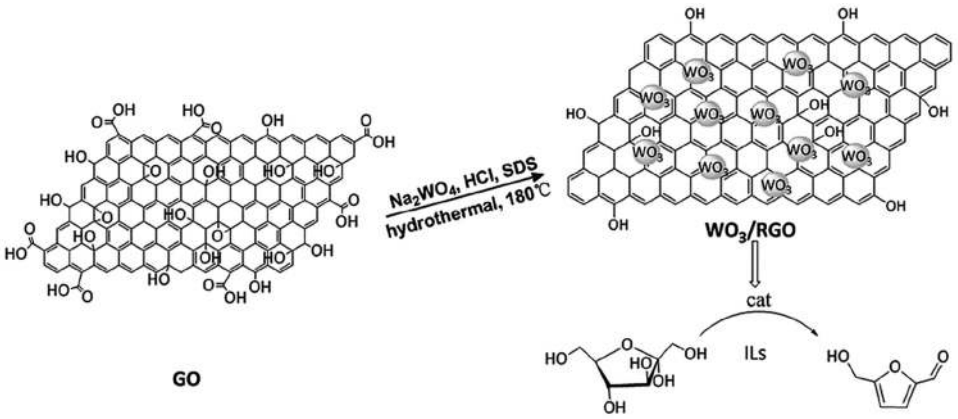

Figure 21. Synthesis and application of WO_3/RGO solid acid for the dehydration of fructose to 5-hydroxymethylfurfural. Reproduced with permission from ref 228. Copyright 2017 Royal Society of Chemistry.

53% HMF yield at 150 °C, while 47% and 31% HMF yields were obtained over MoO_x/ZrO_2 and ZrO_2, respectively. Characterization studies revealed high dispersion of WO_x species on ZrO_2, resulting in superior BET surface area and an optimum amount of acid sites, which are found to be the key reasons for the high catalytic efficiency of WO_x/ZrO_2 solid acid for HMF production. The optimization of MoO_3 (25 wt %)[242] and WO_3 (20 wt %)[243] content in SnO_2 supported catalysts is vital to achieve promising results in the fructose-to-HMF process. It will improve the interaction between WO_3 (MoO_3) and the support, providing adequate amounts of acid sites and inhibiting the leaching of acid sites in aqueous-phase HMF synthesis. The presence of higher surface acid site density and accessible active sites enabled the 20 wt % WO_3/SnO_2 solid acid to produce an excellent yield (93%) of HMF at 120 °C for 2 h.[243] Both WO_3/SnO_2 (five recycles) and MoO_3/SnO_2 (six recycles) solid acids exhibited good reusability with no apparent decrease in HMF yield.

Various carboxylic acids (lauric acid, palmitic acid, myristic acid, and stearic acid) were used to improve the acid-activity performance of the Mo/ZrO_2 solid acid for fructose dehydration in the [BMIM]Cl/H_2O reaction system.[217] The stearic acid-modified Mo/ZrO_2 solid acid exhibited both strong- and medium-strength acid sites that facilitated fructose conversion (91%) with increased HMF yield (54%) at 120 °C within 60 min. The catalyst showed excellent reusability for seven times. The concentration of acid sites was found to increase with increasing WO_3 content (1−20 wt %) in WO_3/ZrO_2 solid acids.[49] The conversion of fructose (strong acid sites) and HMF yield (medium-strength acid sites) depends on the acid sites' strength. However, basic sites are also essential for achieving improved HMF selectivity. About 67% fructose conversion was achieved over 16.8-WO_3/ZrO_2 catalyst, while the conversion of fructose was low (11%) over 5.1-WO_3/ZrO_2 catalyst at 130 °C for a 4 h reaction time. A modified Al−Mo mixed oxide is used as a solid acid for HMF synthesis from fructose.[244] About 50% HMF yield was achieved, and this catalyst is also active for converting glucose and sucrose into HMF with 24.9% and 27.6% yields, respectively. The HMF yield was gradually decreased from 50% (first cycle) to 37% (fourth cycle) due to the adsorption of oligomeric products covering the active sites on the catalyst surface. A remarkable HMF yield (84.2%) at full fructose conversion was obtained when the WO_3 species were dispersed on reduced graphene oxide (WO_3/RGO).[228] Figure 21 shows the structure of WO_3/RGO solid acid. A negligible decrease in HMF yield was found up to five runs, and then, a considerable decrease in HMF yield (74.7%) was found in the sixth run.

3.4.4.4. Other Sugar Derivatives. HMF and lactic acid (LA) are vital platform chemicals for synthesizing polymers and fuel-grade molecules. As discussed in the above sections, acid-catalyzed conversion of glucose and fructose gives HMF, while LA is produced industrially by carbohydrate fermentation. The catalysts' acid sites play a crucial role in the upgradation of HMF and LA. For instance, MoO_x addition to Ru/C catalyst led to more acid sites, which catalyzed the dehydration step during the HDO of HMF to obtain 2,5-dimethylfuran (79.4% yield).[228] Over the MoO_x/C catalyst, only 5-methyl furfural was obtained via dehydration of HMF. The conversion of LA to pyruvic acid via an oxidative dehydrogenation step involves water removal, which could be catalyzed by acid-redox sites.[245] For this, MoO_3/TiO_2 catalysts were developed by varying MoO_3 loadings. Highly dispersed MoO_x species on the TiO_2 surface selectively converted the LA into pyruvic acid (80%) under aerobic conditions. In contrast, considerable yields of propionic acid with pyruvic acid were obtained under anaerobic conditions.

Poly(ethylene terephthalate) (PET) is an essential polymer for synthesizing fibers, containers, and films.[246] Terephthalic acid, a monomer for PET, is synthesized from *p*-xylene (PX). Hence, PX synthesis from biomass is of significant interest. Among the four biobased feedstocks (ethanol, isobutanol, biomass pyrolysis or reformation, and 2,5-dimethylfuran), the conversion route of DMF to PX is of great research interest because of its economic feasibility and the possibility of achieving high product yields. PX synthesis from DMF and ethylene involves Diels−Alder cycloaddition (a Lewis acid-catalyzed step), followed by a dehydration step over Brønsted acid sites. Hence, the solid acid should contain both Brønsted and Lewis acid sites (in optimum amounts) to achieve higher yields of PX from DMF. Tan and co-workers[246] found that, by adjusting the calcination temperature, the ratio of Lewis to Brønsted acid sites can be optimized from 7.4 to 13.4 in a mesoporous WO_3/SBA-15 solid acid. Importantly, more surface active sites are available at lower metal loadings; thus, a higher reaction rate was achieved for DMF production. The reason is that the active sites were blocked when the catalyst contained higher WO_3 loadings. The 0.20-WO_3/SBA-15 catalyst calcined at 700 °C showed a high selectivity (88%) to PX with a 64.4% conversion of DMF. Owing to the mesoporous structure, which can improve the mass transport properties, the WO_3/SBA-15

https://doi.org/10.1021/acscatal.1c03326
ACS Catal. 2021, 11, 13603−13648

solid acid showed higher catalytic performance and carbon resistance ability than a microporous zeolite. The catalyst, after calcination at 550 °C for 6 h in air before each run, showed good reusability for five runs with only a 3% decrease in DMF conversion and no loss in PX selectivity. The isolated $[WO_4]^{2-}$ tetrahedral species acted as Lewis acid sites because of their coordinatively unsaturation.[247] On the basis of DFT calculations, they reported that the WO_x/SiO_2 catalyst mainly accelerates the dehydration step (a Brønsted acid-catalyzed step) in the DMF-to-PX process although WO_x is a Lewis acidic material. This is due to the transformation of Lewis acid sites into Brønsted acid sites by the water generated during the reaction over the WO_x/SiO_2 catalyst.[248]

Erythritol is a C4 platform chemical that can be commercially obtained via fermentation of sugar or starch.[249] Acid-catalyzed dehydration of erythritol gives 1,4-anhydroerythritol, which can be converted into valuable C4 chemicals, such as butanediols (BuDs) over bifunctional catalysts. Pt-WO_x/SiO_2 catalysts with optimum amounts of acid and redox sites showed good activity for the hydrogenolysis of 1,4-anhydroerythritol to 1,3-butanediol (1,3-BuD), which is an essential precursor for polyurethane and polyester resin synthesis. The cleavage of the C−O bond in 1,4-anhydroerythritol is catalyzed by synergistic Pt−WO_x interface sites, a key step toward the 1,3-BuD formation. A more effective Pt−WO_x interface in the as-synthesized catalyst was formed in the presence of water, which induced the conversion of higher valence W^{6+} species to lower valence W^{4+} species between Pt and SiO_2. Hence, this catalyst showed good reusability without the need for prereduction treatment in the presence of water, but a small amount of W (3.5 wt % of total W amount) was leached after the first cycle; then, the leaching was negligible in the subsequent cycles. The loading of W exhibited a remarkable influence on the efficiency of the Pt−WO_x/SiO_2 catalyst, giving about 57% yield of 1,3-BuD at optimized reaction conditions.[250] The synergy between Pt and WO_x is essential to achieve higher yields of 1,3-BuD. No leaching of Pt from the catalyst was found after the reaction, but a traceable amount of WO_x species was found in the liquid sample, which is minimized with the repeated use of the catalyst. Consequently, the catalyst showed good reusability or three runs without loss in the activity and selectivity. The synergy between redox and acid sites of the 2Pd/WO_3−ZrO_2 catalyst also played a crucial role in efficiently removing oxygen from sugar-derived EG via an aqueous-phase HDO process, which proceeds via a dehydration−hydrogenation pathway.[251] The strong acid sites in WO_3−ZrO_2, which induce the coke formation, disappeared after Pd impregnation, resulting in the improved catalytic stability in HDO of EG.

3.5. Valorization of Hemicellulose and Its Derived Compounds. Hemicellulose is a branched heteropolysaccharide, the second most abundant component of lignocellulose biomass.[252] It is composed of mainly C5 sugars (xylose and arabinose) as well as minor amounts of C6 sugars (mannose and glucose), depending on the source. Owing to its ease of availability, hemicellulose conversion is of significance for transforming agricultural waste biomass to bioethanol and other valuable chemicals, such as xylitol, furfural, furfuryl alcohol, and related derivatives. The structure of hemicellulose and acid-catalyzed valorization steps (hydrolysis and dehydration) are shown in Figure 17.

3.5.1. Hydrolysis. SiO_2 and ZrO_2 supported WO_x and MoO_x solid acids were developed for one-pot dehydration of hemicellulose to furfural at 170 °C for 8 h.[253] Two methods, such as sol−gel and wet-impregnation, are used to synthesize these catalysts. For the hemicellulose-to-furfural reaction, the water−toluene biphasic system is essential because the produced furfural can be easily extracted into toluene from water; hence, furfural yields can be improved by suppressing side reactions. The formation of C5 carbohydrates (xylose and arabinose) is also evident because hemicellulose is initially hydrolyzed to C5 carbohydrates and eventually converted into furfural. Small amounts of C6 carbohydrates (glucose, 7%; fructose, 6%) are also observed as the hemicellulose used in this study contained 15% glucose. The impregnated catalysts suffer from the leaching of the active sites during the reaction, which could be due to the weak interaction of WO_x and MoO_x with the supports. The 10 wt % WO_3/SiO_2 solid acid, synthesized by the sol−gel method, gave about 61% furfural yield with excellent reusability for 8 cycles. Compared with the WO_3/SiO_2 solid acid, quite a lower yield of furfural (about 50%) was achieved with MoO_3/ZrO_2 solid acid. A high dispersion of tungsten species in the SiO_2 framework led to the generation of more strong acid sites, which is the reason for the observed catalytic efficacy of 10 wt % WO_3/SiO_2 solid acid. In contrast, the WO_3/ZrO_2 and MoO_3/ZrO_2 solid acids were found to be inactive for this reaction because of the lack of strong acid sites and low concentration of total acid sites. A similar type of sol−gel synthesized WO_3/SiO_2 Lewis acid catalyst was used for furfural synthesis from isolated xylans.[254] Xylan is a group of hemicellulose that predominantly contains β-D-xylose units and is found in plant cell walls and some algae. About 71% furfural yield was obtained over 10 wt % WO_3/SiO_2 solid acid from isolated xylan in a water−toluene (1:2 v/v) solvent system. The WO_3/SiO_2 catalyst shows excellent recyclability for eight catalytic runs in the dehydration of xylan to furfural. Characterization studies reveal that a high dispersion of metal oxide and silicotungstic-type acidic species present on the catalyst's surface was found to be a crucial factor for the dehydration of xylans to furfural. Dedsuksophon et al.[192] investigated hydrolysis and dehydration reactions of xylan (1:1 xylan/acetone molar ratio) at 250 °C over WO_3−ZrO_2 solid acid. WO_3−ZrO_2 efficiently catalyzed the transformation of xylan to furfural. Improved furfural yields were obtained when the dimethyl sulfoxide was added to the xylan/acetone mixture, possibly due to the interference of the acetone−dimethyl sulfoxide mixture.

3.5.2. Dehydration. Xylose is the building block of hemicellulose, and its efficient valorization can lead to the development of efficient, sustainable protocols for directly converting hemicellulose to valuable chemicals.[252] The xylose dehydration to furfural is a crucial reaction in hemicellulose utilization as furfural is a crucial chemical for synthesizing furanic biofuels, such as 2-methyl furan, 2-methyl tetrahydrofuran, etc. Antunes et al.[255] investigated dehydration of xylose to furfural using Zr−(W, Al) mixed oxide solid acids at 170 °C. The effect of the preparation method of ZrO_2 is studied in modifying structural, acid, and catalytic properties of Zr−(W, Al) solid acids. The template-free co-condensation synthesized catalysts have a low concentration of accessible acid sites and small BET surface area, leading to about 35% furfural yield at 99% xylose conversion. The template-assisted synthesized WO_3/ZrO_2 solid acid contains a high specific surface area and large amounts of accessible acid sites because of the mesoporous structure. As a result, increased furfural yields (42%) at comparable xylose conversions were achieved. Further improvement in furfural yield (51%) at high xylose conversions (98%) was achieved by doping Al into the mesoporous WO_3/ZrO_2 solid acid. No

https://doi.org/10.1021/acscatal.1c03326
ACS Catal. 2021, 11, 13603−13648

considerable leaching of the active metal species was found with repeated use of the catalysts; thus, the catalyst represents good reusability. However, a significant drop from 41% to 13% after the second run was found over the nonregenerated WO_3/ZrO_2 solid acid due to the passivation of the catalyst surface by the adsorbed organic residues. Weingarten et al.[256] studied the catalytic performance of WO_x/ZrO_2 solid acid along with γ-Al_2O_3, $SiO_2-Al_2O_3$, Zr−P, and HY zeolite for xylose dehydration in aqueous phase. The acidity of the catalyst is the key to the observed catalytic activity. However, a higher number of Lewis acid sites in the catalysts is essential to achieve promising results in xylose dehydration. On a per active site basis, the WO_x/ZrO_2 solid acid showed higher catalytic activity than $SiO_2-Al_2O_3$, Zr−P, HY zeolite, and HCl but lower activity than γ-Al_2O_3. However, low furfural selectivity was found for the WO_x/ZrO_2 solid acid. Thus, the most active catalysts exhibit the lowest furfural selectivity. Doiseau et al.[257] found a significant effect of reaction medium (water and acetic acid) on the catalytic performance of WO_3/ZrO_2 solid acid prepared by an anionic exchange method in xylose dehydration. In pure water, WO_3/ZrO_2 solid acid shows 30% xylose conversion at 150 °C and 6 h, but poor furfural selectivity is observed due to the formation of levulinic acid and byproducts so-called humins. On the contrary, high selectivity to furfural (41%) was found over WO_3/ZrO_2 solid acid when the reaction was performed in an acetic acid medium. The leaching of W species from the WO_3/ZrO_2 catalyst into the reaction medium is negligible, as investigated by the elemental analysis of the recovered reaction liquid.

3.5.3. Upgrading Furans. Xylose and arabinose are the major components of the hemicellulose, and their dehydration in the presence of acid catalysts gives furfural (Figure 17).[258] Upgrading furfural under hydrogen and oxygen atmospheres can lead to furfuryl alcohol and 2-furancarboxylic acid, respectively, which can be further upgraded to several industrially important chemicals using MoO_x and WO_x solid acids.[259] Moreover, furfural can be used to produce gasoline, diesel, and jet fuel grade molecules.[253] Hydrogenation of furfural gives tetrahydrofurfuryl alcohol, a key precursor for 1,5-pentanediol (1,5-PD) synthesis.[256] 1,5-PD can be used as a monomer to produce polyesters and polyurethanes. Besides, molecules (e.g., furfuryl alcohol, 2-metoxymethylfuran, 2-methylfuran, etc.) obtained from furfural can be upgraded to valuable chemicals. Various acid site-dependent catalytic processes for the utilization of furfural and its derivatives were reviewed in the following sections.

3.5.3.1. Hydroprocessing of Furans. Processing of furfural under the hydrogen atmosphere can give 2-methylfuran (2-MF), 2-methyltetrahydrofuran (2-MTHF), furfuryl alcohol (FA), tetrahydrofurfuryl alcohol (THFA), and tetrahydrofuran-2-carboxylic acid (THFCA). The selectivity of these products is controlled by the acid-redox properties of the catalysts as well as by the processing conditions. These products have applications as biosolvent, fuel additive, etc.

Hydrogenation using monometallic Pt-based catalysts is well-known in heterogeneous catalysis, but its high price limits its uses and imposes the search for alternative catalytic systems, especially bimetallic catalysts. Stucchi et al.[260] developed an efficient Pt−Mo catalyst supported on activated carbon (AC), which showed higher activity for furfural hydrogenation compared with the monometallic Mo and Pt catalysts. HR-TEM of the Pt−Mo/AC catalyst showed the presence of Mo-containing agglomerates with an Mo_4O_{11} orthorhombic phase as well as uniformly dispersed Pt NPs (about 2 nm) in the carbon matrix. The Pt−Mo/AC hybrid catalyst showed selectivity of 20% furfuryl alcohol and 80% ethyl furfuryl ether at 92% furfural conversion. The activity of the Pt−Mo/AC catalyst was decreased up to three runs and then remained constant in the fourth and fifth runs. Recently, it has been observed that cyclopentanol could also be produced by the hydrogenation rearrangement of furfural over Ru−Mo supported on carbon nanotubes in the aqueous phase.[261] The significance of catalyst reduction has been illustrated in the unusual activity with high furfural conversion and selectivity toward rearrangement products (74% selectivity to cyclopentanol and 9% selectivity to cyclopentanone). Without the regeneration step, the RuMo catalyst exhibited good reusability, indicating the catalyst stability under hydrothermal conditions.

1,5-Pentanediol (1,5-PD) is obtained via THFA hydrogenolysis using supported Pt−WO_x catalysts.[262] The WO_x presented as a thin, submonolayer film on the Pt surface, which provided active sites for efficient 1,5-PD production. The atomic layer deposition method was found to be effective to form such thin layers of WO_x onto the Pt nanocrystals. The loading amount of WO_3 (0.5−20 wt %) notably affected the 1,5-PD yields over the $Pt/WO_3/ZrO_2$ catalysts.[263] The 5 wt % WO_3-loaded catalyst exhibited the highest 1,5-PD yield (43% for 15 h reaction) because this catalyst contains the WO_x monolayer on the surface of ZrO_2 with abundant Brønsted acid sites (W−(OH)−Zr), which play a vital role in the selective conversion of THFA to 1,5-PD. Improved selectivity of 1,5-PD (73%) at 83% conversion of THFA was obtained over a $Pt/WO_3@SiO_2$ catalyst, which is composed of the embedded WO_3 in a mesoporous SiO_2.[264] This interesting catalyst system contains the proper amounts of Brønsted acid sites (H_xWO_3), which played an essential role in 1,5-PD synthesis via selective ring-opening of THFA cyclic ether. The mechanism of THFA hydrogenolysis to 1,5-PD over the $Pt/WO_3/SiO_2$ catalyst is shown in Figure 22. The presence of Brønsted acid sites at the boundary site of W−(OH)−Zr promoted the ring-opening of THFA to form 1,5-PD.[263] Compared with W and Re, Mo addition has a significant promoting effect on the activity of the Rh/SiO_2 catalyst in THFA hydrogenolysis to 1,5-PD synthesis.[265] Characterization studies revealed the partial reduction of Mo species, which are strongly bonded to the Rh particles, allowing facile electron transfer and synergistic MoO_x−Rh interaction, and thus, improved yields of 1,5-PD were obtained.

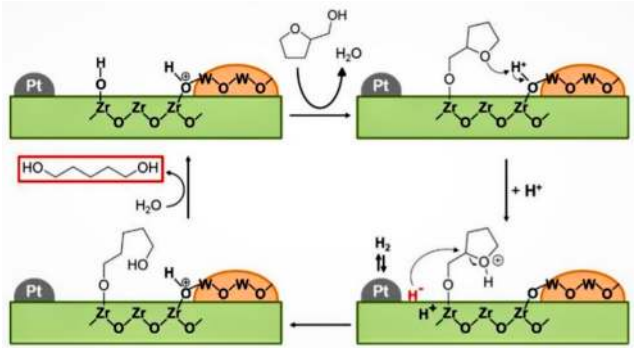

Figure 22. Proposed reaction mechanism of THFA hydrogenolysis to 1,5-pentanediol over the $Pt/WO_3/ZrO_2$ catalyst. Reproduced with permission from ref 263. Copyright 2018 Elsevier.

https://doi.org/10.1021/acscatal.1c03326
ACS Catal. 2021, 11, 13603−13648

The MoO_x−Rh/SiO_2 catalyst also exhibited good reusability, without leaching of the active sites.

Removal of oxygen from the biomass-derived compounds, including furans is essential to produce high-quality fuel-grade molecules. Application of reductive conditions as well as bifunctional catalysts with optimum amounts of acid and redox properties is needed to remove the oxygen effectively. Prasomsri et al.[266] studied MoO_3 catalyzed HDO of biomass-derived oxygenates, including 2-methylfuran, derived from the partial deoxygenation of furfural under low H_2 pressure conditions. MoO_3 shows 53% 2-methylfuran conversion and 97% selectivity toward unsaturated hydrocarbons, along with 43.5% of pentene as a major product. Theoretical calculations indicated the significance of oxygen vacancies in the HDO process. The partial pressure of H_2 played a crucial role in minimizing the catalyst deactivation. A simple calcination step helped to recover the original activity, and the catalytic activity was maintained under hydrothermal conditions. A thorough study of the MoO_x catalyst by adding various metals (Pt, Rh, Ru, Au, Pd, and Ir) and supports (CeO_2, TiO_2, ZrO_2, carbon, SiO_2, and Al_2O_3) was carried out for the HDO of 2-furancarboxylic acid (obtained via furfural oxidation) to valeric acid in a water solvent.[267] The highest valeric acid yield (51%) is obtained over Pt-added MoO_x/TiO_2 catalyst at 150 °C and 15 bar H_2 conditions. The acidic properties of the MoO_x/TiO_2 catalyst with the active metal function may be the reason for the production of valeric acid from 2-furancarboxylic acid, as this reaction involves a couple of dehydration steps under H_2 conditions. The conversion of 2-furancarboxylic acid was decreased drastically from 97% to 64% in the second run. The catalyst deactivation was due to the poisoning of the active sites by the adsorbed carbon residues, since there is no leaching of the active sites and metal aggregation was found.

3.5.3.2. Etherification. Furfural etherification under a hydrogen atmosphere gives 2-methoxymethylfuran, a valuable fuel and chemical. For this, Pizzi et al.[268] screened a wide range of heterogeneous catalysts, including CoO/MoO_3 catalyst supported on Al_2O_3 and Ni/MoO_3 catalyst supported on SiO_2−Al_2O_3. It was found that the acid sites are crucial to achieve a high selectivity of 2-metoxymethylfuran. The catalytic experiments were carried out using a 10 wt % of furfural in methanol solution at 50 bar H_2. Compared with noble-metal-based catalysts, moderate furfural conversion rates were obtained for $CoO/MoO_3/Al_2O_3$ and $Ni/MoO_3/SiO_2$−Al_2O_3 catalysts. Neves et al.[139] studied the catalytic performance of mesostructured Zr−W−Al mixed oxide solid acids for the etherification of furfuryl alcohol with ethanol. The performances of the mesostructured Zr-based mixed oxides were compared with those of conventional WO_3−ZrO_2, Al_2O_3−ZrO_2, and WO_3−Al_2O_3−ZrO_2 solid acids synthesized by the coprecipitation method. The templating route used for the ZrO_2 allowed the stabilization of high purity tetragonal ZrO_2, uniform morphology of the particles, enhanced BET surface area, narrow pore size distribution, and abundant acid sites, compared to the conventional precipitation route. Owing to the higher amount of effective acid sites, the mesostructured Zr−W solid acids exhibited complete furfuryl alcohol conversion, giving about 86% yield of ethyl levulinate and 2-(ethoxymethyl)-furan, which are valuable bioadditives for fuels. The regenerated catalyst by thermal treatment to remove carbon residues showed good reusability without much loss in the catalytic activity.

3.5.3.3. Condensation Reactions. Furfural alcohol-based oligomers are important template chemicals for synthesizing various carbon materials. Chan et al.[269] noticed a comparable activity of the WO_3 catalyst for the liquid-phase furfural alcohol oligomerization to the homogeneous H_2SO_4. Difurfuryl ether and 5-furfuryl-furfuryl alcohol dimers are the primary products. Spectroscopic studies identified the conjugated diene and diketone structures in the oligomers. The WO_3 catalyst showed good recyclability with no modifications in the catalyst structure; therefore, it was suggested as an alternative to the sulfuric acid-based homogeneous catalyst for FA oligomerization. The aldol-condensation reaction carried out at 80 °C with furfural/acetone molar ratios of one revealed that the WO_3−ZrO_2 catalyst (86−90% furfural conversion) shows higher activity than Ti−Zr mixed oxide (68−71% furfural conversion) but similar activity to MgO−ZrO_2.[192] The activity of WO_3−ZrO_2 could be due to the equal amount of acid−base sites. In the case of sequential aldol-condensation/hydrogenation of furfural, almost similar results were found over Pd-added WO_3−ZrO_2, MgO−ZrO_2, and TiO_2−ZrO_2 as the corresponding Pd-free catalysts. Higher yields of water-soluble organic substrates were produced in the case of the Pd/WO_3−ZrO_2 catalyst, attributed to the enhanced activity of the WO_3−ZrO_2 catalyst toward the aldol-condensation reaction.

3.6. Valorization of Lignin and Its Derived Compounds. Lignin, a highly branched aromatic polymer, is one of the key components of lignocellulosic biomass. In pulp and biorefinery industries, lignin is separated from cellulose and hemicellulose using various pretreatment technologies because its presence causes lignocellulose to be recalcitrant for the target application.[270] So, a large amount of lignin is produced annually (about 100 million tons). Some lignin (∼40%) is used in the pulp and paper industry for heat energy, and ∼2% lignin is used to produce chemicals (e.g., vanillin). The remaining fraction (∼56) is waste.[271] Compared to lignin, extensive research has been done toward converting cellulose and hemicellulose into fuels and chemicals. In contrast, lignin is highly underutilized because of its natural complex polymeric structure and high stability; thus, its selective depolymerization to aromatic platform molecules and further upgrading to drop-in chemicals remains a significant challenge. However, when efficient catalysts and appropriate reaction methodologies are used, a variety of valuable chemicals and fuel-grade molecules can be produced from lignin and its derived compounds.

3.6.1. Lignin Valorization. Various lignin processing methods, such as pyrolysis, hydrogenation, ethanolysis, hydrolysis, and hydrodeoxygenation have been developed. The acidic properties of the catalysts play a crucial role in these reactions. Hence, a variety of supported WO_x- and MoO_x-based catalysts was developed for lignin processing. For instance, ethanolysis of Kraft lignin over Al_2O_3 supported Mo catalysts, prepared by an impregnation method, gave various C6−C11 molecules (i.e., alcohols, esters, arenes, benzyl alcohols, and monophenols).[272] No char and tar were formed at the complete conversion of lignin. The product yield initially increases with an increase in the reduction temperature of the catalyst and then decreases in a range of 500−800 °C. Alcohols and esters are the primary products with more than 75 wt % of the total products. Furthermore, the catalyst showed excellent recyclability for up to 5 catalytic runs. A two-stage gas-phase catalytic process was developed to transform lignin into various carboxylic acids and aromatics using a series of catalysts, including WO_3/TiO_2 and vanadium promoted Mo/Al_2O_3, Mo/TiO_2, Mo/ZSM-5, and W/ZSM-5 catalysts.[271] The WO_3/TiO_2 catalyst gave preferentially butyric acid. The W^{6+} Lewis acid sites

https://doi.org/10.1021/acscatal.1c03326
ACS Catal. 2021, 11, 13603−13648

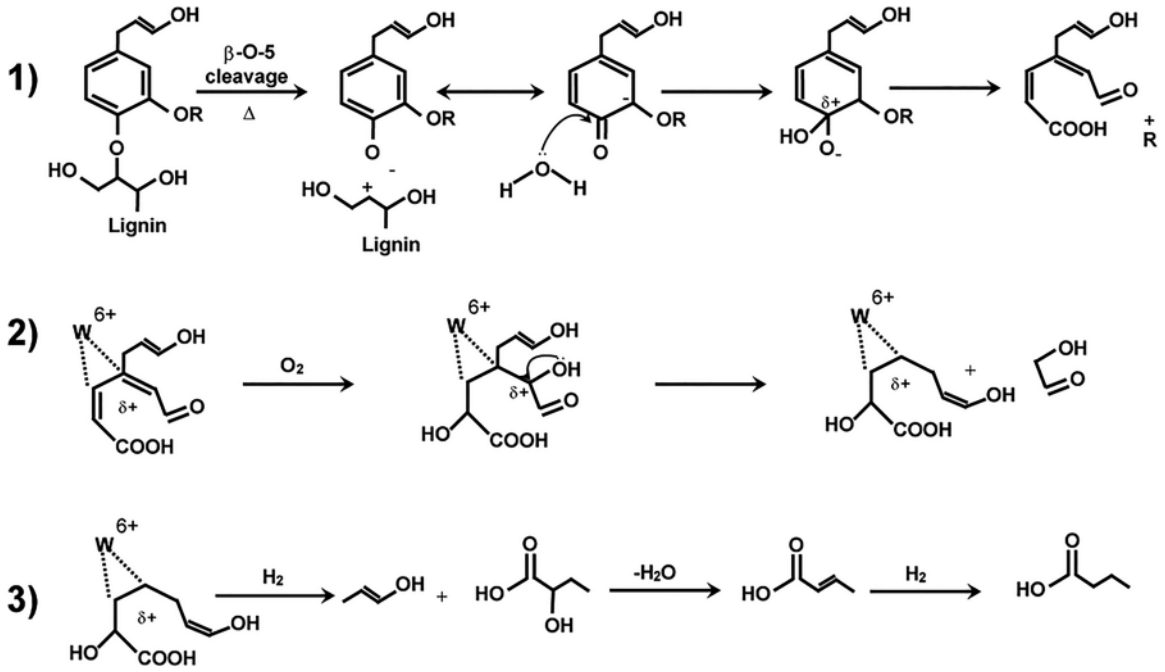

Figure 23. Mechanism for butyric acid formation from lignin over WO_3/TiO_2 catalyst in 3 steps. Reproduced with permission from ref 271. Copyright 2016 Royal Society of Chemistry.

in the WO_3/TiO_2 catalyst played a key role in activating the intermediates (step 2) and hydrogenation/dehydration (step 3) to produce butyric acid preferentially (Figure 23). In contrast, 20% selectivity to maleic acid with 23% and 25% lignin conversions, respectively, were obtained over V−Mo/Al_2O_3 and V−Mo/HZSM-5 catalysts. Lower yields (15.5%) of liquid products were obtained when TiO_2 replaced Al_2O_3 and HZSM-5, but an increased selectivity (45%) to maleic acid was achieved.

Deepa and Dhepe[273] studied solid acid-catalyzed lignin depolymerization to aromatic monomers. A variety of solid acids were tested, including a 10 wt % MoO_3/SiO_2 solid acid, which gave moderate yields (30%) of aromatic monomers. Without a catalyst, only a 10% aromatic monomer yield is obtained, indicating that lignin depolymerization is a catalytic reaction. The acid sites in MoO_3/SiO_2 solid acid effectively cleave the C−O, O−O, or C−C linkages in lignin to give aromatic monomers. The MoO_3/SiO_2 solid acid shows a better catalytic performance than HBEA zeolite, SiO_2−Al_2O_3, Nb_2O_5, and sulfated ZrO_2 and comparable activity to that of the mineral acids, i.e., H_2SO_4 and HCl. Continuous flow depolymerization of sodium lignosulfonate over NiO−MoO_3/Al_2O_3 catalyst gave phenolic compounds, mainly guaiacol and methoxyphenols.[274] The porosity of the catalysts and the reactants' accessibility to the catalyst surface, together with the space−time velocity (contact time), were the key factors influencing the yields and composition of the product mixture obtained. A higher Ni amount led to partial pore blockage. Consequently, the accessibility of the active sites present in the internal surface of the catalyst was inhibited for the lignin dimers and oligomers. Similar results were also observed in the case of higher Mo-loaded catalysts. The role of metal and acid sites in supported NiMo catalysts on lignin depolymerization in formic acid/ethanol media was studied.[275] Ni^0, Mo, and strong Lewis acid sites are responsible for the depolymerization of lignin, giving improved yields of bio-oil. Among those, Ni^0 showed an excellent depolymerization activity, whereas Mo was found to be more effective for the hydrodeoxygenation reactions.

Interestingly, pristine MoO_3 played an effective dual role in lignin valorization, i.e., catalyzing lignin depolymerization into liquid and gas products and then promoting in situ HDO of the resulting liquid product to phenol.[276] Both steps are dependent on the MoO_3 amount and the reaction temperature. The reduction of Mo^{6+} to Mo^{5+}/Mo^{4+} was promoted by lignin carbon rather than hydrogen from carrier gas during the lignin pyrolysis, resulting in the formation of more gas product yield, but Tang et al.[277] demonstrated that the reaction temperature induces the conversion of Mo^{6+} to Mo^{5+} in Mo/sepiolite catalyst, a key reason for efficient lignin depolymerization in supercritical ethanol under nitrogen pressure conditions. Improved yield (63.5%) of liquid products was obtained at 290 °C, 4 h, and 65 bar N_2.

A nanostructured MoO_x/CNT catalyst (CNT: carbon nanotube) was found to be highly selective toward monomeric phenols having an unsaturated substituent at the *p*-position in hydrogenolysis of lignin.[278] The reason is that the MoO_x/CNT catalyst promotes the C−O bond cleavage in β-O-4 units before reducing the double bonds under the H_2 atmosphere. The catalyst showed good reusability performance. An efficient process for producing alkylphenols via depolymerization of lignin-rich corncob residue (LRCR) was developed using a NiMo/Al_2O_3 catalyst under supercritical ethanol.[279] About a 255 mg/g LRCR yield of aromatic compounds with 58 wt % of alkylphenols was achieved with no generation of tar or char. The depolymerization of LRCR is dependent on the solvent, reaction temperature, time, and initial hydrogen pressure. The synergistic Ni−Mo effect was proved, and the $Mo_{1.24}Ni_{0.76}$ was a probable active phase for the depolymerization reaction. Improved yield of aromatic compounds (315.8 mg/g lignin) and the overall higher selectivity (67.5%) of alkylphenols were achieved over a WO_3/γ-Al_2O_3 solid acid, which showed higher catalytic activity compared to that of WO_3 and H_2WO_4 in lignin depolymeriza-

https://doi.org/10.1021/acscatal.1c03326
ACS Catal. 2021, 11, 13603−13648

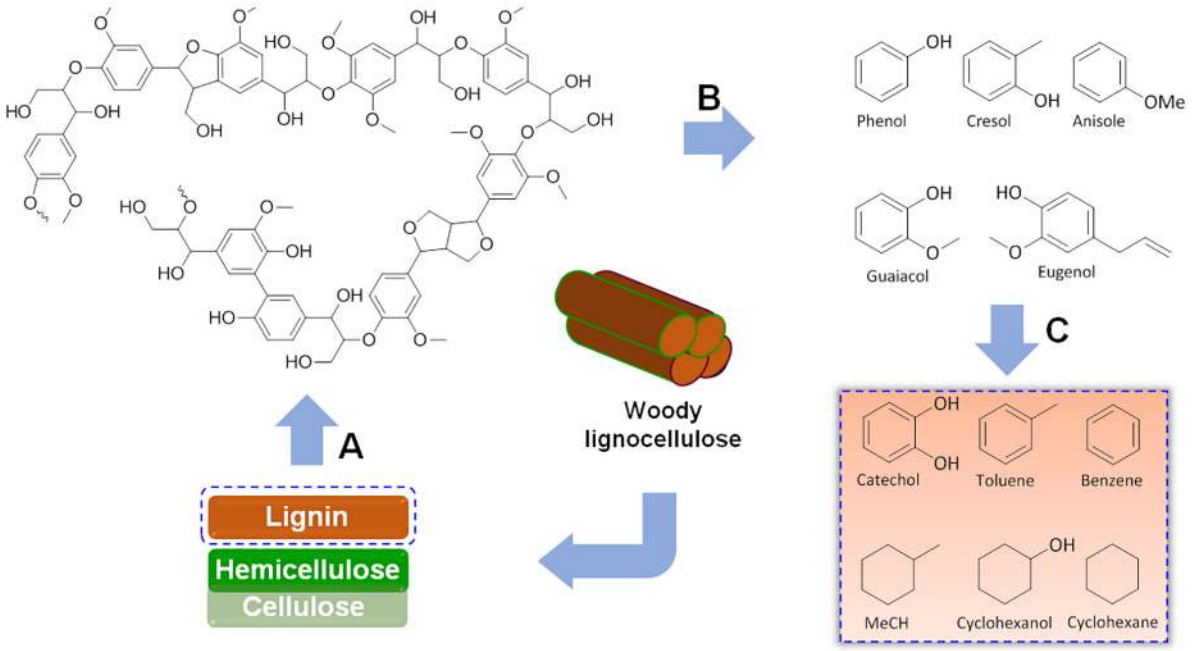

Figure 24. Processing of lignin into drop-in chemicals: (A) extraction of lignin from lignocellulose, (B) selective depolymerization/cleavage of lignin, and (C) selective hydrogenolysis/hydrodeoxygenation of lignin-derived molecules (catalyst's acid sites play a vital role in this process). MeCH: methylcyclohexane.

tion.[280] Efficient depolymerization of lignin was achieved with ethanol solvent, and the $WO_3/\gamma\text{-}Al_2O_3$ catalyst showed good reusability in three cycles.

To study the deoxygenation ability during CFP of lignin, a variety of nanostructured mixed oxides composed of W, Mo, Zr, Ti, or Al were developed. Owing to the optimum amounts of Brønsted and Lewis acid sites, the $WO_3-TiO_2-Al_2O_3$ catalyst showed the highest deoxygenation efficiency by selectively cleaving lignin C−O bonds to produce aromatics, and the subsequent dehydration gives valuable chemicals.[281] This catalyst is also active for synthesizing furans from xylan and cellulose by selectively breaking the C−O bonds by dehydration. As reported by Nolte et al.,[188] benzene and toluene were the main products, accounting for 50−60% of the total aromatics obtained via a bare MoO_3 catalyzed HDO of lignin pyrolysis vapors at low-pressure H_2 (1.8 bar). In the HDO process, the acid sites of a catalyst initiate oxygen removal from bio-oil via dehydration and the resulting oil can meet the transportation fuel standards. In the deoxygenation of lignin during the CFP process, the bare MoO_3 catalyst produces a higher amount of gas (mainly CO_2).[282] MoO_3 catalyst produces more vanillin (30% selectivity) than simple phenolic compounds. A similar yield of phenols, phenol alkoxy, and aromatic hydrocarbons at around 30% was achieved over the MoO_3/H-ZSM5 catalyst. Mullen and Boateng[270] investigated pyrolysis of lignin, obtained from four different sources, at 650 °C using CoO/MoO_3 and compared its performance with HZSM-5 zeolite. It was shown that lignin composition determines the selectivity to a particular aromatic hydrocarbon over both catalysts. Direct deoxygenation of methoxyphenol units is promoted over the CoO/MoO_3 catalyst to give aromatic hydrocarbons.

3.6.2. Valorization of Lignin-Derived Compounds. Lignin bio-oil obtained via pyrolysis can be efficiently upgraded to high-quality transportation fuels compared to cellulose and hemicellulose counterparts.[283] The reason is that lignin-derived aromatic structures exhibit high stability originating from the resonance stabilization; hence, their upgrade will be possible without the formation of unwanted byproducts (liquid and gas) and char. However, the presence of a higher fraction of oxygen-containing compounds (around 40%) in lignin-derived bio-oils is a major concern. This is because oxygen species can adversely affect the bio-oil's properties, inhibiting its practical use in automotive engines.[283,284] Hence, the removal of oxygen from lignin-derived oil via a hydrotreatment similar to catalytic hydrotreating processes employed in a petroleum refinery is required to improve the commercial aspects of bio-oil to be used with petrol. Over the past decade, the catalytic hydrodeoxygenation (HDO) process has been efficiently applied to remove oxygen from lignin bio-oil.[285,286] In addition, the HDO process helps to saturate low aromatic compounds to be compatible with petroleum. Understanding the HDO process of simple model compounds will provide valuable insights into the reaction pathways of lignin upgrading processes, which involve several complex reaction steps. In the following sections, the HDO of lignin-derived compounds, such as guaiacol, cresol, anisole, phenol, eugenol, benzofuran, and dibenzofuran, is discussed with other important upgrading processes (Figure 24).

3.6.2.1. Guaiacols. Lignin mainly contains guaiacyl and syringyl units. Obviously, the depolymerization of lignin can give higher yields of guaiacol, syringol, or their derivatives.[287] Guaiacol is an important precursor for synthesizing various valuable chemicals, such as anisole, phenol, benzene, cyclohexanol, cyclohexane, etc. In guaiacol, the strength of the Ph−OH bond is higher, followed by Ph−OMe and Ph−O−Me. Here, the acid sites of the catalyst play a vital role in the selective cleavage of the C−O bonds. Interestingly, the MoO_3 catalyst is active in the cleavage of the phenolic Ph−OMe bonds over weaker aliphatic Ph−O−Me bonds during HDO of various lignin-derived compounds, including guaiacol, giving higher yields of aromatic hydrocarbons (benzene, toluene, etc.). A simple calcination step helps to regenerate the activity of the

https://doi.org/10.1021/acscatal.1c03326
ACS Catal. 2021, 11, 13603−13648

spent catalyst. Both the support and the nature of the active site could play a crucial role in tuning the efficiency of Mo-based catalysts in guaiacol HDO reaction in a batch reactor at 350 °C and 4000 kPa of H_2.[288] Various supports, including SiO_2, Al_2O_3, NaY zeolite, MgO, activated carbon, and graphite, were used in this work. Mo catalyst on activated carbon showed the best performance toward guaiacol demethoxylation (99.9% conversion) with 72% and 19% selectivity to phenol and cresols, respectively. The high performance of MoO_x/activated carbon catalyst is due to the high surface area, larger porosity, and limited and localized acidity. Mechanistic studies revealed that the partial reduction of the superficial Mo^{6+} to Mo^{4+} clusters with coordination is crucial in initiating the HDO catalytic cycle. The acidic strength of the catalyst plays a pivotal role in controlling the reaction mechanism and product selectivity. The demethoxylation route to give phenol is promoted by weak acid sites, while catechol is formed via the demethylation route over strong acid sites. The porosity of the catalyst seems to play a determinant effect in guaiacol conversion and controlling product selectivity in HDO of guaiacol over bimetallic MoO_3−NiO catalysts supported on SBA-15, Ti-SBA-15 (Si/Ti = 10), mesoporous aluminosilicate (Si/Al = 20), and their respective γ-alumina composites.[289] Owing to strong acidity and high dispersion of $NiMoO_x$ sites, the MoO_3−NiO catalyst supported on mesoporous aluminosilicate showed higher guaiacol conversion with cyclohexane as a major product. In contrast, high selectivity to benzene was achieved over SBA-15 and Ti-SBA-15 supported catalysts. The variation in the product selectivity could be related to the porous structure of the composite-based catalyst, which has smaller-sized pores but a higher percentage of dispersed active sites compared with the parent catalyst. Another interesting observation is that Ni helps to achieve a suitable oxidation state of Mo for the hydrogenolysis step, indicating a strong Ni−Mo interaction in the MoO_3−NiO catalyst.

An in situ copyrolysis method was used to develop a novel magnetic Co-doped MoO_2@C catalyst, which showed excellent catalytic performance for the guaiacol HDO reaction.[290] Solvent plays a crucial role in controlling the selectivity of arenes or substituted phenols. The enhanced activation of H_2 and ethanol, induced by metal−metal and metal−support synergy, led to higher guaiacol conversion and product selectivity at 8 bar initial H_2 pressure. The leaching of the active sites as well as phase transformation of MoO_2 and the formation of oxidized Co species occurred during the recycling of the catalyst, resulting in the activity loss of the catalyst. The addition of Mo to NiCu/SiO_2 led to improved catalytic activity in the hydrotreatment of guaiacol.[291] This is due to the formation of active NiMo(Cu) solid solution and optimum oxidation states (4+ and 5+) of Mo on the catalyst surface. The selective demethoxylation of lignin-derived 4-propylguaiacol to 4-propylphenol was achieved by supported MoO_3 catalysts (SiO_2, Al_2O_3, TiO_2, CeO_2, and active carbon).[292] 4-Propylguaiacol can be obtained via reductive depolymerization of lignin. The catalyst support, which contains high cation electronegativity, such as Si, showed the best catalytic performance in converting 4-propyiguaicaol into 4-propylphenol, giving >80% selectivity at >60% conversion for >10 h. The aggregation of MoO_3 particles was not noticed in the spent MoO_3/SiO_2 catalyst, indicating its high stability due to a strong MoO_3−SiO_2 interaction. A bare MoO_3 is also effective in HDO of the acetone/guaiacol mixture, giving benzene as a major product. Reduction of MoO_3 to MoO_2 and coke formation were the key reasons for the catalyst deactivation in HDO of biomass pyrolysis vapors.[293]

3.6.2.2. Anisole. Anisole is another important lignin-derived compound with numerous applications in the chemical industry. In the vapor-phase HDO reaction of anisole using MoO_3/ZrO_2 catalysts, an improved HDO performance was achieved when the catalyst contains monolayer coverage of MoO_3 over the ZrO_2 surface (i.e., up to 15 wt % MoO_3 loading).[294] At higher MoO_3 loadings, the catalysts exceed the monolayer coverage, resulting in low reaction rates, which is attributed to a decreased amount of redox-active species (MoO_2). However, intermediate and higher-loaded MoO_3/ZrO_2 catalysts (10−36 wt %) exhibit a high selectivity toward fully deoxygenated aromatics (40% on a C-mol basis), while only 13% and 24% selectivities were found for 1 and 5 wt % MoO_3-loaded catalysts, respectively. This could be attributed to the presence of different oxidation states of Mo in high-loaded (Mo^{4+}/Mo^{3+}) and low/intermediate-loaded (Mo^{5+}/Mo^{6+}) catalysts. The kinetic models on gas-phase hydrotreatment of anisole over a 10 wt % MoO_3/ZrO_2 catalyst suggest that oxygen vacancy sites (Lewis acid character) present on the catalyst surface activates anisole for HDO reaction.[295] The presence of oxygen vacancies leads to enhanced oxophilicity of the catalyst surface, which is the key reason for the formation of deoxygenated products from the anisole HDO reaction. The treatment of MoO_3/ZrO_2 catalysts under H_2/CH_4 (80/20 vol %) atmosphere at 550 and 700 °C gave a high concentration of Mo^{5+} and Mo^{4+} species.[296] The presence of Mo^{5+} species was predicted to achieve improved catalyst stability and higher turnover frequency because of their higher capacity in deoxygenation, although a low initial anisole conversion was noticed.

The addition of Co to Mo catalysts supported on Al_2O_3, ZrO_2, and TiO_2 improved anisole conversion and product selectivity, which was due to the presence of more Mo^{5+} species.[297] This indicates the charge transfer from Mo to Co in bimetallic catalysts. The initial activity, catalyst stability, and product selectivity were improved over alumina-, titania-, and zirconia-supported catalysts, respectively. The TiO_2-based catalysts exhibited good stability over a 50 h reaction time, while higher HDO selectivity was found over ZrO_2-based catalysts. Reduction of active Mo^{5+} species to lower Mo states (Mo^{3+} and Mo^{4+}) and coke formation are the reasons for the catalyst deactivation. The beneficial role of Mo^{5+} species in improving the HDO rate of anisole was also noticed in the TiO_2-supported Re-MoO_x catalyst. The formation of Mo^{5+} species was controlled by Re^{4+} sites via a strong Re−Mo interaction.[298]

The significance of nanostructured support (γ-alumina) in improving the activity of the Mo catalyst was realized for gas-phase hydrotreatment of anisole, which was mainly attributed to the high surface area of the nanosized support compared with the bulk support.[299] Catalyst deactivation by coke deposition was minimized in the case of nanoscale γ-alumina supported catalyst. Anisole conversion was increased with reaction temperature but decreased selectivity to benzene was found due to the formation of unwanted byproducts and/or coke. The acid sites of the Ni−Mo/SiO_2 catalyst significantly promoted the methyl radicals transfer reaction, which prevented carbon loss during the gas-phase HDO of anisole and guaiacol.[300] As a result, high conversion (98.7%) and more than 96% selectivity to aromatic hydrocarbons were obtained. The regeneration of the catalyst was achieved by thermally treating it at 550 °C in air flow, leading to a stable performance for up to 14 recycles.

https://doi.org/10.1021/acscatal.1c03326
ACS Catal. 2021, 11, 13603−13648

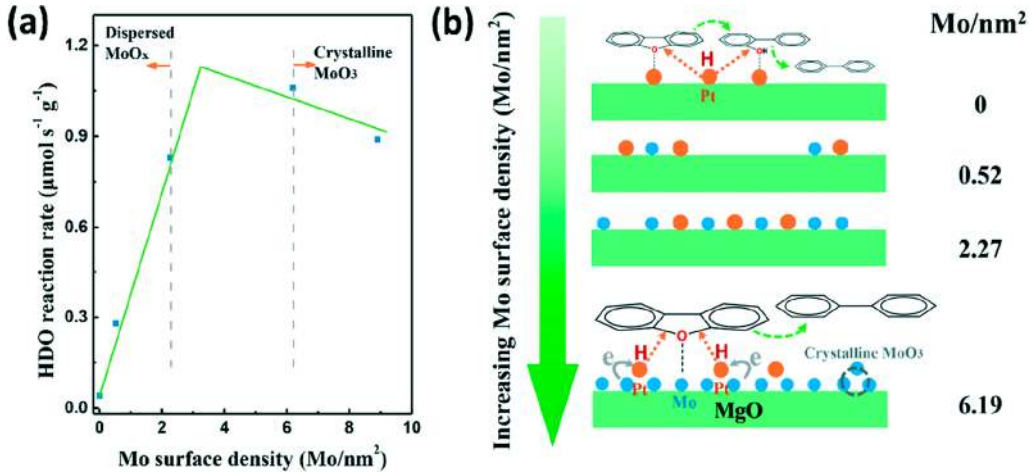

Figure 25. (a) Hydrodeoxygenation (HDO) reaction rate with Mo surface density (Mo per nm^2) for Pt/MoO_x/MgO catalysts at the contact time of 0.15 min and (b) the corresponding proposed reaction mechanism. Reproduced with permission from ref 311. Copyright 2020 Royal Society of Chemistry.

3.6.2.3. Cresols (Methylphenols). Cresols are important lignin-derived phenolic compounds obtained via catalytic pyrolysis processes. Pristine MoO_3 displayed the highest conversion of 4-methylphenol compared with MoO_2, MoS_2, and MoP catalysts.[301] This is due to the partial reduction of MoO_3 to a mixed oxide containing MoO_2, Mo_4O_{11}, and Mo phases, which provide more active sites, such as Brønsted acid sites and anionic vacancies for the HDO of 4-methylphenol to toluene as the major product via the C−O hydrogenolysis step. Better results in terms of the dispersion of MoO_x particles, Mo reducibility, and hence, the catalytic activity were achieved over an acidic support Al_2O_3-based MoO_x catalyst compared with SBA−15 and SiO_2 supported catalysts in HDO of *m*-cresol.[302] The direct C−O bond scission to toluene formation was the primary route over all catalysts. Oxygen vacancies, formed via the partial reduction of Mo species, were found to be the HDO active sites for the adsorption/activation of the reactant molecules. The use of high-pressure hydrogen (32 bar) preserved the active sites during the reaction, thus inhibiting the catalyst deactivation. Another work reported that the catalysts with a high concentration of Mo^{5+} and Mo^{3+} species exhibit higher activity in the vapor-phase HDO of *m*-cresol.[303] The support plays a crucial role in stabilizing these partially reduced Mo species. Hence, the MoO_3/ZrO_2 and MoO_3/TiO_2 catalysts showed the highest activity with 23.4 and 13.9 h^{-1} initial site time yields, respectively. Coke formation is induced by acid sites present in $MoO_3/\gamma Al_2O_3$ and MoO_3/SiO_2 catalysts. The presence of strong acid sites in γ-Al_2O_3 and SiO_2 induced the graphitic coke formation on the catalyst surface, enabling them undesirable to use as supports for HDO reactions. In contrast, the activity of spent MoO_3/ZrO_2 and MoO_3/TiO_2 catalysts can be recovered after calcination at 400 °C, because of the weak acidic character of the ZrO_2 and TiO_2 supports. The addition of Pt helps to stabilize the active WO_x species on a carbon support, giving a high selectivity (94%) to toluene from HDO of *m*-cresol.[304] Oxygen vacancies (or redox sites) present in WO_x act as anchoring sites for *m*-cresol. Among the various promoters (Pt, Cu, and Cu) added to a MoO_{3-x}/TiO_2 catalyst, higher HDO conversion of *p*-cresol was achieved over the Pt-based catalyst, followed by Cu- and Ni-promoted catalysts.[305] This is due to the high electronegativity of Pt and density of state near the Fermi level, which efficiently enabled the H_2 dissociation and improved the catalyst's activity at milder reaction conditions.

3.6.2.4. Phenol and Alkylated Phenols. Phenol and alkylated phenols are abundantly available in lignin-derived bio-oil because the pyrolysis at higher temperatures can promote demethoxylation from guaiacol and syringol units.[5] Compared to anisole and guaiacol, oxygen removal from phenol using Mo/ZrO_2 catalysts was found to be more efficient due to a simple reaction pathway involved during HDO of phenol. Benzene was the main product (95% selectivity) with phenol conversions up to 80%. As noticed by Boullosa-Eiras et al.,[306] the MoO_3/TiO_2 catalyst showed similar activity as the nitrides and phosphide catalysts for the HDO reaction of phenol. Benzene is the primary product with minor amounts of cyclohexene. A higher HDO efficacy of phenol was found over the 15 wt % Mo_2C/TiO_2 at 350 °C and 25 bar. The observed catalyst deactivation was attributed to the structural changes occurring during the reaction. The Ni−W/activated carbon catalysts, prepared using different tungsten precursors, namely, silicotungstic, phosphotungstic, and tungstic acids, showed promising activity in continuous-flow HDO of phenol at 15 bar H_2 pressure.[283] Ni addition enhanced the activity of the W/activated carbon catalysts for all tungsten precursors. Owing to the strong interaction of Ni and W phases on activated carbon, a low coke formation was found with respect to an alumina-supported catalyst. The addition of Ni and Co improved the deoxygenation rate of the Mo/Al_2O_3 catalyst for continuous-flow HDO of 2-ethylphenol at 340 °C and 70 bar pressure.[307] The deoxygenation route was controlled by the adsorption geometry of the reactant molecule. The acidity of the support induced disproportionation and isomerization reactions, giving minor yields of phenolic products. In the case of Mo/Al_2O_3 and NiMo/Al_2O_3 catalysts, coke formation occurred, leading to the catalyst deactivation.

3.6.2.5. Other Lignin-Derived Compounds. Eugenol, an important lignin monomer, is obtained by hydroprocessing and pyrolysis of lignin. In HDO of eugenol, the NiMo/Laponite catalyst showed complete eugenol conversion and high selectivity to 3- and 4-propyl phenols with considerable yields of complete deoxygenated products (benzene and 4-propyl cyclohexene).[308] This excellent performance was attributed to high catalyst stability, improved metal dispersions, and strong

https://doi.org/10.1021/acscatal.1c03326
ACS Catal. 2021, 11, 13603−13648

metal−support interaction in Laponite composite supported NiMo catalyst. The effect of the preparation method and the morphology of the catalyst were studied in this work. The activated catalyst before each run at 400 °C for 3 h using 10% H_2/He showed good reusability for up to five cycles, which was attributed to the high thermal stability of the catalyst. The HDO of isomeric dihydroxybenzenes (*o*-, *m*-, and *p*-) was analyzed using a MoO_3−NiO−Al_2O_3 catalyst by changing the reaction temperature and the effects of added H_2O and MeOH during the reaction.[309] At a 350 °C reaction temperature, the HDO activity of *o*- and *p*-dihydroxybenzenes is higher than phenol, while *m*-dihydroxybenzene is much less reactive. Interestingly, about 60% of phenol was obtained from HDO of *o*-dihydroxybenzene, but the saturation of the benzene ring has occurred in the case of *m*- and *p*-dihydroxybenzene. All three isomers were completely converted at 500 °C. The MoO_3−NiO−Al_2O_3 catalyst is also found to be active for the HDO of various methoxy- and methyl-phenols. The lignin-derived bio-oil also contains considerable amounts of furans (furan, benzofuran, and dibenzofuran).[310] The incorporation of Mo into the silica-supported Pt or Pd catalysts led to higher HDO efficiency of dibenzofuran, attributed to the improved acidity, reducibility, and metal dispersion controlled by the metal−Mo interaction. Mainly, in the case of the Mo−Pd/SiO_2 catalyst, higher yields of oxygen-free products were achieved, attributed to the ability of Mo species in the C−O bond cleavage. It was found that the oxophilic Mo species improve the Pt reducibility and acid site concentration in the Pt/MoO_x/MgO catalysts, resulting in the significantly improved conversion of dibenzofuran toward biphenyl formation.[311] The reason is that these oxophilic Mo species, optimized at near monolayer on the support, promote the adsorption/activation of the C−O bond in dibenzofuran (Figure 25). Lower catalytic activity was achieved when the catalyst contained higher MoO_x surface density (>6.19 Mo per nm^2) because of inactive MoO_3 crystallites formation.

3.6.3. Nonhydroprocessing of Lignin Model Compounds. The catalytic benzylation of anisole in the liquid phase was studied using WO_3 solid acids supported on an ordered mesoporous zirconium oxophosphate (M-ZrPO).[312] The high dispersion of WO_3 species led to a strong WO_3−support interaction that controlled the sintering and leaching of active species for the benzylation of anisole. Improved anisole conversion and product selectivity were achieved over 20 wt % WO_3-loaded catalyst due to highly dispersed WO_3 species and the strong Brønsted acidity, outperforming the conventional zeolite catalysts (H-ZSM5 and H-Beta). The WO_3/M-ZrPO solid acid is successfully reused up to five cycles without much loss in activity and selectivity. Cui et al.[285] developed an efficient route for converting guaiacol to alkylphenols over MoO_3 in supercritical ethanol under hydrogen-free conditions. The complete conversion of guaiacol (99%) with the maximum yields of alkylphenols up to 94% was obtained at 280 °C for 4 h. The formation of higher alkylphenols from guaiacol involves the demethylation of guaiacol to the catechol intermediate and then its ethylation without phenol formation. The methyl and ethyl species derived from ethanol attack the activated hydrogen on the α-carbon of ethylphenol, giving higher alkylphenols. The Mo^{5+} species were found to be active species as investigated by postcatalytic characterization studies. Hence, the consumption of Mo^{5+} and the carbon deposition are the reasons for the catalyst deactivation, but the activity can be recovered using a simple calcination step at 600 °C for 2 h under air atmosphere.

4. HYDROTHERMAL STABILITY AND LIMITATIONS OF WO_x- AND MoO_x-BASED SOLID ACIDS

The hydrothermal stability of metal oxides is a significant concern, especially during biomass conversion due to the presence of high water content in the original biomass raw material. Biomass contains a variety of oxygen-containing functional groups (alcohol, acid, aldehyde, etc.) that can decompose into the water during biomass processing. While coupled together with biological processes, water as a green solvent is most preferred to develop sustainable biomass upgrading processes. In many biomass valorization processes, water as a solvent has shown improved selectivity compared to organic solvent by either dissolving reactant molecules more efficiently or involving in the reaction mechanism.[313−316] Moreover, water is a key reagent and byproduct in various biomass conversion reactions, such as hydrolysis, esterification, dehydration, acetalization, etc. Harsh reaction conditions are usually required for the conversion of biomass molecules because of their bulky, complex structure and low solubility in most solvents, including water. Under those harsh conditions, water induces catalyst deactivation by acting as the catalyst's poison and/or leaching the active sites into the reaction medium.

The catalyst's poison, i.e., water forms a passive layer around the protons present on the catalyst surface, hinders the acid sites' accessibility to the reactant molecules. The catalyst's poison can be reversible by thermally treating the recovered catalyst after the reaction at higher temperatures (300−500 °C) in air flow, which is highlighted in numerous research works in this Review. In contrast, leaching of the active sites, which is irreversible, is considered a key concern in aqueous-phase biomass processing. Under hydrothermal conditions, water can exhibit both acid and base properties because of its high ionic product values. Metal oxides like MoO_x and WO_x are unstable under acidic and alkaline conditions; thus, leaching of these active species is induced under hydrothermal conditions, and the catalyst deactivation is inevitable. In some biomass upgrading reactions, for example, cellulose hydrogenolysis where polyols like EG are the desired products, the leaching of the MoO_x and WO_x species and structural changes are evident because of their ability as a chelating agent to bind strongly with metal sites.[204] This Review highlights several methods for enhancing hydrothermal stability of MoO_x and WO_x metal oxides, such as selection/optimization of the catalyst's synthesis method (e.g., sol−gel),[253] optimization of metal loading,[130] development of robust mixed oxides (WNbO),[147] precise encapsulation or incorporation of MoO_x and WO_x species into the host material (e.g., mesoporous silica),[115−117] the addition of heteroatoms, and development of strong mesoporous metal oxides.[139,170,223] Chen et al.[317] studied the hydrothermal stability of supported WO_x catalysts. They found severe textural and structural changes of the WO_x/$CeZrO_x$ catalyst under hydrothermal conditions, but the incorporation of silica into the catalyst structure not only prevented the sintering and aggregation of active particles but also remarkably improved hydrothermal stability.

Both MoO_x and WO_x are highly redox metal oxides, which can be stabilized in different oxidation states on the supporting materials. The oxidation state of these metal oxides can significantly affect the reaction rate and mechanism. Harsh reaction conditions (temperature and pressure) are often needed for biomass processing because of the complex structure of the biomass molecules and their low solubility in most

https://doi.org/10.1021/acscatal.1c03326
ACS Catal. 2021, 11, 13603−13648

solvents, but there is a possibility of transforming the active oxides to inactive oxides under such harsh conditions. For instance, in cellulose hydrogenolysis, which requires higher temperature and pressure conditions, inactive $NiWO_4$ species were formed during the multiple uses of the Ni/W/AC catalyst, resulting in decreased polyol yield.[204] The application of in situ studies could provide more information about structural changes in the catalyst during biomass conversion reactions. Besides, leaching of the active metal sites due to the unavoidable application of harsh conditions for biomass processing is another key concern that could significantly limit their applications in biorefinery research. Therefore, biomass processing conditions need to be optimized to avoid the changes in the structure of metal oxides and leaching of the active sites to achieve stable catalytic activity. In higher-loaded MoO_3 catalysts (10−36 wt %), the lower oxidation state of Mo species (Mo^{4+}/Mo^{3+}) was enriched on the catalyst surface, which is found to be less active for HDO of biomass molecules like anisole.[294] In contrast, an improved HDO performance was achieved when the catalyst contains MoO_3 loading of up to 15 wt % due to the presence of more Mo^{5+}/Mo^{6+} species on the support surface, but metal loading and the formation of active/inactive metal oxides also depend on the nature of the support, limiting the scope of the supporting materials for MoO_x and WO_x solid acids.

In gas-phase processing of biomass molecules, coke formation over MoO_x and WO_x solid acids is a key concern because strong acid sites present in these materials promote coke formation, resulting in rapid catalyst deactivation.[152] However, the presence of strong acid sites is essential for numerous biomass conversion reactions like transesterification of triglycerides, esterification of fatty acids, esterification/acetalization of glycerol, cellulose hydrolysis, and dehydration of fructose. Calcination of MoO_x and WO_x solid acids at higher temperatures (400−700 °C) is required to obtain the desired catalytic properties. Concurrently, the transformation of polymeric metal oxide clusters, which contain abundant Brønsted acid sites (bridged −OH groups, exist as metal−OH−metal) needed for various acid-catalyzed biomass conversions (cellulose hydrolysis and fructose dehydration), to the inactive metal oxide crystallites is possible under higher calcination temperatures. In contrast, isolated WO_x and MoO_x species exhibit the Lewis acidic nature, which needs to be optimized depending on the reaction (e.g., glucose hydrogenolysis).[233] Hence, the optimization of the acidic properties of MoO_x and WO_x solid acids to avail their versatile application in biorefinery research is challenging. In the case of mesoporous supporting materials like SiO_2, the isolated metal oxides can migrate and block the active sites, inhibiting the accessibility of the active sites to the reactant molecules that will show a negative effect on the reaction rates and product selectivity.[222] Therefore, the versatile application of MoO_x and WO_x solid acids supported on mesoporous materials is limited in the conversion of biomass and its derivatives, which typically contain bulky structures. Above all, the scarcity and high cost of these materials have a huge limitation on their industrial uses.

5. CONCLUSIONS AND CHALLENGES

In summary, efficient development/utilization of renewable energy replacing fossil fuels is one of the primary goals of the scientific community, providing a sustainable economy and society to the present and future generations. Biomass, the only available renewable organic carbon source, has received much attention because of its high abundance, biodegradability, and resemblance to carbon−hydrogen and carbon−oxygen structures with petrochemicals and their derivatives. Efficient biomass valorization controls the carbon footprint because photosynthesis utilizes CO_2 released from the biorefinery industry for biomass production, thus mitigating environmental pollution. So, several processes have been developed for sustainable biomass conversion to produce fuels/fuel additives and chemicals (fine, bulk, and drop-in) as well as new materials.

Catalysis, especially using acid materials, can efficiently convert biomass and its model compounds to valuable fuels and chemicals at mild processing conditions. A variety of steps in biomass processing are catalyzed by acids, namely, hydrolysis, pyrolysis, dehydration, esterification, acetalization, condensation, hydrogenolysis, hydrodeoxygenation, etc. Although quite faster reaction rates in biomass conversion are evident with homogeneous acid catalysts like HF, HCl, H_3PO_4, and H_2SO_4, these methods suffer from reactor damage, active site leaching, trivial catalyst's reusability, and the requirement of multiple steps for product isolation/purification, resulting in increased production cost and huge amounts of waste generation. Using heterogeneous solid acid catalysts for biomass conversion is a potential solution to overcome the above challenges. Various solid acids are developed for biomass conversion: zeolites, pure metal oxides and supported metal oxides, ion-exchange resins, functionalized silicas, heteropolyacids, immobilized ionic liquids, carbonaceous acids, and metal−organic frameworks. Using filtration or centrifugation, these solid-phase acid materials can be efficiently separated from the reaction mixture and reused (after regeneration if needed) for the next cycle. This approach provides a high purity reaction mixture, reducing the number of steps required to separate and purify the desirable product, thus improving the process's energy efficiency.

Among the solid acids developed for biomass conversion, supported MoO_x and WO_x materials are of particular interest because these materials are nontoxic, inexpensive, and exhibit excellent acidic properties like H_2SO_4 liquid acid. The remarkable stability of these solid acids in various atmospheres (water, hydrogen, and oxygen) is another unique property that allows them to inhibit the poisoning/leaching of the acid sites by water, a typically used reactant and reaction medium, or byproduct formed in most acid-catalyzed biomass conversions, achieving improved turnover frequency values and excellent catalyst reusability. The hydroxyl groups present on the oxide supports (e.g., Al_2O_3, SiO_2, and ZrO_2) act as Brønsted acid sites, but their interaction with the metal sites (W or Mo) determines the acidic strength. Concurrently, the Brønsted acidic strength of the hydroxyl species associated with poly-WO_x and -MoO_x species cannot be ruled out. On the other hand, the number and strength of the Lewis acid sites strongly depend on the dispersion of isolated and oligomeric WO_x and MoO_x species and their coordination chemistry on the supports. The concentration of Brønsted/Lewis acid sites in supported WO_x and MoO_x catalysts can be controlled by metal loading, support, synthesis method, and reaction medium (i.e., water and H_2). At low metal loadings, coordinatively unsaturated M^{+4} species in oxide supports, for instance, Zr^{4+} in ZrO_2, are also available as Lewis acid sites as they exhibit electron-deficient character. Above all, the key versatile nature of these supported WO_x and MoO_x solid acids is that they can form a synergistic interaction with redox metals (Pd, Ru, Pt, Cu, Co, Ni, etc.), enabling them to be an essential choice of heterogeneous catalysts for a variety of biomass conversion reactions. This is because biomass conversion to practically valuable fuels and chemicals requires efficient cleavage of biomass to model compounds and the

https://doi.org/10.1021/acscatal.1c03326
ACS Catal. 2021, 11, 13603−13648

subsequent deoxygenation, in which bifunctional acid-redox sites play a crucial role.

This Review highlighted the importance of the interplay of coordination chemistry and acidity of supported MoO_x and WO_x catalysts with respect to their catalytic performance for various biomass conversion reactions. Metal site density and its coordination environment via grafting metal precursors onto the OH functional groups of supports, mainly oxides, can affect the acidic properties and the catalytic efficiency of supported MoO_x and WO_x solid acids. To understand this, the coordination nature of MoO_x and WO_x by taking typical metal oxide supports, namely, Al_2O_3, SiO_2, and ZrO_2, is discussed. Similar types of coordination modes were found for both MoO_x and WO_x on different oxide supports. Mono- and dioxo species are formed at low surface coverage, whereas the formation of distorted polymetalate species of different natures was favored at high surface coverage. Metal loading and the properties of the oxide supports (Hüttig temperature and surface hydroxyl group density) determine the degree of polymerization and the formation of polymetalate species. When the metal loading above the monolayer coverage (ca., >4.6 Mo atoms per nm^2 and >4.5 W per nm^2) was increased, the formation of crystalline MoO_3 and WO_3 particles was noticed because of the lack of the hydroxyl groups on the support for metal grafting, resulting in decreased surface acidity and lower catalytic performance in most biomass conversions. However, in the case of WO_x/ZrO_2 solid acid, the formation of disordered Zr−WO_x clusters above the monolayer coverage is observed; this cluster is responsible for improved acidity, but the catalytic performance of this material in biomass conversion is unclear.

A systematic catalytic activity study of supported MoO_x and WO_x solid acids for biomass conversion was reported by taking different feedstocks (oils, fats, and lignocellulose), constituents (fatty acids, cellulose, hemicellulose, and lignin), and derived compounds (cellobiose, glucose, fructose, xylose, furans, levulinic acid, aromatics, glycerol, etc.). Supported MoO_x and WO_x solid acids are beneficial for biodiesel production via transesterification of oils and fats feedstock with methanol or ethanol because they prevent the saponification of free fatty acids (a base-catalyzed step) present in the feedstock, resulting in high purity biodiesel production at economically viable conditions. As a result, these solid acids exhibited good catalytic activities for the transesterification of waste cooking oil, containing higher amounts of free fatty acids, to obtain biodiesel. In the case of biodiesel industry byproduct, i.e., glycerol, four important valorization reactions, namely, esterification, acetalization, (oxidative) dehydration, and hydrogenolysis, are realized over the supported MoO_x and WO_x solid acids. The resulting products can be used as fuel additives (glycerol acetins/acetals) and monomers (acrylic acid and propanediols) for the polymer industry. For esterification and acetalization of glycerol, a greater number of acid sites with higher Brønsted acidity compared with Lewis acidity is crucial for achieving improved conversion and product selectivity. The nature of the acid sites (Brønsted/Lewis) determines the reaction mechanism in glycerol acetalization. Glycerol dehydration to acrolein was promoted by Brønsted acid sites, while both redox and acid sites are needed for efficient production of acrylic acid from glycerol via the oxidative dehydration route. For glycerol hydrogenolysis, which involves a two-step dehydration−hydrogenation mechanism, Brønsted acid sites in synergy with metal redox sites provide higher conversions and improved product selectivity.

Fuel grade molecules and value-added chemicals can be produced from lignocellulose, abundantly available nonedible biomass, via catalytic fast pyrolysis using MoO_x- and WO_x-based catalysts. The acid sites of these catalysts can promote deoxygenation of bio-oil produced from the fast pyrolysis of lignocellulose, giving high-quality bio-oil that can be used alone or blended with petrochemicals in the automotive industry. The potential catalytic role of supported MoO_x and WO_x solid acids for biomass valorization is evidenced in the case of lignocellulose constituents (cellulose, hemicellulose, and lignin) and their derived compounds (cellobiose, glucose, fructose, xylose, furans, levulinic acid, lignin-based aromatics, etc.). The reason is that most reactions (hydrolysis, dehydration, isomerization, etherification, hydrogenolysis, and hydrodeoxygenation) developed for converting these substrates into value-added fuels and chemicals can be catalyzed by solid acids. Harsh reaction conditions are often required for these reactions, which will induce the leaching of the catalyst's active sites. Owing to high hydrothermal stability and a good amount of Brønsted/Lewis acid sites, supported MoO_x and WO_x solid acids are preferred for these reactions. Brønsted acid sites are needed to depolymerize cellulose or hemicellulose to the respective building blocks (glucose and xylose). Conversion of glucose to value-added products (e.g., HMF) via fructose formation requires both Brønsted and Lewis acid sites, but a higher percentage of Brønsted to Lewis acid sites is favorable for improved HMF formation because Brønsted acid sites efficiently catalyze the fructose-to-HMF dehydration step that eventually increases glucose conversion by inducing the glucose-to-fructose isomerization step.[232] The excellent synergistic effect of acid sites of supported MoO_x and WO_x catalysts with redox metals is beneficial for the hydroprocessing of sugars and their furan derivatives. Interestingly, there is no role of Brønsted acid sites in Pd−WO_x/Al_2O_3 for the hydroprocessing of glucose to produce 1,2-propanediol.[233] The porous nature of the support (SiO_2) provided improved accessibility of acid sites and also optimized the concentration of Brønsted acid sites (H_xWO_3) in a Pt/WO_3@SiO_2 catalyst, which showed excellent catalytic efficiency in 1,5-pentanediol synthesis via THFA hydrogenolysis.[264] With the increase of W/Si molar ratio, both the total pore volume and the BET surface area of the catalyst were decreased, which can negatively affect the active site accessibility.

To enhance the practical applications of lignin-derived aromatics (guaiacol, cresol, anisole, phenol, eugenol, etc.), the removal of oxygen from these molecules via the hydrodeoxygenation (HDO) route is recommended. For an efficient HDO process, both acid and redox properties are needed with a synergetic interaction. In this case, the combination of supported WO_x and MoO_x solid acids with redox metals (e.g., Pd, Pt, Ru, Re, Ni, Cu, Co) provides synergetic acid-redox properties. Good to excellent catalytic activity/selectivity results and improved catalyst reusability were achieved for HDO of lignin-derived aromatics. Especially, MoO_x-based catalysts are found to be highly active for HDO reactions because of the strong ability of Mo species in C−O bond cleavage, which is the key for efficient oxygen removal from lignin derivates. Interestingly, electron-deficient oxygen vacancies (Lewis acid sites), formed via the partial reduction of Mo species, were found to be the active sites for the adsorption/activation of the reactants during the HDO reaction. The oxidation state of Mo (4+ and 5+) is also important for efficient HDO reactions. In some cases, pure MoO_3 and WO_3 as well as their mixed oxides also exhibited reasonably good catalytic activity for biomass

https://doi.org/10.1021/acscatal.1c03326
ACS Catal. 2021, 11, 13603−13648

conversion, but the correlation of their catalytic performances (in terms of turnover frequency values and catalyst's reusability) with that of supported MoO_x and WO_x solid acids can provide valuable insights to develop advanced solid acid catalysts.

This Review indeed reveals the significant progress achieved toward developing efficient supported MoO_x and WO_x solid acids for biomass conversion. However, to achieve sustainable biomass conversion at mild reaction conditions, further developments of supported MoO_x and WO_x solid acids are essential, corresponding to the in-depth characterization of acid sites and their optimization, acid site accessibility, the effect of added redox metal on the catalyst's acidity, the interaction between catalyst and reaction medium/byproducts/gases, and catalyst deactivation/regeneration, which are discussed below.

1. In-depth characterization of acid sites and their optimization: Containing more acid sites is not always beneficial for catalysis because excess acid sites may often induce side reactions, resulting in lower selectivity of the desired products. Thus, the optimization of the acid sites is vital to achieving improved catalytic activity and selectivity of supported MoO_x and WO_x solid acids. For this, an in-depth understanding of the acid site species is essential. Although several coordination models of MoO_x and WO_x on the supports were reported, the precise identification of the acid sites remains a significant challenge. As noticed in the WO_3/ZrO_2 catalyst, which contains ∼1 nm Zr−WO_x catalytically active clusters, the visualization and distinguishability of different structures of MoO_x and WO_x as well as the supports at the atomic scale using advanced electron microscopy techniques and identifying true active sites during the reaction using in situ spectroscopy techniques with the complementary theoretical studies can provide valuable solutions to optimize the acid sites and the catalyst synthesis methods that will help catalysis researchers to design advanced MoO_x and WO_x solid acids.
2. Acid site accessibility: Higher reaction rates and improved product selectivity are generally possible when the catalyst exhibits facile accessibility of the active sites to the reactants and intermediates. The mesoporous network of the support can also prevent agglomeration of the active MoO_x and WO_x species, especially during high-temperature gas-phase reactions, thus improving the catalyst durability. In addition, coke deposition on MoO_x and WO_x species can also be prevented because of the enhanced diffusion of the coke precursors through the support's pores. Although a few studies are reported using mesoporous silica as a support to incorporate MoO_x and WO_x species, more stimulating efforts are needed in this direction, for instance, studying the effect of different types of porous materials with different pore sizes on the structure−activity performance of MoO_x and WO_x solid acids for biomass conversion.
3. Effect of added redox metal on the catalyst's acidity: The bifunctional role of acid and redox sites in supported M-MoO_x (WO_x) catalysts (M = Pd, Pt, Ru, Re, Ni, Cu, Co) in activating reactants/intermediates involving different cascade reactions in biomass conversion is investigated in many studies, but less attention has been paid to understand the effect of redox metal on the acidity of supported MoO_x (WO_x) catalysts. Because of the different electronegativity nature and multiple oxidation states, the added redox metal can significantly alter the electronic properties of MoO_x (WO_x) species as well as the oxide supports (e.g., ZrO_2 and TiO_2) that can modify the acidic properties of the catalysts. This information is crucial to select a suitable redox metal depending on the reaction and to optimize its amount in the catalyst that will help researchers to design new bifunctional solid catalysts for biomass conversion and other important cascade chemical transformations.
4. Interaction between catalyst and reaction medium/byproducts/gases: Understanding the catalyst's interaction with the reactants and the derivation of reaction mechanisms are essential studies in catalysis research. However, there is a lack of understanding of how the reaction medium (solvents), byproducts (water, carbon particles, etc.), or gases (hydrogen is compulsory for biomass hydroprocessing) can interact with the acid sites of the catalyst, and it is crucial to achieve improved product selectivities in biomass conversion. For instance, the in situ generated water during the reaction of DMF to *p*-xylene induced the transformation of Lewis acid sites into Brønsted acid sites in the WO_x/SiO_2 catalyst.[248] The formed Brønsted acids promoted an unwanted hydrolysis reaction of DMF into the 2,5-hexanedione byproduct, resulting in lower selectivity of the desirable *p*-xylene product. It is also reported that the interaction of hydrogen with the WO_3/ZrO_2 solid acid creates Brønsted acid sites, promoting the fast hydride transfer steps toward 2,5-hexanedione from cellulose, whereas lactic acid is the primary product in the presence of He.[50] Coke formation is the key reason for the catalyst deactivation in high-temperature gas-phase biomass conversion reactions. Interestingly, coke particles, formed during glycerol dehydration, covered the active sites of the WO_3/TiO_2 solid acid responsible for the side reactions, resulting in increased acrolein selectivity with time-on-stream.[155] These studies indicate the interaction of water, hydrogen, and coke particles with acid catalysts that significantly affected tuning acidity and catalytic activity/selectivity. Thus, more investigations need to be done to understand these unusual interactions that will help us to optimize the process conditions and catalysts' properties for efficient biomass conversion.
5. Catalyst deactivation and regeneration strategies: Catalyst deactivation either by poisoning or leaching of the acid sites usually occurs by polar solvents; in situ generated water or byproducts like humins in liquid-phase reactions or carbon deposition on the active sites in gas-phase reactions is obvious during biomass conversion over supported MoO_x and WO_x solid acids. The optimization of metal loading or the addition of appropriate amounts of another metal oxide can improve the metal−support interaction that will inhibit the leaching of acid sites as noticed in aqueous-phase HMF synthesis over SnO_2-supported MoO_x and WO_x solid acids.[243] For the inhibition of coke formation, several strategies are reported: (i) the addition of another metal oxide, like vanadium oxide to a MoO_x/Al_2O_3 solid acid,[157] which can promote coke oxidation with its labile lattice oxygen via the Mars-van Krevelen mechanism; (ii) using the porous supporting materials like mesoporous silica, which can enhance the diffusion of the coke precursors through the pores; (iii) partial oxidation of coke using oxygen during

https://doi.org/10.1021/acscatal.1c03326
ACS Catal. 2021, 11, 13603−13648

the reaction, for instance, in the case of oxidative dehydration of glycerol; (iv) the presence of atmospheric pressure H_2 in the reactor, which was also found to minimize the production of char and coke.[186]

The aforesaid challenges and prospects indicate the urgency of performing more studies for biomass valorization using different types of supported MoO_x and WO_x solid acids at various atmospheres as well as exploring the effect of various factors (redox metal, reaction medium, byproducts, gases, etc.) and investing reaction mechanisms using advanced (in situ) electron microscopy and optical spectroscopy techniques with the support of theoretical studies. In this context, we believe this informative Review will act as a critical reference to catalysis researchers with valuable insights for the rational design of new solid acids for catalytic biomass valorization and other challenging acid-catalyzed processes.

AUTHOR INFORMATION

Corresponding Author

Putla Sudarsanam − *Catalysis and Inorganic Chemistry Division, CSIR-National Chemical Laboratory, Pune 411 008, India; Academy of Scientific and Innovative Research (AcSIR), Ghaziabad, Uttar Pradesh 201 002, India;* orcid.org/0000-0001-5574-2819; Email: s.putla@ncl.res.in

Authors

Navneet Kumar Gupta − *Technical University of Darmstadt, Department of Chemistry, Ernst-Berl-Institut für Technische und Makromolekulare Chemie, 64287 Darmstadt, Germany*

Baithy Mallesham − *Chemical Engineering Department, Indian Institute of Technology Hyderabad, Sangareddy 502285, India*

Nittan Singh − *Catalysis and Inorganic Chemistry Division, CSIR-National Chemical Laboratory, Pune 411 008, India; Academy of Scientific and Innovative Research (AcSIR), Ghaziabad, Uttar Pradesh 201 002, India*

Pavan Narayan Kalbande − *Catalysis and Inorganic Chemistry Division, CSIR-National Chemical Laboratory, Pune 411 008, India; Academy of Scientific and Innovative Research (AcSIR), Ghaziabad, Uttar Pradesh 201 002, India*

Benjaram M. Reddy − *Catalysis and Fine Chemicals Department, CSIR-Indian Institute of Chemical Technology, Hyderabad 500 007, India;* orcid.org/0000-0002-5451-7289

Bert F. Sels − *Center for Sustainable Catalysis and Engineering, Faculty of Bioscience Engineering, KU Leuven, 3001 Heverlee, Belgium;* orcid.org/0000-0001-9657-1710

Complete contact information is available at: https://pubs.acs.org/10.1021/acscatal.1c03326

Notes

The authors declare no competing financial interest.

ACKNOWLEDGMENTS

P.S. acknowledges the funding support from the CSIR-National Chemical Laboratory, Pune. N.K.G. gratefully acknowledges support from the Alexander von Humboldt foundation. B.M. thanks the Department of Science and Technology (DST)-SERB, New Delhi, for the award of a National Post-Doctoral Fellowship (PDF/2018/002244). N.S. and P.N.K. acknowledge the Council of Scientific and Industrial Research (CSIR), New Delhi, for research fellowships. B.F.S. acknowledges the EoS FWO BIOFACT project, the VLAIO SBO BIOWOOD project, the iBOF NEXTBIOREF project, and the Catalysti Moonschot NIBCON project for financial support.

REFERENCES

(1) Zhang, R.; Liu, N.; Lei, Z.; Chen, B. Selective Transformation of Various Nitrogen-Containing Exhaust Gases toward N_2 over Zeolite Catalysts. *Chem. Rev.* **2016**, *116* (6), 3658−3721.

(2) Zhang, X.; Wilson, K.; Lee, A. F. Heterogeneously Catalyzed Hydrothermal Processing of C_5−C_6 Sugars. *Chem. Rev.* **2016**, *116* (19), 12328−12368.

(3) Raheem, A.; Prinsen, P.; Vuppaladadiyam, A. K.; Zhao, M.; Luque, R. A Review on Sustainable Microalgae Based Biofuel and Bioenergy Production: Recent Developments. *J. Cleaner Prod.* **2018**, *181*, 42−59.

(4) Lee, A. F.; Bennett, J. A.; Manayil, J. C.; Wilson, K. Heterogeneous Catalysis for Sustainable Biodiesel Production via Esterification and Transesterification. *Chem. Soc. Rev.* **2014**, *43* (22), 7887−7916.

(5) Lødeng, R.; Ranga, C.; Rajkhowa, T.; Alexiadis, V. I.; Bjørkan, H.; Chytil, S.; Svenum, I. H.; Walmsley, J.; Thybaut, J. W. Hydrodeoxygenation of Phenolics in Liquid Phase over Supported MoO_3 and Carburized Analogues. *Biomass Convers. Biorefin.* **2017**, *7* (3), 343−359.

(6) Huang, W. Oxide Nanocrystal Model Catalysts. *Acc. Chem. Res.* **2016**, *49* (3), 520−527.

(7) Munnik, P.; de Jongh, P. E.; de Jong, K. P. Recent Developments in the Synthesis of Supported Catalysts. *Chem. Rev.* **2015**, *115* (14), 6687−6718.

(8) Takagaki, A.; Tagusagawa, C.; Hayashi, S.; Hara, M.; Domen, K. Nanosheets as Highly Active Solid Acid Catalysts for Green Chemical Syntheses. *Energy Environ. Sci.* **2010**, *3* (1), 82−93.

(9) Hu, S.; Jiang, F.; Hsieh, Y.-L. 1D Lignin-Based Solid Acid Catalysts for Cellulose Hydrolysis to Glucose and Nanocellulose. *ACS Sustainable Chem. Eng.* **2015**, *3* (10), 2566−2574.

(10) Fu, G.; Cirujano, F. G.; Krajnc, A.; Mali, G.; Henrion, M.; Smolders, S.; De Vos, D. E. Unexpected Linker-Dependent Brønsted Acidity in the (Zr)UiO-66 Metal Organic Framework and Application to Biomass Valorization. *Catal. Sci. Technol.* **2020**, *10* (12), 4002−4009.

(11) Sudarsanam, P.; Zhong, R.; Van den Bosch, S.; Coman, S. M.; Parvulescu, V. I.; Sels, B. F. Functionalised Heterogeneous Catalysts for Sustainable Biomass Valorisation. *Chem. Soc. Rev.* **2018**, *47* (22), 8349−8402.

(12) Hu, L.; Lin, L.; Wu, Z.; Zhou, S.; Liu, S. Chemocatalytic Hydrolysis of Cellulose into Glucose over Solid Acid Catalysts. *Appl. Catal., B* **2015**, *174*−*175*, 225−243.

(13) Zeng, D.; Liu, S.; Gong, W.; Chen, H.; Wang, G. A Nano-Sized Solid Acid Synthesized from Rice Hull Ash for Biodiesel Production. *RSC Adv.* **2014**, *4* (39), 20535−20539.

(14) Okuhara, T. Water-Tolerant Solid Acid Catalysts. *Chem. Rev.* **2002**, *102* (10), 3641−3666.

(15) Zhou, W.; Soultanidis, N.; Xu, H.; Wong, M. S.; Neurock, M.; Kiely, C. J.; Wachs, I. E. Nature of Catalytically Active Sites in the Supported WO_3/ZrO_2 Solid Acid System: A Current Perspective. *ACS Catal.* **2017**, *7* (3), 2181−2198.

(16) Poyraz, A. S.; Kuo, C.-H.; Kim, E.; Meng, Y.; Seraji, M. S.; Suib, S. L. Tungsten-Promoted Mesoporous Group 4 (Ti, Zr, and Hf) Transition-Metal Oxides for Room-Temperature Solvent-Free Acetalization and Ketalization Reactions. *Chem. Mater.* **2014**, *26* (9), 2803−2813.

(17) Lecarpentier, S.; van Gestel, J.; Thomas, K.; Gilson, J.-P.; Houalla, M. Influence of W Loading on the Environment of Si in WO_3/ZrO_2−SiO_2 Catalysts. *Appl. Catal., A* **2010**, *374* (1−2), 137−141.

(18) Mallesham, B.; Sudarsanam, P.; Reddy, B. M. Eco-Friendly Synthesis of Bio-Additive Fuels from Renewable Glycerol Using Nanocrystalline SnO_2-Based Solid Acids. *Catal. Sci. Technol.* **2014**, *4* (3), 803−813.

(19) Rao, B. G.; Sudarsanam, P.; Mallesham, B.; Reddy, B. M. Highly Efficient Continuous-Flow Oxidative Coupling of Amines Using Promising Nanoscale CeO_2-M/SiO_2 (M = MoO_3 and WO_3) Solid Acid Catalysts. *RSC Adv.* **2016**, *6* (97), 95252−95262.

(20) Mallesham, B.; Govinda Rao, B.; Reddy, B. M. Production of Biofuel Additives by Esterification and Acetalization of Bioglycerol. *C. R. Chim.* **2016**, *19* (10), 1194−1202.
(21) Mallesham, B.; Sudarsanam, P.; Reddy, B. M. Production of Biofuel Additives from Esterification and Acetalization of Bioglycerol over SnO_2 -Based Solid Acids. *Ind. Eng. Chem. Res.* **2014**, *53* (49), 18775−18785.
(22) Reddy, P. S.; Sudarsanam, P.; Mallesham, B.; Raju, G.; Reddy, B. M. Acetalisation of Glycerol with Acetone over Zirconia and Promoted Zirconia Catalysts under Mild Reaction Conditions. *J. Ind. Eng. Chem.* **2011**, *17* (3), 377.
(23) Sudarsanam, P.; Mallesham, B.; Prasad, A. N.; Reddy, P. S.; Reddy, B. M. Synthesis of Bio−Additive Fuels from Acetalization of Glycerol with Benzaldehyde over Molybdenum Promoted Green Solid Acid Catalysts. *Fuel Process. Technol.* **2013**, *106*, 539−545.
(24) Mallesham, B.; Rangaswamy, A.; Rao, B. G.; Rao, T. V.; Reddy, B. M. Solvent-Free Production of Glycerol Carbonate from Bioglycerol with Urea Over Nanostructured Promoted SnO_2 Catalysts. *Catal. Lett.* **2020**, *150* (12), 3626−3641.
(25) Mallesham, B.; Sudarsanam, P.; Raju, G.; Reddy, B. M. Design of Highly Efficient Mo and W-Promoted SnO_2 Solid Acids for Heterogeneous Catalysis: Acetalization of Bio-Glycerol. *Green Chem.* **2013**, *15* (2), 478−489.
(26) Reddy, P. S.; Sudarsanam, P.; Raju, G.; Reddy, B. M. Synthesis of Bio-Additives: Acetylation of Glycerol over Zirconia-Based Solid Acid Catalysts. *Catal. Commun.* **2010**, *11* (15), 1224−1228.
(27) Corma, A.; García, H. Lewis Acids as Catalysts in Oxidation Reactions: From Homogeneous to Heterogeneous Systems. *Chem. Rev.* **2002**, *102* (10), 3837−3892.
(28) Busca, G. Acid Catalysts in Industrial Hydrocarbon Chemistry. *Chem. Rev.* **2007**, *107* (11), 5366−5410.
(29) Reddy, B. M.; Patil, M. K. Organic Syntheses and Transformations Catalyzed by Sulfated Zirconia. *Chem. Rev.* **2009**, *109* (6), 2185−2208.
(30) Rousseau, R.; Dixon, D. A.; Kay, B. D.; Dohnálek, Z. Dehydration, Dehydrogenation, and Condensation of Alcohols on Supported Oxide Catalysts Based on Cyclic $(WO_3)_3$ and $(MoO_3)_3$ Clusters. *Chem. Soc. Rev.* **2014**, *43* (22), 7664−7680.
(31) Kouva, S.; Honkala, K.; Lefferts, L.; Kanervo, J. Review: Monoclinic Zirconia, Its Surface Sites and Their Interaction with Carbon Monoxide. *Catal. Sci. Technol.* **2015**, *5* (7), 3473−3490.
(32) Bianchi, D.; Gass, J.-L.; Khalfallah, M.; Teichner, S. J. Intermediate Species on Zirconia Supported Methanol Aerogel Catalysts. *Appl. Catal., A* **1993**, *101* (2), 297−315.
(33) Morierra, C.; Aschieri, R.; Volante, M. Surface Characterization of Zirconium Oxide. I. Surface Activation and the Development of a Strong Lewis Acidity. *Mater. Chem. Phys.* **1988**, *20* (6), 539−557.
(34) Ma, Z.-Y.; Yang, C.; Wei, W.; Li, W.-H.; Sun, Y.-H. Surface Properties and CO Adsorption on Zirconia Polymorphs. *J. Mol. Catal. A: Chem.* **2005**, *227* (1−2), 119−124.
(35) Jung, K. T.; Bell, A. T. The Effects of Synthesis and Pretreatment Conditions on the Bulk Structure and Surface Properties of Zirconia. *J. Mol. Catal. A: Chem.* **2000**, *163* (1−2), 27−42.
(36) Merle-Méjean, T.; Barberis, P.; Othmane, S. B.; Nardou, F.; Quintard, P. E. Chemical Forms of Hydroxyls on/in Zirconia: An FT-IR Study. *J. Eur. Ceram. Soc.* **1998**, *18* (11), 1579−1586.
(37) Hu, H.; Wachs, I. E. Catalytic Properties of Supported Molybdenum Oxide Catalysts: In Situ Raman and Methanol Oxidation Studies. *J. Phys. Chem.* **1995**, *99* (27), 10911−10922.
(38) Fu, T.; Wang, Y.; Wernbacher, A.; Schlögl, R.; Trunschke, A. Single-Site Vanadyl Species Isolated within Molybdenum Oxide Monolayers in Propane Oxidation. *ACS Catal.* **2019**, *9* (6), 4875−4886.
(39) Digne, M.; Sautet, P.; Raybaud, P.; Euzen, P.; Toulhoat, H. Hydroxyl Groups on γ-Alumina Surfaces: A DFT Study. *J. Catal.* **2002**, *211* (1), 1−5.
(40) Zhuravlev, L. T. The Surface Chemistry of Amorphous Silica. Zhuravlev Model. *Colloids Surf., A* **2000**, *173* (1−3), 1−38.
(41) Sneh, O.; George, S. M. Thermal Stability of Hydroxyl Groups on a Well-Defined Silica Surface. *J. Phys. Chem.* **1995**, *99* (13), 4639−4647.
(42) Mukhamed'yarova, A.; Nesterova, O.; Boretsky, K.; Skibina, J.; Boretskaya, A.; Egorova, S.; Lamberov, A. Influence of the Obtaining Method on the Properties of Amorphous Aluminum Compounds. *Coatings* **2019**, *9* (1), 41.
(43) Tregubenko, V. Y.; Belyi, A. S. Characterization of Acid-Modified Alumina as a Support for Reforming Catalysts. *Kinet. Catal.* **2020**, *61* (1), 130−136.
(44) Kim, G.; Kwon, G.; Lee, H. The Role of Surface Hydroxyl Groups on a Single-Atomic Rh_1/ZrO_2 Catalyst for Direct Methane Oxidation. *Chem. Commun.* **2021**, *57* (13), 1671−1674.
(45) Hino, M.; Arata, K. Synthesis of Solid Superacid of Tungsten Oxide Supported on Zirconia and Its Catalytic Action for Reactions of Butane and Pentane. *J. Chem. Soc., Chem. Commun.* **1988**, *18*, 1259.
(46) Rao Ginjupalli, S.; Mugawar, S.; Rajan, N. P.; Kumar Balla, P.; Chary Komandur, V. R. Vapour Phase Dehydration of Glycerol to Acrolein over Tungstated Zirconia Catalysts. *Appl. Surf. Sci.* **2014**, *309*, 153−159.
(47) Znaiguia, R.; Brandhorst, L.; Christin, N.; Bellière Baca, V.; Rey, P.; Millet, J.-M. M.; Loridant, S. Toward Longer Life Catalysts for Dehydration of Glycerol to Acrolein. *Microporous Mesoporous Mater.* **2014**, *196*, 97−103.
(48) Giang, C.; Osatiashtiani, A.; dos Santos, V.; Lee, A.; Wilson, D.; Waldron, K.; Wilson, K. Valorisation of Vietnamese Rice Straw Waste: Catalytic Aqueous Phase Reforming of Hydrolysate from Steam Explosion to Platform Chemicals. *Catalysts* **2014**, *4* (4), 414−426.
(49) Kourieh, R.; Rakic, V.; Bennici, S.; Auroux, A. Relation between Surface Acidity and Reactivity in Fructose Conversion into 5-HMF Using Tungstated Zirconia Catalysts. *Catal. Commun.* **2013**, *30*, 5−13.
(50) Chambon, F.; Rataboul, F.; Pinel, C.; Cabiac, A.; Guillon, E.; Essayem, N. Conversion of Cellulose to 2,5-Hexanedione Using Tungstated Zirconia in Hydrogen Atmosphere. *Appl. Catal., A* **2015**, *504*, 664−671.
(51) Ciptonugroho, W.; Al-Shaal, M. G.; Mensah, J. B.; Palkovits, R. One Pot Synthesis of WO_x/Mesoporous-ZrO_2 Catalysts for the Production of Levulinic-Acid Esters. *J. Catal.* **2016**, *340*, 17−29.
(52) Kim, D. S.; Ostromecki, M.; Wachs, I. E. Surface Structures of Supported Tungsten Oxide Catalysts under Dehydrated Conditions. *J. Mol. Catal. A: Chem.* **1996**, *106* (1−2), 93−102.
(53) Lee, E. L.; Wachs, I. E. In Situ Spectroscopic Investigation of the Molecular and Electronic Structures of SiO_2 Supported Surface Metal Oxides. *J. Phys. Chem. C* **2007**, *111* (39), 14410−14425.
(54) Chempath, S.; Zhang, Y.; Bell, A. T. DFT Studies of the Structure and Vibrational Spectra of Isolated Molybdena Species Supported on Silica. *J. Phys. Chem. C* **2007**, *111* (3), 1291−1298.
(55) Amakawa, K.; Sun, L.; Guo, C.; Hävecker, M.; Kube, P.; Wachs, I. E.; Lwin, S.; Frenkel, A. I.; Patlolla, A.; Hermann, K.; Schlögl, R.; Trunschke, A. How Strain Affects the Reactivity of Surface Metal Oxide Catalysts. *Angew. Chem., Int. Ed.* **2013**, *52* (51), 13553−13557.
(56) Banares, M. A.; Hu, H. C.; Wachs, I. E. Molybdena on Silica Catalysts: Role of Preparation Methods on the Structure-Selectivity Properties for the Oxidation of Methanol. *J. Catal.* **1994**, *150* (2), 407−420.
(57) Zhao, Q.; Chen, S.-L.; Gao, J.; Xu, C. Effect of Tungsten Oxide Loading on Metathesis Activity of Ethene and 2-Butene over WO_3/SiO_2 Catalysts. *Transition Met. Chem.* **2009**, *34* (6), 621−627.
(58) Ross-Medgaarden, E. I.; Wachs, I. E. Structural Determination of Bulk and Surface Tungsten Oxides with UV−vis Diffuse Reflectance Spectroscopy and Raman Spectroscopy. *J. Phys. Chem. C* **2007**, *111* (41), 15089−15099.
(59) de Lucas, A.; Valverde, J.; Cañizares, P.; Rodriguez, L. Partial Oxidation of Methane to Formaldehyde over W/SiO_2 Catalysts. *Appl. Catal., A* **1999**, *184* (1), 143−152.
(60) Lwin, S.; Wachs, I. E. Olefin Metathesis by Supported Metal Oxide Catalysts. *ACS Catal.* **2014**, *4* (8), 2505−2520.
(61) Lei, N.; Zhao, X.; Hou, B.; Yang, M.; Zhou, M.; Liu, F.; Wang, A.; Zhang, T. Effective Hydrogenolysis of Glycerol to 1,3-Propanediol over

https://doi.org/10.1021/acscatal.1c03326
ACS Catal. 2021, 11, 13603−13648

Metal-Acid Concerted Pt/WO_x/Al_2O_3 Catalysts. *ChemCatChem* **2019**, *11* (16), 3903−3912.
(62) Handzlik, J.; Sautet, P. Structure of Isolated Molybdenum(VI) Oxide Species on γ-Alumina: A Periodic Density Functional Theory Study. *J. Phys. Chem. C* **2008**, *112* (37), 14456−14463.
(63) Handzlik, J.; Sautet, P. Structure of Dimeric Molybdenum(VI) Oxide Species on γ-Alumina: A Periodic Density Functional Theory Study. *J. Phys. Chem. C* **2010**, *114* (45), 19406−19414.
(64) Wachs, I. E.; Kim, T.; Ross, E. I. Catalysis Science of the Solid Acidity of Model Supported Tungsten Oxide Catalysts. *Catal. Today* **2006**, *116* (2), 162−168.
(65) Wachs, I. E. Raman and IR Studies of Surface Metal Oxide Species on Oxide Supports: Supported Metal Oxide Catalysts. *Catal. Today* **1996**, *27* (3−4), 437−455.
(66) Barton, D. G.; Soled, S. L.; Meitzner, G. D.; Fuentes, G. A.; Iglesia, E. Structural and Catalytic Characterization of Solid Acids Based on Zirconia Modified by Tungsten Oxide. *J. Catal.* **1999**, *181* (1), 57−72.
(67) Lai, J.-K.; Wachs, I. E. A Perspective on the Selective Catalytic Reduction (SCR) of NO with NH_3 by Supported V_2O_5−WO_3/TiO_2 Catalysts. *ACS Catal.* **2018**, *8* (7), 6537−6551.
(68) Samaranch, B.; Ramírez de la Piscina, P.; Clet, G.; Houalla, M.; Homs, N. Study of the Structure, Acidic, and Catalytic Properties of Binary Mixed-Oxide MoO_3−ZrO_2 Systems. *Chem. Mater.* **2006**, *18* (6), 1581−1586.
(69) Xie, S.; Chen, K.; Bell, A. T.; Iglesia, E. Structural Characterization of Molybdenum Oxide Supported on Zirconia. *J. Phys. Chem. B* **2000**, *104* (43), 10059−10068.
(70) Liu, Q.; Zhang, T.; Liao, Y.; Cai, C.; Tan, J.; Wang, T.; Qiu, S.; He, M.; Ma, L. Production of C_5/C_6 Sugar Alcohols by Hydrolytic Hydrogenation of Raw Lignocellulosic Biomass over Zr Based Solid Acids Combined with Ru/C. *ACS Sustainable Chem. Eng.* **2017**, *5* (7), 5940−5950.
(71) Chary, K. Structure and Catalytic Properties of Molybdenum Oxide Catalysts Supported on Zirconia. *J. Catal.* **2004**, *226* (2), 283−291.
(72) Zhao, B.; Wang, X.; Ma, H.; Tang, Y. Raman Spectroscopy Studies on the Structure of MoO_3ZrO_2 Solid Superacid. *J. Mol. Catal. A: Chem.* **1996**, *108* (3), 167−174.
(73) Rossmedgaarden, E.; Knowles, W.; Kim, T.; Wong, M.; Zhou, W.; Kiely, C.; Wachs, I. New Insights into the Nature of the Acidic Catalytic Active Sites Present in ZrO_2-Supported Tungsten Oxide Catalysts. *J. Catal.* **2008**, *256* (1), 108−125.
(74) Zhou, W.; Ross-Medgaarden, E. I.; Knowles, W. V.; Wong, M. S.; Wachs, I. E.; Kiely, C. J. Identification of Active Zr−WO_x Clusters on a ZrO_2 Support for Solid Acid Catalysts. *Nat. Chem.* **2009**, *1* (9), 722−728.
(75) Soultanidis, N.; Zhou, W.; Psarras, A. C.; Gonzalez, A. J.; Iliopoulou, E. F.; Kiely, C. J.; Wachs, I. E.; Wong, M. S. Relating n-Pentane Isomerization Activity to the Tungsten Surface Density of WO_x/ZrO_2. *J. Am. Chem. Soc.* **2010**, *132* (38), 13462−13471.
(76) Zhou, W.; Wachs, I. E.; Kiely, C. J. Nanostructural and Chemical Characterization of Supported Metal Oxide Catalysts by Aberration Corrected Analytical Electron Microscopy. *Curr. Opin. Solid State Mater. Sci.* **2012**, *16* (1), 10−22.
(77) Aihara, T.; Miura, H.; Shishido, T. Effect of Perimeter Interface Length between 2D WO_3 Monolayer Domain and γ-Al_2O_3 on Selective Hydrogenolysis of Glycerol to 1,3-Propanediol. *Catal. Sci. Technol.* **2019**, *9* (19), 5359−5367.
(78) Zhang, J.; Zhao, C.; Li, C.; Li, S.; Tsang, C.-W.; Liang, C. The Role of Oxophilic Mo Species in Pt/MgO Catalysts as Extremely Active Sites for Enhanced Hydrodeoxygenation of Dibenzofuran. *Catal. Sci. Technol.* **2020**, *10* (9), 2948−2960.
(79) Lee, E. L.; Wachs, I. E. In Situ Spectroscopic Investigation of the Molecular and Electronic Structures of SiO_2 Supported Surface Metal Oxides. *J. Phys. Chem. C* **2007**, *111* (39), 14410−14425.
(80) Chauvin, J.; Thomas, K.; Clet, G.; Houalla, M. Comparative Influence of Surface Tungstate Species and Bulk Amorphous WO_3 Particles on the Acidity and Catalytic Activity of Tungsten Oxide Supported on Silica. *J. Phys. Chem. C* **2015**, *119* (22), 12345−12355.
(81) Hahn, T.; Bentrup, U.; Armbrüster, M.; Kondratenko, E. V.; Linke, D. The Enhancing Effect of Brønsted Acidity of Supported MoO_x Species on Their Activity and Selectivity in Ethylene/Trans−2-Butene Metathesis. *ChemCatChem* **2014**, *6* (6), 1664−1672.
(82) Kitano, T.; Okazaki, S.; Shishido, T.; Teramura, K.; Tanaka, T. Brønsted Acid Generation of Alumina-Supported Molybdenum Oxide Calcined at High Temperatures: Characterization by Acid-Catalyzed Reactions and Spectroscopic Methods. *J. Mol. Catal. A: Chem.* **2013**, *371*, 21−28.
(83) Laverty, D. Possible Role of Hydrido-Metal Complexes in Metathesis, Isomerization, Dimerization, and Polymerization of Alkenes. *J. Catal.* **1976**, *45* (1), 110−113.
(84) Xia, T.; Li, Q.; Liu, X.; Meng, J.; Cao, X. Morphology-Controllable Synthesis and Characterization of Single-Crystal Molybdenum Trioxide. *J. Phys. Chem. B* **2006**, *110* (5), 2006−2012.
(85) Barton, D. G.; Soled, S. L.; Iglesia, E. Solid Acid Catalysts Based on Supported Tungsten Oxides. *Top. Catal.* **1998**, *6* (1), 87−99.
(86) Baertsch, C. D.; Komala, K. T.; Chua, Y.-H.; Iglesia, E. Genesis of Brønsted Acid Sites during Dehydration of 2-Butanol on Tungsten Oxide Catalysts. *J. Catal.* **2002**, *205* (1), 44−57.
(87) Kuba, S.; Lukinskas, P.; Grasselli, R. K.; Gates, B. C.; Knözinger, H. Structure and Properties of Tungstated Zirconia Catalysts for Alkane Conversion. *J. Catal.* **2003**, *216* (1−2), 353−361.
(88) Knözinger, H. Heterogeneously Catalyzed Alkane Isomerization °C towards 100% Selectivity. In *Surface Chemistry in Biomedical and Environmental Science*; Blitz, J. P., Gun'ko, V. M., Eds.; Springer Netherlands: Dordrecht, 2006; Vol. *228*, pp 349−358; DOI: 10.1007/1-4020-4741-X_31.
(89) Santiesteban, J.; Vartuli, J.; Han, S.; Bastian, R.; Chang, C. Influence of the Preparative Method on the Activity of Highly Acidic WO_x/ZrO_2 and the Relative Acid Activity Compared with Zeolites. *J. Catal.* **1997**, *168* (2), 431−441.
(90) Song, K.; Zhang, H.; Zhang, Y.; Tang, Y.; Tang, K. Preparation and Characterization of WO_x/ZrO_2 Nanosized Catalysts with High WO_x Dispersion Threshold and Acidity. *J. Catal.* **2013**, *299* (19), 119−128.
(91) Kim, T. Y.; Park, D. S.; Choi, Y.; Baek, J.; Park, J. R.; Yi, J. Preparation and Characterization of Mesoporous Zr-WO_x/SiO_2 Catalysts for the Esterification of 1-Butanol with Acetic Acid. *J. Mater. Chem.* **2012**, *22* (19), 10021−10028.
(92) Zheng, A.; Liu, S.-B.; Deng, F. ^{31}P NMR Chemical Shifts of Phosphorus Probes as Reliable and Practical Acidity Scales for Solid and Liquid Catalysts. *Chem. Rev.* **2017**, *117* (19), 12475−12531.
(93) Huang, J.; Jiang, Y.; Reddy Marthala, V. R.; Ooi, Y. S.; Weitkamp, J.; Hunger, M. Concentration and Acid Strength of Hydroxyl Groups in Zeolites La,Na-X and La,Na-Y with Different Lanthanum Exchange Degrees Studied by Solid-State NMR Spectroscopy. *Microporous Mesoporous Mater.* **2007**, *104* (1−3), 129−136.
(94) Hunger, M. Multinuclear Solid-State NMR Studies of Acidic and Non-Acidic Hydroxyl Protons in Zeolites. *Solid State Nucl. Magn. Reson.* **1996**, *6* (1), 1−29.
(95) Zheng, A.; Zhang, H.; Chen, L.; Yue, Y.; Ye, C.; Deng, F. Relationship Between 1 H Chemical Shifts of Deuterated Pyridinium Ions and Brønsted Acid Strength of Solid Acids. *J. Phys. Chem. B* **2007**, *111* (12), 3085−3089.
(96) Gao, W.; Qi, G.; Wang, Q.; Wang, W.; Li, S.; Hung, I.; Gan, Z.; Xu, J.; Deng, F. Dual Active Sites on Molybdenum/ZSM-5 Catalyst for Methane Dehydroaromatization: Insights from Solid-State NMR Spectroscopy. *Angew. Chem., Int. Ed.* **2021**, *60* (19), 10709−10715.
(97) Zhu, H.; Ramanathan, A.; Wu, J.-F.; Subramaniam, B. Genesis of Strong Brønsted Acid Sites in WZr-KIT-6 Catalysts and Enhancement of Ethanol Dehydration Activity. *ACS Catal.* **2018**, *8* (6), 4848−4859.
(98) Hu, J. Z.; Kwak, J. H.; Wang, Y.; Hu, M. Y.; Turcu, R. V.; Peden, C. H. F. Characterizing Surface Acidic Sites in Mesoporous-Silica-Supported Tungsten Oxide Catalysts Using Solid-State NMR and Quantum Chemistry Calculations. *J. Phys. Chem. C* **2011**, *115* (47), 23354−23362.

(99) Mollar-Cuni, A.; Byrne, J. P.; Borja, P.; Vicent, C.; Albrecht, M.; Mata, J. A. Selective Conversion of Various Monosaccharaides into Sugar Acids by Additive-Free Dehydrogenation in Water. *ChemCatChem* **2020**, *12* (14), 3746−3752.
(100) Chu, Y.; Yu, Z.; Zheng, A.; Fang, H.; Zhang, H.; Huang, S.-J.; Liu, S.-B.; Deng, F. Acidic Strengths of Brønsted and Lewis Acid Sites in Solid Acids Scaled by ^{31}P NMR Chemical Shifts of Adsorbed Trimethylphosphine. *J. Phys. Chem. C* **2011**, *115* (15), 7660−7667.
(101) Li, S.; Zhou, H.; Jin, C.; Feng, N.; Liu, F.; Deng, F.; Wang, J.-Q.; Huang, W.; Xiao, L.; Fan, J. Formation of Subnanometer Zr-WO_x Clusters within Mesoporous W−Zr Mixed Oxides as Strong Solid Acid Catalysts for Friedel−Crafts Alkylation. *J. Phys. Chem. C* **2014**, *118* (12), 6283−6290.
(102) Wang, Y.; Xin, S.; Chu, Y.; Xu, J.; Qi, G.; Wang, Q.; Xia, Q.; Deng, F. Influence of Trimethylphosphine Oxide Loading on the Measurement of Zeolite Acidity by Solid-State NMR Spectroscopy. *J. Phys. Chem. C* **2021**, *125* (17), 9497−9506.
(103) Hernandez-Tamargo, C. E.; Roldan, A.; De Leeuw, N. H. DFT Modeling of the Adsorption of Trimethylphosphine Oxide at the Internal and External Surfaces of Zeolite MFI. *J. Phys. Chem. C* **2016**, *120* (34), 19097−19106.
(104) Wang, A.; Sudarsanam, P.; Xu, Y.; Zhang, H.; Li, H.; Yang, S. Functionalized Magnetic Nanosized Materials for Efficient Biodiesel Synthesis via Acid−Base/Enzyme Catalysis. *Green Chem.* **2020**, *22* (10), 2977−3012.
(105) Sahu, G.; Gupta, N. K.; Kotha, A.; Saha, S.; Datta, S.; Chavan, P.; Kumari, N.; Dutta, P. A Review on Biodiesel Production through Heterogeneous Catalysis Route. *ChemBioEng Rev.* **2018**, *5* (4), 231−252.
(106) Tan, X.; Sudarsanam, P.; Tan, J.; Wang, A.; Zhang, H.; Li, H.; Yang, S. Sulfonic Acid-Functionalized Heterogeneous Catalytic Materials for Efficient Biodiesel Production: A Review. *J. Environ. Chem. Eng.* **2021**, *9* (1), 104719.
(107) Zhang, Q.; Li, H.; Liu, X.; Qin, W.; Zhang, Y.; Xue, W.; Yang, S. Modified Porous Zr−Mo Mixed Oxides as Strong Acid Catalysts for Biodiesel Production. *Energy Technol.* **2013**, *1* (12), 735−742.
(108) Sun, D.; Yamada, Y.; Sato, S.; Ueda, W. Glycerol as a Potential Renewable Raw Material for Acrylic Acid Production. *Green Chem.* **2017**, *19* (14), 3186−3213.
(109) Xie, W.; Yang, D. Transesterification of Soybean Oil over WO_3 Supported on $AlPO_4$ as a Solid Acid Catalyst. *Bioresour. Technol.* **2012**, *119*, 60−65.
(110) Xie, W.; Wang, T. Biodiesel Production from Soybean Oil Transesterification Using Tin Oxide-Supported WO_3 Catalysts. *Fuel Process. Technol.* **2013**, *109*, 150−155.
(111) Navajas, A.; Reyero, I.; Jiménez-Barrera, E.; Romero-Sarria, F.; Llorca, J.; Gandía, L. M. Catalytic Performance of Bulk and Al_2O_3-Supported Molybdenum Oxide for the Production of Biodiesel from Oil with High Free Fatty Acids Content. *Catalysts* **2020**, *10* (2), 158.
(112) López, D. E.; Goodwin, J. G.; Bruce, D. A.; Furuta, S. Esterification and Transesterification Using Modified-Zirconia Catalysts. *Appl. Catal., A* **2008**, *339* (1), 76−83.
(113) Guldhe, A.; Singh, P.; Ansari, F. A.; Singh, B.; Bux, F. Biodiesel Synthesis from Microalgal Lipids Using Tungstated Zirconia as a Heterogeneous Acid Catalyst and Its Comparison with Homogeneous Acid and Enzyme Catalysts. *Fuel* **2017**, *187*, 180−188.
(114) Furuta, S.; Matsuhashi, H.; Arata, K. Biodiesel Fuel Production with Solid Superacid Catalysis in Fixed Bed Reactor under Atmospheric Pressure. *Catal. Commun.* **2004**, *5* (12), 721−723.
(115) Aziz, M. A. A.; Puad, K.; Triwahyono, S.; Jalil, A. A.; Khayoon, M. S.; Atabani, A. E.; Ramli, Z.; Majid, Z. A.; Prasetyoko, D.; Hartanto, D. Transesterification of Croton Megalocarpus Oil to Biodiesel over WO_3 Supported on Silica Mesoporous-Macroparticles Catalyst. *Chem. Eng. J.* **2017**, *316*, 882−892.
(116) Sudarsanam, P.; Peeters, E.; Makshina, E. V.; Parvulescu, V. I.; Sels, B. F. Advances in Porous and Nanoscale Catalysts for Viable Biomass Conversion. *Chem. Soc. Rev.* **2019**, *48* (8), 2366−2421.
(117) Jiménez-López, A.; Jiménez-Morales, I.; Santamaría-González, J.; Maireles-Torres, P. Biodiesel Production from Sunflower Oil by Tungsten Oxide Supported on Zirconium Doped MCM-41 Silica. *J. Mol. Catal. A: Chem.* **2011**, *335* (1−2), 205−209.
(118) Xie, W.; Zhao, L. Heterogeneous CaO−MoO_3−SBA-15 Catalysts for Biodiesel Production from Soybean Oil. *Energy Convers. Manage.* **2014**, *79*, 34−42.
(119) Chen, C.; Cai, L.; Zhang, L.; Fu, W.; Hong, Y.; Gao, X.; Jiang, Y.; Li, L.; Yan, X.; Wu, G. Transesterification of Rice Bran Oil to Biodiesel Using Mesoporous NaBeta Zeolite-Supported Molybdenum Catalyst: Experimental and Kinetic Studies. *Chem. Eng. J.* **2020**, *382*, 122839.
(120) Alhassan, F. H.; Rashid, U.; Taufiq-Yap, Y. H. Biodiesel Synthesis Catalyzed by Transition Metal Oxides: Ferric-Manganese Doped Tungstated/Molybdena Nanoparticle Catalyst. *J. Oleo Sci.* **2015**, *64* (1), 91−99.
(121) Jacobson, K.; Gopinath, R.; Meher, L.; Dalai, A. Solid Acid Catalyzed Biodiesel Production from Waste Cooking Oil. *Appl. Catal., B* **2008**, *85* (1−2), 86−91.
(122) Komintarachat, C.; Chuepeng, S. Solid Acid Catalyst for Biodiesel Production from Waste Used Cooking Oils. *Ind. Eng. Chem. Res.* **2009**, *48* (20), 9350−9353.
(123) Kaur, M.; Malhotra, R.; Ali, A. Tungsten Supported Ti/SiO_2 Nanoflowers as Reusable Heterogeneous Catalyst for Biodiesel Production. *Renewable Energy* **2018**, *116*, 109−119.
(124) Veillette, M.; Giroir-Fendler, A.; Faucheux, N.; Heitz, M. Esterification of Free Fatty Acids with Methanol to Biodiesel Using Heterogeneous Catalysts: From Model Acid Oil to Microalgae Lipids. *Chem. Eng. J.* **2017**, *308*, 101−109.
(125) Park, Y.-M.; Lee, D.-W.; Kim, D.-K.; Lee, J.-S.; Lee, K.-Y. The Heterogeneous Catalyst System for the Continuous Conversion of Free Fatty Acids in Used Vegetable Oils for the Production of Biodiesel. *Catal. Today* **2008**, *131* (1−4), 238−243.
(126) Bail, A.; dos Santos, V. C.; de Freitas, M. R.; Ramos, L. P.; Schreiner, W. H.; Ricci, G. P.; Ciuffi, K. J.; Nakagaki, S. Investigation of a Molybdenum-Containing Silica Catalyst Synthesized by the Sol−Gel Process in Heterogeneous Catalytic Esterification Reactions Using Methanol and Ethanol. *Appl. Catal., B* **2013**, *130*−*131*, 314−324.
(127) dos Santos, V. C.; Wilson, K.; Lee, A. F.; Nakagaki, S. Physicochemical Properties of WO_x/ZrO_2 Catalysts for Palmitic Acid Esterification. *Appl. Catal., B* **2015**, *162*, 75−84.
(128) Rao, K. N.; Sridhar, A.; Lee, A. F.; Tavener, S. J.; Young, N. A.; Wilson, K. Zirconium Phosphate Supported Tungsten Oxide Solid Acid Catalysts for the Esterification of Palmitic Acid. *Green Chem.* **2006**, *8* (9), 790.
(129) Mutlu, V. N.; Yilmaz, S. Esterification of Cetyl Alcohol with Palmitic Acid over WO_3/Zr-SBA-15 and Zr-SBA-15 Catalysts. *Appl. Catal., A* **2016**, *522*, 194−200.
(130) Jiménez-Morales, I.; Santamaría-González, J.; Maireles-Torres, P.; Jiménez-López, A. Zirconium Doped MCM-41 Supported WO_3 Solid Acid Catalysts for the Esterification of Oleic Acid with Methanol. *Appl. Catal., A* **2010**, *379* (1−2), 61−68.
(131) Zhang, Q.; Li, H.; Yang, S. Facile and Low-Cost Synthesis of Mesoporous Ti−Mo Bi-Metal Oxide Catalysts for Biodiesel Production from Esterification of Free Fatty Acids in *Jatropha Curcas* Crude Oil. *J. Oleo Sci.* **2018**, *67* (5), 579−588.
(132) Zhang, Q.; Wei, F.; Ma, P.; Zhang, Y.; Wei, F.; Chen, H. Mesoporous Al−Mo Oxides as an Effective and Stable Catalyst for the Synthesis of Biodiesel from the Esterification of Free-Fatty Acids in Non-Edible Oils. *Waste Biomass Valorization* **2018**, *9* (6), 911−918.
(133) Sarkar, A.; Ghosh, S. K.; Pramanik, P. Investigation of the Catalytic Efficiency of a New Mesoporous Catalyst SnO_2/WO_3 towards Oleic Acid Esterification. *J. Mol. Catal. A: Chem.* **2010**, *327* (1−2), 73−79.
(134) Ketzer, F.; Celante, D.; de Castilhos, F. Catalytic Performance and Ultrasonic-Assisted Impregnation Effects on WO_3/USY Zeolites in Esterification of Oleic Acid with Methyl Acetate. *Microporous Mesoporous Mater.* **2020**, *291*, 109704.
(135) Kong, P. S.; Aroua, M. K.; Daud, W. M. A. W.; Lee, H. V.; Cognet, P.; Pérès, Y. Catalytic Role of Solid Acid Catalysts in Glycerol

https://doi.org/10.1021/acscatal.1c03326
ACS Catal. 2021, 11, 13603−13648

Acetylation for the Production of Bio-Additives: A Review. *RSC Adv.* **2016**, *6* (73), 68885−68905.
(136) Galhardo, T. S.; Simone, N.; Gonçalves, M.; Figueiredo, F. C. A.; Mandelli, D.; Carvalho, W. A. Preparation of Sulfonated Carbons from Rice Husk and Their Application in Catalytic Conversion of Glycerol. *ACS Sustainable Chem. Eng.* **2013**, *1* (11), 1381−1389.
(137) Ghoreishi, K. B.; Yarmo, M. A.; Nordin, N. M.; Samsudin, M. W. Enhanced Catalyst Activity of WO_3 Using Polypyrrole as Support for Acidic Esterification of Glycerol with Acetic Acid. *J. Chem.* **2013**, *2013*, 1−10.
(138) Stawicka, K.; Díaz-Álvarez, A. E.; Calvino-Casilda, V.; Trejda, M.; Bañares, M. A.; Ziolek, M. The Role of Brønsted and Lewis Acid Sites in Acetalization of Glycerol over Modified Mesoporous Cellular Foams. *J. Phys. Chem. C* **2016**, *120* (30), 16699−16711.
(139) Neves, P.; Russo, P. A.; Fernandes, A.; Antunes, M. M.; Farinha, J.; Pillinger, M.; Ribeiro, M. F.; Castanheiro, J. E.; Valente, A. A. Mesoporous Zirconia-Based Mixed Oxides as Versatile Acid Catalysts for Producing Bio-Additives from Furfuryl Alcohol and Glycerol. *Appl. Catal., A* **2014**, *487*, 148−157.
(140) Umbarkar, S. B.; Kotbagi, T. V.; Biradar, A. V.; Pasricha, R.; Chanale, J.; Dongare, M. K.; Mamede, A.-S.; Lancelot, C.; Payen, E. Acetalization of Glycerol Using Mesoporous MoO_3/SiO_2 Solid Acid Catalyst. *J. Mol. Catal. A: Chem.* **2009**, *310* (1−2), 150−158.
(141) Li, Z.; Miao, Z.; Wang, X.; Zhao, J.; Zhou, J.; Si, W.; Zhuo, S. One-Pot Synthesis of ZrMo-KIT-6 Solid Acid Catalyst for Solvent-Free Conversion of Glycerol to Solketal. *Fuel* **2018**, *233*, 377−387.
(142) Ulgen, A.; Hoelderich, W. F. Conversion of Glycerol to Acrolein in the Presence of WO_3/TiO_2 Catalysts. *Appl. Catal., A* **2011**, *400* (1), 34−38.
(143) Massa, M.; Andersson, A.; Finocchio, E.; Busca, G.; Lenrick, F.; Wallenberg, L. R. Performance of ZrO_2-Supported Nb- and W-Oxide in the Gas-Phase Dehydration of Glycerol to Acrolein. *J. Catal.* **2013**, *297*, 93−109.
(144) Dalil, M.; Carnevali, D.; Dubois, J.-L.; Patience, G. S. Transient Acrolein Selectivity and Carbon Deposition Study of Glycerol Dehydration over WO_3/TiO_2 Catalyst. *Chem. Eng. J.* **2015**, *270*, 557−563.
(145) Chai, S.-H.; Tao, L.-Z.; Yan, B.; Vedrine, J. C.; Xu, B.-Q. Sustainable Production of Acrolein: Effects of Reaction Variables, Modifiers Doping and ZrO_2 Origin on the Performance of WO_3/ZrO_2 Catalyst for the Gas-Phase Dehydration of Glycerol. *RSC Adv.* **2014**, *4* (9), 4619−4630.
(146) Chai, S.-H.; Wang, H.-P.; Liang, Y.; Xu, B.-Q. Sustainable Production of Acrolein: Investigation of Solid Acid−Base Catalysts for Gas-Phase Dehydration of Glycerol. *Green Chem.* **2007**, *9* (10), 1130.
(147) Delgado, D.; Fernández-Arroyo, A.; Domine, M. E.; García-González, E.; López Nieto, J. M. W−Nb−O Oxides with Tunable Acid Properties as Efficient Catalysts for the Transformation of Biomass-Derived Oxygenates in Aqueous Systems. *Catal. Sci. Technol.* **2019**, *9* (12), 3126−3136.
(148) Cecilia, J. A.; García-Sancho, C.; Mérida-Robles, J. M.; Santamaría González, J.; Moreno-Tost, R.; Maireles-Torres, P. WO_3 Supported on Zr Doped Mesoporous SBA-15 Silica for Glycerol Dehydration to Acrolein. *Appl. Catal., A* **2016**, *516*, 30−40.
(149) Massa, M.; Andersson, A.; Finocchio, E.; Busca, G. Gas-Phase Dehydration of Glycerol to Acrolein over Al_2O_3-, SiO_2-, and TiO_2-Supported Nb- and W-Oxide Catalysts. *J. Catal.* **2013**, *307*, 170−184.
(150) Aihara, T.; Asazuma, K.; Miura, H.; Shishido, T. Highly Active and Durable WO_3/Al_2O_3 Catalysts for Gas-Phase Dehydration of Polyols. *RSC Adv.* **2020**, *10* (61), 37538−37544.
(151) Lauriol-Garbey, P.; Loridant, S.; Bellière-Baca, V.; Rey, P.; Millet, J.-M. M. Gas Phase Dehydration of Glycerol to Acrolein over WO_3/ZrO_2 Catalysts: Improvement of Selectivity and Stability by Doping with SiO_2. *Catal. Commun.* **2011**, *16* (1), 170−174.
(152) Yu, W.; Wang, P.; Zhou, C.; Zhao, H.; Tong, D.; Zhang, H.; Yang, H.; Ji, S.; Wang, H. Acid-Activated and WO_x-Loaded Montmorillonite Catalysts and Their Catalytic Behaviors in Glycerol Dehydration. *Chin. J. Catal.* **2017**, *38* (6), 1087−1100.
(153) Akizuki, M.; Sano, K.; Oshima, Y. Effect of Supercritical Water on the Stability of WO_x/TiO_2 and NbO_x/TiO_2 Catalysts during Glycerol Dehydration. *J. Supercrit. Fluids* **2016**, *113*, 158−165.
(154) Akizuki, M.; Oshima, Y. Kinetics of Glycerol Dehydration with WO_3/TiO_2 in Supercritical Water. *Ind. Eng. Chem. Res.* **2012**, *51* (38), 12253−12257.
(155) Dalil, M.; Carnevali, D.; Edake, M.; Auroux, A.; Dubois, J.-L.; Patience, G. S. Gas Phase Dehydration of Glycerol to Acrolein: Coke on WO_3/TiO_2 Reduces by-Products. *J. Mol. Catal. A: Chem.* **2016**, *421*, 146−155.
(156) Santos, R. C. R.; Braga, D. M. V; Pinheiro, A. N.; Leite, E. R.; Freire, V. N.; Longhinotti, E.; Valentini, A. Role of Cu, Ni and Co Metals in the Acidic and Redox Properties of Mo Catalysts Supported on Al_2O_3 Spheres for Glycerol Conversion. *Catal. Sci. Technol.* **2016**, *6* (13), 4986−5002.
(157) Bezerra, F.; Altino, H.; Soares, R. Oxidative Dehydration of Glycerol over Molybdenum- and Vanadium-Based Catalysts. *J. Braz. Chem. Soc.* **2018**, *30* (5), 1025−1033.
(158) Possato, L. G.; Acevedo, M. D.; Padró, C. L.; Briois, V.; Passos, A. R.; Pulcinelli, S. H.; Santilli, C. V.; Martins, L. Activation of Mo and V Oxides Supported on ZSM-5 Zeolite Catalysts Followed by in Situ XAS and XRD and Their Uses in Oxydehydration of Glycerol. *Mol. Catal.* **2020**, *481*, 110158.
(159) Nakagawa, Y.; Tamura, M.; Tomishige, K. Catalytic Materials for the Hydrogenolysis of Glycerol to 1,3-Propanediol. *J. Mater. Chem. A* **2014**, *2* (19), 6688−6702.
(160) Shozi, M. L.; Dasireddy, V. D. B. C.; Singh, S.; Mohlala, P.; Morgan, D. J.; Friedrich, H. B. Hydrogenolysis of Glycerol to Monoalcohols over Supported Mo and W Catalysts. *ACS Sustainable Chem. Eng.* **2016**, *4* (10), 5752−5760.
(161) Zhu, S.; Gao, X.; Zhu, Y.; Cui, J.; Zheng, H.; Li, Y. SiO_2 Promoted $Pt/WO_x/ZrO_2$ Catalysts for the Selective Hydrogenolysis of Glycerol to 1,3-Propanediol. *Appl. Catal., B* **2014**, *158−159*, 391−399.
(162) Kurosaka, T.; Maruyama, H.; Naribayashi, I.; Sasaki, Y. Production of 1,3-Propanediol by Hydrogenolysis of Glycerol Catalyzed by $Pt/WO_3/ZrO_2$. *Catal. Commun.* **2008**, *9* (6), 1360−1363.
(163) Fan, Y.; Cheng, S.; Wang, H.; Tian, J.; Xie, S.; Pei, Y.; Qiao, M.; Zong, B. Pt−WO on Monoclinic or Tetrahedral ZrO_2: Crystal Phase Effect of Zirconia on Glycerol Hydrogenolysis to 1,3-Propanediol. *Appl. Catal., B* **2017**, *217*, 331−341.
(164) Edake, M.; Dalil, M.; Darabi Mahboub, M. J.; Dubois, J.-L.; Patience, G. S. Catalytic Glycerol Hydrogenolysis to 1,3-Propanediol in a Gas−Solid Fluidized Bed. *RSC Adv.* **2017**, *7* (7), 3853−3860.
(165) García-Fernández, S.; Gandarias, I.; Requies, J.; Soulimani, F.; Arias, P. L.; Weckhuysen, B. M. The Role of Tungsten Oxide in the Selective Hydrogenolysis of Glycerol to 1,3-Propanediol over $Pt/WO_x/Al_2O_3$. *Appl. Catal., B* **2017**, *204*, 260−272.
(166) Aihara, T.; Miura, H.; Shishido, T. Investigation of the Mechanism of the Selective Hydrogenolysis of C−O Bonds over a $Pt/WO_3/Al_2O_3$ Catalyst. *Catal. Today* **2020**, *352*, 73−79.
(167) Aihara, T.; Miura, H.; Shishido, T. Effect of Perimeter Interface Length between 2D WO_3 Monolayer Domain and γ-Al_2O_3 on Selective Hydrogenolysis of Glycerol to 1,3-Propanediol. *Catal. Sci. Technol.* **2019**, *9* (19), 5359−5367.
(168) Wang, B.; Liu, F.; Guan, W.; Wang, A.; Zhang, T. Promoting the Effect of Au on the Selective Hydrogenolysis of Glycerol to 1,3-Propanediol over the $Pt/WO_x/Al_2O_3$ Catalyst. *ACS Sustainable Chem. Eng.* **2021**, *9* (16), 5705−5715.
(169) Bhowmik, S.; Enjamuri, N.; Darbha, S. Hydrogenolysis of Glycerol in an Aqueous Medium over Pt/WO_3/Zirconium Phosphate Catalysts Studied by ^1H NMR Spectroscopy. *New J. Chem.* **2021**, *45* (11), 5013−5022.
(170) Liu, L.; Zhang, Y.; Wang, A.; Zhang, T. Mesoporous WO_3 Supported Pt Catalyst for Hydrogenolysis of Glycerol to 1,3-Propanediol. *Chin. J. Catal.* **2012**, *33* (7), 1257−1261.
(171) Gong, L.; Lu, Y.; Ding, Y.; Lin, R.; Li, J.; Dong, W.; Wang, T.; Chen, W. Selective Hydrogenolysis of Glycerol to 1,3-Propanediol over a $Pt/WO_3/TiO_2/SiO_2$ Catalyst in Aqueous Media. *Appl. Catal., A* **2010**, *390* (1−2), 119−126.

https://doi.org/10.1021/acscatal.1c03326
ACS Catal. 2021, 11, 13603−13648

(172) Koso, S.; Watanabe, H.; Okumura, K.; Nakagawa, Y.; Tomishige, K. Comparative Study of Rh−MoO_x and Rh−ReO_x Supported on SiO_2 for the Hydrogenolysis of Ethers and Polyols. *Appl. Catal., B* **2012**, *111*−*112*, 27−37.
(173) Checa, M.; Montes, V.; Hidalgo-Carrillo, J.; Marinas, A.; Urbano, F. Influence of Boron, Tungsten and Molybdenum Modifiers on Zirconia Based Pt Catalyst for Glycerol Valorization. *Nanomaterials* **2019**, *9* (4), 509.
(174) Samudrala, S.; Bhattacharya, S. Toward the Sustainable Synthesis of Propanols from Renewable Glycerol over MoO_3-Al_2O_3 Supported Palladium Catalysts. *Catalysts* **2018**, *8* (9), 385.
(175) Li, D.; Zhou, Z.; Qin, J.; Li, Y.; Liu, Z.; Wu, W. Cu-WO_x-TiO_2 Catalysts by Modified Evaporation-Induced Self-Assembly Method for Glycerol Hydrogenolysis to 1,3-Propanediol. *ChemistrySelect* **2018**, *3* (9), 2479−2486.
(176) Lan, H.; Zeng, J.; Zhang, B.; Jiang, Y. CeO_2 Promoting Allyl Alcohol Synthesis from Glycerol Direct Conversion over MoFe/CeO_2 Oxide Catalysts: Morphology and Particle Sizes Dependent. *Res. Chem. Intermed.* **2019**, *45* (3), 1565−1580.
(177) Mitran, G.; Pavel, O. D.; Florea, M.; Mieritz, D. G.; Seo, D.-K. Hydrogen Production from Glycerol Steam Reforming over Molybdena−Alumina Catalysts. *Catal. Commun.* **2016**, *77*, 83−88.
(178) Kabir, G.; Hameed, B. H. Recent Progress on Catalytic Pyrolysis of Lignocellulosic Biomass to High-Grade Bio-Oil and Bio-Chemicals. *Renewable Sustainable Energy Rev.* **2017**, *70*, 945−967.
(179) Wang, H.; Male, J.; Wang, Y. Recent Advances in Hydrotreating of Pyrolysis Bio-Oil and Its Oxygen-Containing Model Compounds. *ACS Catal.* **2013**, *3* (5), 1047−1070.
(180) Yang, Z.; Kumar, A.; Apblett, A. Integration of Biomass Catalytic Pyrolysis and Methane Aromatization over Mo/HZSM-5 Catalysts. *J. Anal. Appl. Pyrolysis* **2016**, *120*, 484−492.
(181) Ciddor, L.; Bennett, J. A.; Hunns, J. A.; Wilson, K.; Lee, A. F. Catalytic Upgrading of Bio-Oils by Esterification. *J. Chem. Technol. Biotechnol.* **2015**, *90* (5), 780−795.
(182) Shao, S.; Zhang, H.; Xiao, R.; Shen, D. Back Cover: Catalytic Conversion of Furan to Hydrocarbons Using HZSM-5: Coking Behavior and Kinetic Modeling Including Coke Deposition. *Energy Technol.* **2017**, *5*, 111.
(183) Liu, C.; Wang, H.; Karim, A. M.; Sun, J.; Wang, Y. Catalytic Fast Pyrolysis of Lignocellulosic Biomass. *Chem. Soc. Rev.* **2014**, *43* (22), 7594−7623.
(184) Murugappan, K.; Mukarakate, C.; Budhi, S.; Shetty, M.; Nimlos, M. R.; Román-Leshkov, Y. Supported Molybdenum Oxides as Effective Catalysts for the Catalytic Fast Pyrolysis of Lignocellulosic Biomass. *Green Chem.* **2016**, *18* (20), 5548−5557.
(185) Budhi, S.; Mukarakate, C.; Iisa, K.; Pylypenko, S.; Ciesielski, P. N.; Yung, M. M.; Donohoe, B. S.; Katahira, R.; Nimlos, M. R.; Trewyn, B. G. Molybdenum Incorporated Mesoporous Silica Catalyst for Production of Biofuels and Value-Added Chemicals via Catalytic Fast Pyrolysis. *Green Chem.* **2015**, *17* (5), 3035−3046.
(186) Wang, K.; Dayton, D. C.; Peters, J. E.; Mante, O. D. Reactive Catalytic Fast Pyrolysis of Biomass to Produce High-Quality Bio-Crude. *Green Chem.* **2017**, *19* (14), 3243−3251.
(187) Yang, Z.; Kumar, A.; Apblett, A. W.; Moneeb, A. M. Co-Pyrolysis of Torrefied Biomass and Methane over Molybdenum Modified Bimetallic HZSM-5 Catalyst for Hydrocarbons Production. *Green Chem.* **2017**, *19* (3), 757−768.
(188) Nolte, M. W.; Zhang, J.; Shanks, B. H. Ex Situ Hydrodeoxygenation in Biomass Pyrolysis Using Molybdenum Oxide and Low Pressure Hydrogen. *Green Chem.* **2016**, *18* (1), 134−138.
(189) Eschenbacher, A.; Saraeian, A.; Shanks, B. H.; Jensen, P. A.; Li, C.; Duus, J. Ø.; Hansen, A. B.; Mentzel, U. V.; Henriksen, U. B.; Ahrenfeldt, J.; Jensen, A. D. Enhancing Bio-Oil Quality and Energy Recovery by Atmospheric Hydrodeoxygenation of Wheat Straw Pyrolysis Vapors Using Pt and Mo-Based Catalysts. *Sustain. Energy Fuels* **2020**, *4* (4), 1991−2008.
(190) Bhaumik, P.; Dhepe, P. L. From Lignocellulosic Biomass to Furfural: Insight into the Active Species of a Silica-Supported Tungsten Oxide Catalyst. *ChemCatChem* **2017**, *9* (14), 2709−2716.
(191) Grilc, M.; Veryasov, G.; Likozar, B.; Jesih, A.; Levec, J. Hydrodeoxygenation of Solvolysed Lignocellulosic Biomass by Unsupported MoS_2, MoO_2, Mo_2C and WS_2 Catalysts. *Appl. Catal., B* **2015**, *163*, 467−477.
(192) Dedsuksophon, W.; Faungnawakij, K.; Champreda, V.; Laosiripojana, N. Hydrolysis/Dehydration/Aldol-Condensation/Hydrogenation of Lignocellulosic Biomass and Biomass-Derived Carbohydrates in the Presence of Pd/WO_3−ZrO_2 in a Single Reactor. *Bioresour. Technol.* **2011**, *102* (2), 2040−2046.
(193) de Almeida, R. M.; de Albuquerque, N. J. A.; Souza, F. T. C.; Meneghetti, S. M. P. Catalysts Based on TiO_2 Anchored with MoO_3 or SO_4^{2-} for Conversion of Cellulose into Chemicals. *Catal. Sci. Technol.* **2016**, *6* (9), 3137−3142.
(194) Kobayashi, H.; Komanoya, T.; Guha, S. K.; Hara, K.; Fukuoka, A. Conversion of Cellulose into Renewable Chemicals by Supported Metal Catalysis. *Appl. Catal., A* **2011**, *409*−*410*, 13−20.
(195) Geboers, J.; Van de Vyver, S.; Carpentier, K.; Jacobs, P.; Sels, B. Efficient Hydrolytic Hydrogenation of Cellulose in the Presence of Ru-Loaded Zeolites and Trace Amounts of Mineral Acid. *Chem. Commun.* **2011**, *47* (19), 5590−5592.
(196) Chambon, F.; Rataboul, F.; Pinel, C.; Cabiac, A.; Guillon, E.; Essayem, N. Cellulose Hydrothermal Conversion Promoted by Heterogeneous Brønsted and Lewis Acids: Remarkable Efficiency of Solid Lewis Acids to Produce Lactic Acid. *Appl. Catal., B* **2011**, *105* (1−2), 171−181.
(197) Chambon, F.; Rataboul, F.; Pinel, C.; Cabiac, A.; Guillon, E.; Essayem, N. Cellulose Conversion with Tungstated-Alumina-Based Catalysts: Influence of the Presence of Platinum and Mechanistic Studies. *ChemSusChem* **2013**, *6* (3), 500−507.
(198) de Almeida, R. M.; de Albuquerque, N. J. A.; Souza, F. T. C.; Meneghetti, S. M. P. Catalysts Based on TiO_2 Anchored with MoO_3 or SO_4^{2-} for Conversion of Cellulose into Chemicals. *Catal. Sci. Technol.* **2016**, *6* (9), 3137−3142.
(199) Wiesfeld, J. J.; Peršolja, P.; Rollier, F. A.; Elemans-Mehring, A. M.; Hensen, E. J. M. Cellulose Conversion to Ethylene Glycol by Tungsten Oxide-Based Catalysts. *Mol. Catal.* **2019**, *473* (March), 110400.
(200) Lucas, M.; Fabičovicová, K.; Claus, P. Hydrothermally Stable Ruthenium−Zirconium−Tungsten Catalyst for Cellulose Hydrogenolysis to Polyols. *ChemCatChem* **2018**, *10* (3), 612−618.
(201) Baek, I. G.; You, S. J.; Park, E. D. Direct Conversion of Cellulose into Polyols over Ni/W/SiO_2-Al_2O_3. *Bioresour. Technol.* **2012**, *114*, 684−690.
(202) Xiao, Z.; Mao, J.; Ji, J.; Sha, R.; Fan, Y.; Xing, C. Preparation of Nano-Scale Nickel-Tungsten Catalysts by pH Value Control and Application in Hydrogenolysis of Cellulose to Polyols. *J. Fuel Chem. Technol.* **2017**, *45* (6), 641−650.
(203) Xiao, Z.; Xu, Y.; Yu, H.; Mao, J.; Cai, C.; Sha, R. Selective Transformation of Cellulose to C_2−C_3 Polyols on M-W/SBA-15 (M = Ni, Pd, Zn, Cu) under Low Hydrogen Pressure. *IOP Conf. Ser. Earth Environ. Sci.* **2017**, *69* (1), No. 012066.
(204) Fabičovicová, K.; Malter, O.; Lucas, M.; Claus, P. Hydrogenolysis of Cellulose to Valuable Chemicals over Activated Carbon Supported Mono- and Bimetallic Nickel/Tungsten Catalysts. *Green Chem.* **2014**, *16* (7), 3580−3588.
(205) Ji, N.; Zhang, T.; Zheng, M.; Wang, A.; Wang, H.; Wang, X.; Chen, J. G. Direct Catalytic Conversion of Cellulose into Ethylene Glycol Using Nickel-Promoted Tungsten Carbide Catalysts. *Angew. Chem., Int. Ed.* **2008**, *47* (44), 8510−8513.
(206) Wang, A.; Zhang, T. One-Pot Conversion of Cellulose to Ethylene Glycol with Multifunctional Tungsten-Based Catalysts. *Acc. Chem. Res.* **2013**, *46* (7), 1377−1386.
(207) Chai, J.; Zhu, S.; Cen, Y.; Guo, J.; Wang, J.; Fan, W. Effect of Tungsten Surface Density of WO_3−ZrO_2 on Its Catalytic Performance in Hydrogenolysis of Cellulose to Ethylene Glycol. *RSC Adv.* **2017**, *7* (14), 8567−8574.
(208) Liu, Y.; Luo, C.; Liu, H. Tungsten Trioxide Promoted Selective Conversion of Cellulose into Propylene Glycol and Ethylene Glycol on

https://doi.org/10.1021/acscatal.1c03326
ACS Catal. 2021, 11, 13603−13648

a Ruthenium Catalyst. *Angew. Chem., Int. Ed.* **2012**, *51* (13), 3249−3253.
(209) Zheng, M.; Pang, J.; Sun, R.; Wang, A.; Zhang, T. Selectivity Control for Cellulose to Diols: Dancing on Eggs. *ACS Catal.* **2017**, *7* (3), 1939−1954.
(210) Zhang, K.; Yang, G.; Lyu, G.; Jia, Z.; Lucia, L. A.; Chen, J. One-Pot Solvothermal Synthesis of Graphene Nanocomposites for Catalytic Conversion of Cellulose to Ethylene Glycol. *ACS Sustainable Chem. Eng.* **2019**, *7* (13), 11110−11117.
(211) Yang, M.; Qi, H.; Liu, F.; Ren, Y.; Pan, X.; Zhang, L.; Liu, X.; Wang, H.; Pang, J.; Zheng, M.; Wang, A.; Zhang, T. One-Pot Production of Cellulosic Ethanol via Tandem Catalysis over a Multifunctional Mo/Pt/WO_x Catalyst. *Joule* **2019**, *3* (8), 1937−1948.
(212) Nolte, M. W.; Saraeian, A.; Shanks, B. H. Hydrodeoxygenation of Cellulose Pyrolysis Model Compounds Using Molybdenum Oxide and Low Pressure Hydrogen. *Green Chem.* **2017**, *19* (15), 3654−3664.
(213) Luo, J.; Lee, J. D.; Yun, H.; Wang, C.; Monai, M.; Murray, C. B.; Fornasiero, P.; Gorte, R. J. Base Metal-Pt Alloys: A General Route to High Selectivity and Stability in the Production of Biofuels from HMF. *Appl. Catal., B* **2016**, *199*, 439−446.
(214) Wang, Q.; Yu, Z.; Feng, J.; Fornasiero, P.; He, Y.; Li, D. Insight into the Effect of Dual Active Cu^0/Cu^+ Sites in a Cu/ZnO-Al_2O_3 Catalyst on 5-Hydroxylmethylfurfural Hydrodeoxygenation. *ACS Sustainable Chem. Eng.* **2020**, *8* (40), 15288−15298.
(215) Chhabra, T.; Bahuguna, A.; Dhankhar, S. S.; Nagaraja, C. M.; Krishnan, V. Sulfonated Graphitic Carbon Nitride as a Highly Selective and Efficient Heterogeneous Catalyst for the Conversion of Biomass-Derived Saccharides to 5-Hydroxymethylfurfural in Green Solvents. *Green Chem.* **2019**, *21* (21), 6012−6026.
(216) Pal, P.; Saravanamurugan, S. Recent Advances in the Development of 5-Hydroxymethylfurfural Oxidation with Base (Non-precious)-Metal-Containing Catalysts. *ChemSusChem* **2019**, *12* (1), 145−163.
(217) Li, H.; Zhang, Q.; Liu, J.; Liu, X.; Chang, F.; Liu, Y.; Xue, W.; Yang, S. Selective Transformation of Carbohydrates into HMF Promoted by Carboxylic Acids Modified ZrMo Mixed Oxides. *Biomass Convers. Biorefin.* **2014**, *4* (1), 59−66.
(218) Aid, T.; Koel, M.; Lopp, M.; Vaher, M. Metal-Catalyzed Degradation of Cellulose in Ionic Liquid Media. *Inorganics* **2018**, *6* (3), 78.
(219) Yin, W.; Venderbosch, R. H.; Alekseeva, M. V.; Figueirêdo, M. B.; Heeres, H.; Khromova, S. A.; Yakovlev, V. A.; Cannilla, C.; Bonura, G.; Frusteri, F.; Heeres, H. J. Hydrotreatment of the Carbohydrate-Rich Fraction of Pyrolysis Liquids Using Bimetallic Ni Based Catalyst: Catalyst Activity and Product Property Relations. *Fuel Process. Technol.* **2018**, *169*, 258−268.
(220) Levi, N.; Khenkin, A. M.; Hailegnaw, B.; Neumann, R. Depolymerization of Cellulose in Water Catalyzed by Phenylboronic Acid Derivatives. *ACS Sustainable Chem. Eng.* **2016**, *4* (10), 5799−5803.
(221) Kourieh, R.; Bennici, S.; Marzo, M.; Gervasini, A.; Auroux, A. Investigation of the WO_3/ZrO_2 Surface Acidic Properties for the Aqueous Hydrolysis of Cellobiose. *Catal. Commun.* **2012**, *19*, 119−126.
(222) Wang, H.; Guo, Y.; Chang, C.; Zhu, X.; Liu, X.; Han, J.; Ge, Q. Enhancing Tungsten Oxide/SBA-15 Catalysts for Hydrolysis of Cellobiose through Doping ZrO_2. *Appl. Catal., A* **2016**, *523*, 182−192.
(223) Tagusagawa, C.; Takagaki, A.; Iguchi, A.; Takanabe, K.; Kondo, J. N.; Ebitani, K.; Tatsumi, T.; Domen, K. Synthesis and Characterization of Mesoporous Ta−W Oxides as Strong Solid Acid Catalysts. *Chem. Mater.* **2010**, *22* (10), 3072−3078.
(224) Vilcocq, L.; Rebmann, É.; Cheah, Y. W.; Fongarland, P. Hydrolysis of Cellobiose and Xylan over TiO_2-Based Catalysts. *ACS Sustainable Chem. Eng.* **2018**, *6* (4), 5555−5565.
(225) Guo, J.; Zhu, S.; Cen, Y.; Qin, Z.; Wang, J.; Fan, W. Ordered Mesoporous Nb−W Oxides for the Conversion of Glucose to Fructose, Mannose and 5-Hydroxymethylfurfural. *Appl. Catal., B* **2017**, *200*, 611−619.
(226) Yatoo, M. A.; Saravanamurugan, S. Tin Grafted on Modified Alumina-Catalyzed Isomerisation of Glucose to Fructose. *Appl. Catal., A* **2019**, *582*, 117094.
(227) Wiesfeld, J. J.; Gaquere, R.; Hensen, E. J. M. Mesoporous Doped Tungsten Oxide for Glucose Dehydration to 5-Hydroxymethylfurfural. *ACS Sustainable Chem. Eng.* **2019**, *7* (8), 7552−7562.
(228) Han, H.; Zhao, H.; Liu, Y.; Li, Z.; Song, J.; Chu, W.; Sun, Z. Efficient Conversion of Fructose into 5-Hydroxymethylfurfural over WO_3/Reduced Graphene Oxide Catalysts. *RSC Adv.* **2017**, *7* (7), 3790−3795.
(229) Kawamura, K.; Yasuda, T.; Hatanaka, T.; Hamahiga, K.; Matsuda, N.; Ueshima, M.; Nakai, K. In Situ UV−VIS Spectrophotometry within the Second Time Scale as a Research Tool for Solid-State Catalyst and Liquid-Phase Reactions at High Temperatures: Its Application to the Formation of HMF from Glucose and Cellulose. *Chem. Eng. J.* **2017**, *307*, 1066−1075.
(230) Ganji, P.; Roy, S. Trade-Off between Acidic Sites and Crystallinity of the $WO_3−TiO_2$ Catalyst toward Dehydration of Glucose to 5-Hydroxymethylfurfural. *Energy Fuels* **2019**, *33* (6), 5293−5303.
(231) Córdova-Pérez, G. E.; Torres-Torres, G.; Ortíz-Chi, F.; Godavarthi, S.; Silahua-Pavón, A. A.; Izquierdo-Colorado, A.; Da Costa, P.; Hernández-Como, N.; Aleman, M.; Espinosa-González, C. G. Effect of Acid-Basic Sites Ratio on the Catalytic Activity to Obtain 5-HMF from Glucose Using Al_2O_3-TiO_2-W Catalysts. *ChemistrySelect* **2018**, *3* (45), 12854−12864.
(232) Guo, B.; He, L.; Tang, G.; Zhang, L.; Ye, L.; Yue, B.; Tsang, S. C. E.; He, H. Dehydration of Sugars to 5-Hydroxymethylfurfural and Non-Stoichiometric Formic and Levulinic Acids over Mesoporous Ta and Ta-W Oxide Solid Acid Catalysts. *Chin. J. Catal.* **2020**, *41* (8), 1248−1260.
(233) Liu, C.; Zhang, C.; Sun, S.; Liu, K.; Hao, S.; Xu, J.; Zhu, Y.; Li, Y. Effect of WO_x on Bifunctional Pd−WO_x/Al_2O_3 Catalysts for the Selective Hydrogenolysis of Glucose to 1,2-Propanediol. *ACS Catal.* **2015**, *5* (8), 4612−4623.
(234) Liu, Y.; Liu, Y.; Zhang, Y. The Synergistic Effects of Ru and WO_x for Aqueous-Phase Hydrogenation of Glucose to Lower Diols. *Appl. Catal., B* **2019**, *242*, 100−108.
(235) Liu, Y.; Liu, Y.; Wu, Q.; Zhang, Y. Catalytic Conversion of Glucose into Lower Diols over Highly Dispersed SiO_2-Supported Ru-W. *Catal. Commun.* **2019**, *129* (June), 105731.
(236) Hu, H.; Liu, S.; Zhang, W.; An, J.; Xia, H. Efficient Epimerization of Glucose to Mannose over Molybdenum-Based Catalyst in Aqueous Media. *ChemistrySelect* **2020**, *5* (5), 1728−1733.
(237) Zhang, Y.; Chen, H.; Gao, Y.; Yao, Z.; Wang, J.; Zhang, B.; Luo, K.; Du, S.; Su, D. S.; Zhang, J. MoO_x Nanoparticle Catalysts for D-Glucose Epimerization and Their Electrical Immobilization in a Continuous Flow Reactor. *ACS Appl. Mater. Interfaces* **2019**, *11* (47), 44118−44123.
(238) Yang, X.; Zhang, Y.; Zhou, L.; Gao, B.; Lu, T.; Su, Y.; Xu, J. Production of Lactic Acid Derivatives from Sugars over Post-Synthesized Sn-Beta Zeolite Promoted by WO_3. *Food Chem.* **2019**, *289*, 285−291.
(239) de Souza, R. L.; Yu, H.; Rataboul, F.; Essayem, N. 5-Hydroxymethylfurfural (5-HMF) Production from Hexoses: Limits of Heterogeneous Catalysis in Hydrothermal Conditions and Potential of Concentrated Aqueous Organic Acids as Reactive Solvent System. *Challenges* **2012**, *3* (2), 212−232.
(240) Sun, H.; Song, F.; Zhou, C.; Wan, X.; Jin, Y.; Dai, Y.; Zheng, J.; Yao, S.; Yang, Y. Lattice-Water-Induced Acid Sites in Tungsten Oxide Hydrate for Catalyzing Fructose Dehydration. *Catal. Commun.* **2021**, *149*, 106254.
(241) Wang, J.; Qu, T.; Liang, M.; Zhao, Z. Microwave Assisted Rapid Conversion of Fructose into 5-HMF over Solid Acid Catalysts. *RSC Adv.* **2015**, *5* (128), 106053−106060.
(242) dos Santos, T. V.; da Silva Avelino, D. O.; Meneghetti, M. R.; Meneghetti, S. M. P. Mixed Oxides Based on SnO_2 Impregnated with MoO_3: A Robust System to Apply in Fructose Conversion. *Catal. Commun.* **2018**, *114*, 120−123.

https://doi.org/10.1021/acscatal.1c03326
ACS Catal. 2021, 11, 13603−13648

(243) Raveendra, G.; Surendar, M.; Sai Prasad, P. S. Selective Conversion of Fructose to 5-Hydroxymethylfurfural over WO_3/SnO_2 Catalysts. *New J. Chem.* **2017**, *41* (16), 8520−8529.
(244) Zhang, Q.; Liu, X.; Yang, T.; Pu, Q.; Yue, C.; Zhang, S.; Zhang, Y. Catalytic Transfer of Fructose to 5-Hydroxymethylfurfural over Bimetal Oxide Catalysts. *Int. J. Chem. Eng.* **2019**, *2019*, 1−6.
(245) Liu, K.; Huang, X.; Pidko, E. A.; Hensen, E. J. M. MoO_3−TiO_2 Synergy in Oxidative Dehydrogenation of Lactic Acid to Pyruvic Acid. *Green Chem.* **2017**, *19* (13), 3014−3022.
(246) Feng, X.; Shen, C.; Ji, K.; Yin, J.; Tan, T. Production of p -Xylene from Bio-Based 2,5-Dimethylfuran over High Performance Catalyst WO_3/SBA-15. *Catal. Sci. Technol.* **2017**, *7* (23), 5540−5549.
(247) Cui, Z.; Fang, Y.; Tan, T. Mechanistic Insight of the Catalytic Role of WO_x/SiO_2 Catalyst in 2,5-Dimethylfuran to Para-Xylene Conversion by DFT Calculation. *Catal. Lett.* **2020**, *150* (3), 794−801.
(248) Cui, Z.; Feng, X.; Li, H.; Tan, T. Interconversion of Lewis Acid and Brønsted Acid Catalysts in Biomass-Derived Paraxylene Synthesis. *Chem. Eng. Sci.* **2020**, *227* (6), 115942.
(249) Liu, L.; Asano, T.; Nakagawa, Y.; Gu, M.; Li, C.; Tamura, M.; Tomishige, K. Structure and Performance Relationship of Silica-Supported Platinum-Tungsten Catalysts in Selective C-O Hydrogenolysis of Glycerol and 1,4-Anhydroerythritol. *Appl. Catal., B* **2021**, *292*, 120164.
(250) Liu, L.; Asano, T.; Nakagawa, Y.; Tamura, M.; Tomishige, K. One-Pot Synthesis of 1,3-Butanediol by 1,4-Anhydroerythritol Hydrogenolysis over a Tungsten-Modified Platinum on Silica Catalyst. *Green Chem.* **2020**, *22* (8), 2375−2380.
(251) Liu, C.; Sun, J.; Brown, H. M.; Marin-Flores, O. G.; Bays, J. T.; Karim, A. M.; Wang, Y. Aqueous Phase Hydrodeoxygenation of Polyols over Pd/WO_3-ZrO_2: Role of Pd-WO_3 Interaction and Hydrodeoxygenation Pathway. *Catal. Today* **2016**, *269*, 103−109.
(252) Zhu, S.; Wang, J.; Fan, W. Graphene-Based Catalysis for Biomass Conversion. *Catal. Sci. Technol.* **2015**, *5* (8), 3845−3858.
(253) Bhaumik, P.; Kane, T.; Dhepe, P. L. Silica and Zirconia Supported Tungsten, Molybdenum and Gallium Oxide Catalysts for the Synthesis of Furfural. *Catal. Sci. Technol.* **2014**, *4* (9), 2904−2907.
(254) Bhanja, P.; Bhaumik, A. Organic-Inorganic Hybrid Metal Phosphonates as Recyclable Heterogeneous Catalysts. *ChemCatChem* **2016**, *8* (9), 1607−1616.
(255) Antunes, M. M.; Lima, S.; Fernandes, A.; Candeias, J.; Pillinger, M.; Rocha, S. M.; Ribeiro, M. F.; Valente, A. A. Catalytic Dehydration of D-Xylose to 2-Furfuraldehyde in the Presence of Zr-(W,Al) Mixed Oxides. Tracing by-Products Using Two-Dimensional Gas Chromatography-Time-of-Flight Mass Spectrometry. *Catal. Today* **2012**, *195* (1), 127−135.
(256) Weingarten, R.; Tompsett, G. A.; Conner, W. C.; Huber, G. W. Design of Solid Acid Catalysts for Aqueous-Phase Dehydration of Carbohydrates: The Role of Lewis and Brønsted Acid Sites. *J. Catal.* **2011**, *279* (1), 174−182.
(257) Doiseau, A.-C.; Rataboul, F.; Burel, L.; Essayem, N. Synergy Effect between Solid Acid Catalysts and Concentrated Carboxylic Acids Solutions for Efficient Furfural Production from Xylose. *Catal. Today* **2014**, *226*, 176−184.
(258) Xu, C.; Paone, E.; Rodríguez-Padrón, D.; Luque, R.; Mauriello, F. Recent Catalytic Routes for the Preparation and the Upgrading of Biomass Derived Furfural and 5-Hydroxymethylfurfural. *Chem. Soc. Rev.* **2020**, *49* (13), 4273−4306.
(259) Pardo Cuervo, O. H.; Romanelli, G. P.; Cubillos, J. A.; Rojas, H. A.; Martínez, J. J. Selective Catalytic Dehydration of Xylose to Furfural and Fructose and Glucose to 5-Hydroximethylfurfural (HMF) Using Preyssler Heteropolyacid. *ChemistrySelect* **2020**, *5* (14), 4186−4193.
(260) Stucchi, M.; Alijani, S.; Manzoli, M.; Villa, A.; Lahti, R.; Galloni, M. G.; Lassi, U.; Prati, L. A Pt-Mo Hybrid Catalyst for Furfural Transformation. *Catal. Today* **2020**, *357*, 122−131.
(261) Wang, L.; Weng, Y.; Wang, X.; Yin, H.; Wang, F.; Xue, X.; Liu, X.; Wang, F.; Duan, P.; Zhang, Y. Synergistic Bimetallic RuMo Catalysts for Selective Rearrangement of Furfural to Cyclopentanol in Aqueous Phase. *Catal. Commun.* **2019**, *129*, 105745.
(262) Wang, C.; Lee, J. D.; Ji, Y.; Onn, T. M.; Luo, J.; Murray, C. B.; Gorte, R. J. A Study of Tetrahydrofurfuryl Alcohol to 1,5-Pentanediol Over Pt−WO_x/C. *Catal. Lett.* **2018**, *148* (4), 1047−1054.
(263) Feng, S.; Nagao, A.; Aihara, T.; Miura, H.; Shishido, T. Selective Hydrogenolysis of Tetrahydrofurfuryl Alcohol on $Pt/WO_3/ZrO_2$ Catalysts: Effect of WO_3 Loading Amount on Activity. *Catal. Today* **2018**, *303*, 207−212.
(264) Kuang, B.; Zhang, Q.; Fang, Y.; Bai, Y.; Qiu, S.; Wu, P.; Qin, Y.; Wang, T. Ring Opening of Cyclic Ether for Selective Synthesis of Renewable 1,5-Pentanediol over $Pt/WO_3@SiO_2$ Catalysts. *Ind. Eng. Chem. Res.* **2020**, *59* (20), 9372−9381.
(265) Koso, S.; Ueda, N.; Shinmi, Y.; Okumura, K.; Kizuka, T.; Tomishige, K. Promoting Effect of Mo on the Hydrogenolysis of Tetrahydrofurfuryl Alcohol to 1,5-Pentanediol over Rh/SiO_2. *J. Catal.* **2009**, *267* (1), 89−92.
(266) Prasomsri, T.; Nimmanwudipong, T.; Román-Leshkov, Y. Effective Hydrodeoxygenation of Biomass-Derived Oxygenates into Unsaturated Hydrocarbons by MoO_3 Using Low H_2 Pressures. *Energy Environ. Sci.* **2013**, *6* (6), 1732−1738.
(267) Asano, T.; Tamura, M.; Nakagawa, Y.; Tomishige, K. Selective Hydrodeoxygenation of 2-Furancarboxylic Acid to Valeric Acid over Molybdenum-Oxide-Modified Platinum Catalyst. *ACS Sustainable Chem. Eng.* **2016**, *4* (12), 6253−6257.
(268) Pizzi, R.; van Putten, R.-J.; Brust, H.; Perathoner, S.; Centi, G.; van der Waal, J. High-Throughput Screening of Heterogeneous Catalysts for the Conversion of Furfural to Bio-Based Fuel Components. *Catalysts* **2015**, *5* (4), 2244−2257.
(269) Chan, X.; Nan, W.; Mahajan, D.; Kim, T. Comprehensive Investigation of the Biomass Derived Furfuryl Alcohol Oligomer Formation over Tungsten Oxide Catalysts. *Catal. Commun.* **2015**, *72*, 11−15.
(270) Mullen, C. A.; Boateng, A. A. Catalytic Pyrolysis-GC/MS of Lignin from Several Sources. *Fuel Process. Technol.* **2010**, *91* (11), 1446−1458.
(271) Lotfi, S.; Boffito, D. C.; Patience, G. S. Gas−Solid Conversion of Lignin to Carboxylic Acids. *React. Chem. Eng.* **2016**, *1* (4), 397−408.
(272) Ma, X.; Cui, K.; Hao, W.; Ma, R.; Tian, Y.; Li, Y. Alumina Supported Molybdenum Catalyst for Lignin Valorization: Effect of Reduction Temperature. *Bioresour. Technol.* **2015**, *192*, 17−22.
(273) Deepa, A. K.; Dhepe, P. L. Solid Acid Catalyzed Depolymerization of Lignin into Value Added Aromatic Monomers. *RSC Adv.* **2014**, *4* (25), 12625−12629.
(274) Horáček, J.; Mikkola, J.-P.; Samikannu, A.; Šťávová, G.; Larsson, W.; Hora, L.; Kubička, D. Studies on Sodium Lignosulfonate Depolymerization Over Al_2O_3 Supported Catalysts Loaded with Metals and Metal Oxides in a Continuous Flow Reactor. *Top. Catal.* **2013**, *56* (9), 794−799.
(275) Oregui-Bengoechea, M.; Gandarias, I.; Miletić, N.; Simonsen, S. F.; Kronstad, A.; Arias, P. L.; Barth, T. Thermocatalytic Conversion of Lignin in an Ethanol/Formic Acid Medium with NiMo Catalysts: Role of the Metal and Acid Sites. *Appl. Catal., B* **2017**, *217*, 353−364.
(276) Huang, Y.; Hu, Y.; Ye, F.; Fang, Y. Lignin Pyrolysis and in Situ Hydrodeoxygenation over MoO_3: Interaction between MoO_3 and Lignin. *Energy Fuels* **2017**, *31* (8), 8356−8362.
(277) Tang, Z.; Wang, Y.; Chen, M.; Zhang, J.; Wang, C.; Yang, Z.; Zhang, H.; Wang, J. Study of Mo-Based Sepiolite Catalyst on Depolymerization of Lignin under Supercritical Ethanol. *Int. J. Energy Res.* **2020**, *44* (1), 257−268.
(278) Xiao, L.-P.; Wang, S.; Li, H.; Li, Z.; Shi, Z.-J.; Xiao, L.; Sun, R.-C.; Fang, Y.; Song, G. Catalytic Hydrogenolysis of Lignins into Phenolic Compounds over Carbon Nanotube Supported Molybdenum Oxide. *ACS Catal.* **2017**, *7* (11), 7535−7542.
(279) Bai, Y.; Cui, K.; Sang, Y.; Wu, K.; Yan, F.; Mai, F.; Ma, Z.; Wen, Z.; Chen, H.; Chen, M.; Li, Y. Catalytic Depolymerization of a Lignin-Rich Corncob Residue into Aromatics in Supercritical Ethanol over an Alumina-Supported NiMo Alloy Catalyst. *Energy Fuels* **2019**, *33* (9), 8657−8665.
(280) Mai, F.; Wen, Z.; Bai, Y.; Ma, Z.; Cui, K.; Wu, K.; Yan, F.; Chen, H.; Li, Y. Selective Conversion of Enzymatic Hydrolysis Lignin into

Alkylphenols in Supercritical Ethanol over a WO_3/γ-Al_2O_3 Catalyst. *Ind. Eng. Chem. Res.* **2019**, *58* (24), 10255−10263.
(281) Zheng, A.; Huang, Z.; Wei, G.; Zhao, K.; Jiang, L.; Zhao, Z.; Tian, Y.; Li, H. Controlling Deoxygenation Pathways in Catalytic Fast Pyrolysis of Biomass and Its Components by Using Metal-Oxide Nanocomposites. *iScience* **2020**, *23* (1), 100814.
(282) Ma, Z.; Custodis, V.; van Bokhoven, J. A. Selective Deoxygenation of Lignin during Catalytic Fast Pyrolysis. *Catal. Sci. Technol.* **2014**, *4* (3), 766−772.
(283) Echeandia, S.; Arias, P. L.; Barrio, V. L.; Pawelec, B.; Fierro, J. L. G. Synergy Effect in the HDO of Phenol over Ni−W Catalysts Supported on Active Carbon: Effect of Tungsten Precursors. *Appl. Catal., B* **2010**, *101* (1), 1−12.
(284) Leiva, K.; Sepúlveda, C.; García, R.; Fierro, J. L. G.; Aguila, G.; Baeza, P.; Villarroel, M.; Escalona, N. Effect of P Content in the Conversion of Guaiacol over Mo/γ-Al_2O_3 Catalysts. *Appl. Catal., A* **2013**, *467*, 568−574.
(285) Cui, K.; Yang, L.; Ma, Z.; Yan, F.; Wu, K.; Sang, Y.; Chen, H.; Li, Y. Selective Conversion of Guaiacol to Substituted Alkylphenols in Supercritical Ethanol over MoO_3. *Appl. Catal., B* **2017**, *219*, 592−602.
(286) Sudarsanam, P.; Li, H.; Sagar, T. V. TiO_2-Based Water-Tolerant Acid Catalysis for Biomass-Based Fuels and Chemicals. *ACS Catal.* **2020**, *10* (16), 9555−9584.
(287) Prasomsri, T.; Shetty, M.; Murugappan, K.; Román-Leshkov, Y. Insights into the Catalytic Activity and Surface Modification of MoO_3 during the Hydrodeoxygenation of Lignin-Derived Model Compounds into Aromatic Hydrocarbons under Low Hydrogen Pressures. *Energy Environ. Sci.* **2014**, *7* (8), 2660−2669.
(288) Ansaloni, S.; Russo, N.; Pirone, R. Hydrodeoxygenation of Guaiacol over Molybdenum-Based Catalysts: The Effect of Support and the Nature of the Active Site. *Can. J. Chem. Eng.* **2017**, *95* (9), 1730−1744.
(289) Selvaraj, M.; Shanthi, K.; Maheswari, R.; Ramanathan, A. Hydrodeoxygenation of Guaiacol over MoO_3-NiO/Mesoporous Silicates: Effect of Incorporated Heteroatom. *Energy Fuels* **2014**, *28* (4), 2598−2607.
(290) Liu, G.-H.; Zong, Z.-M.; Liu, Z.-Q.; Liu, F.-J.; Zhang, Y.-Y.; Wei, X.-Y. Solvent-Controlled Selective Hydrodeoxygenation of Bio-Derived Guaiacol to Arenes or Phenols over a Biochar Supported Co-Doped MoO_2 Catalyst. *Fuel Process. Technol.* **2018**, *179*, 114−123.
(291) Alekseeva (Bykova), M. V.; Rekhtina, M. A.; Lebedev, M. Y.; Zavarukhin, S. G.; Kaichev, V. V.; Venderbosch, R. H.; Yakovlev, V. A. Hydrotreatment of 2-Methoxyphenol over High Ni-Loaded Sol-Gel Catalysts: The Influence of Mo on Catalyst Activity and Reaction Pathways. *ChemistrySelect* **2018**, *3* (18), 5153−5164.
(292) Song, S.; Zhang, J.; Yan, N. Support Effects in the De-Methoxylation of Lignin Monomer 4-Propylguaiacol over Molybdenum-Based Catalysts. *Fuel Process. Technol.* **2020**, *199*, 106224.
(293) Zhou, G.; Jensen, P. A.; Le, D. M.; Knudsen, N. O.; Jensen, A. D. Atmospheric Hydrodeoxygenation of Biomass Fast Pyrolysis Vapor by MoO_3. *ACS Sustainable Chem. Eng.* **2016**, *4* (10), 5432−5440.
(294) Shetty, M.; Murugappan, K.; Green, W. H.; Román-Leshkov, Y. Structural Properties and Reactivity Trends of Molybdenum Oxide Catalysts Supported on Zirconia for the Hydrodeoxygenation of Anisole. *ACS Sustainable Chem. Eng.* **2017**, *5* (6), 5293−5301.
(295) Shetty, M.; Anderson, E. M.; Green, W. H.; Román-Leshkov, Y. Kinetic Analysis and Reaction Mechanism for Anisole Conversion over Zirconia-Supported Molybdenum Oxide. *J. Catal.* **2019**, *376*, 248−257.
(296) Ranga, C.; Lødeng, R.; Alexiadis, V. I.; Rajkhowa, T.; Bjørkan, H.; Chytil, S.; Svenum, I. H.; Walmsley, J.; Detavernier, C.; Poelman, H.; Van Der Voort, P.; Thybaut, J. W. Effect of Composition and Preparation of Supported MoO_3 Catalysts for Anisole Hydrodeoxygenation. *Chem. Eng. J.* **2018**, *335*, 120−132.
(297) Ranga, C.; Alexiadis, V. I.; Lauwaert, J.; Lødeng, R.; Thybaut, J. W. Effect of Co Incorporation and Support Selection on Deoxygenation Selectivity and Stability of (Co)Mo Catalysts in Anisole HDO. *Appl. Catal., A* **2019**, *571*, 61−70.
(298) Ghampson, I. T.; Pecchi, G.; Fierro, J. L. G.; Videla, A.; Escalona, N. Catalytic Hydrodeoxygenation of Anisole over $Re\text{-}MoO_x/TiO_2$ and $Re\text{-}VO_x/TiO_2$ Catalysts. *Appl. Catal., B* **2017**, *208*, 60−74.
(299) Saidi, M.; Rahzani, B.; Rahimpour, M. R. Characterization and Catalytic Properties of Molybdenum Supported on Nano Gamma Al_2O_3 for Upgrading of Anisole Model Compound. *Chem. Eng. J.* **2017**, *319*, 143−154.
(300) He, T.; Liu, X.; Ge, Y.; Han, D.; Li, J.; Wang, Z.; Wu, J. Gas Phase Hydrodeoxygenation of Anisole and Guaiacol to Aromatics with a High Selectivity over $Ni\text{-}Mo/SiO_2$. *Catal. Commun.* **2017**, *102*, 127−130.
(301) Whiffen, V. M. L.; Smith, K. J. Hydrodeoxygenation of 4-Methylphenol over Unsupported MoP, MoS_2, and MoO_x Catalysts. *Energy Fuels* **2010**, *24* (9), 4728−4737.
(302) Gonçalves, V. O. O.; Ciotonea, C.; Arrii-Clacens, S.; Guignard, N.; Roudaut, C.; Rousseau, J.; Clacens, J.-M.; Royer, S.; Richard, F. Effect of the Support on the Hydrodeoxygenation of M-Cresol over Molybdenum Oxide Based Catalysts. *Appl. Catal., B* **2017**, *214*, 57−66.
(303) Shetty, M.; Murugappan, K.; Prasomsri, T.; Green, W. H.; Román-Leshkov, Y. Reactivity and Stability Investigation of Supported Molybdenum Oxide Catalysts for the Hydrodeoxygenation (HDO) of m-Cresol. *J. Catal.* **2015**, *331*, 86−97.
(304) Wang, C.; Mironenko, A. V.; Raizada, A.; Chen, T.; Mao, X.; Padmanabhan, A.; Vlachos, D. G.; Gorte, R. J.; Vohs, J. M. Mechanistic Study of the Direct Hydrodeoxygenation of M-Cresol over WO_x-Decorated Pt/C Catalysts. *ACS Catal.* **2018**, *8* (9), 7749−7759.
(305) Itthibenchapong, V.; Chakthranont, P.; Sattayanon, C.; Butburee, T.; Faungnawakij, K.; Namuangruk, S. Understanding the Promoter Effect of Bifunctional (Pt, Ni, Cu)-MoO_{3-x}/TiO_2 Catalysts for the Hydrodeoxygenation of p-Cresol: A Combined DFT and Experimental Study. *Appl. Surf. Sci.* **2021**, *547*, 149170.
(306) Boullosa-Eiras, S.; Lødeng, R.; Bergem, H.; Stöcker, M.; Hannevold, L.; Blekkan, E. A. Catalytic Hydrodeoxygenation (HDO) of Phenol over Supported Molybdenum Carbide, Nitride, Phosphide and Oxide Catalysts. *Catal. Today* **2014**, *223*, 44−53.
(307) Romero, Y.; Richard, F.; Brunet, S. Hydrodeoxygenation of 2-Ethylphenol as a Model Compound of Bio-Crude over Sulfided Mo-Based Catalysts: Promoting Effect and Reaction Mechanism. *Appl. Catal., B* **2010**, *98* (3), 213−223.
(308) Krishnan, P. S.; Tamizhdurai, P.; Theres, G. S.; Shanthi, K. Molybdenum Hybrid − Nanocrystals Supported on Modified Laponite Composite as Superior Catalyst for Vapour Phase Hydrodeoxygenation of Clove Oil. *Renewable Energy* **2020**, *148*, 451−466.
(309) Kallury, R. K. M. R.; Restivo, W. M.; Tidwell, T. T.; Boocock, D. G. B.; Crimi, A.; Douglas, J. Hydrodeoxygenation of Hydroxy, Methoxy and Methyl Phenols with Molybdenum Oxide/Nickel Oxide/Alumina Catalyst. *J. Catal.* **1985**, *96* (2), 535−543.
(310) Ballesteros-Plata, D.; Infantes-Molina, A.; Rodríguez-Cuadrado, M.; Rodríguez-Aguado, E.; Braos-García, P.; Rodríguez-Castellón, E. Incorporation of Molybdenum into Pd and Pt Catalysts Supported on Commercial Silica for Hydrodeoxygenation Reaction of Dibenzofuran. *Appl. Catal., A* **2017**, *547*, 86−95.
(311) Zhang, J.; Zhao, C.; Li, C.; Li, S.; Tsang, C.-W.; Liang, C. The Role of Oxophilic Mo Species in Pt/MgO Catalysts as Extremely Active Sites for Enhanced Hydrodeoxygenation of Dibenzofuran. *Catal. Sci. Technol.* **2020**, *10* (9), 2948−2960.
(312) Miao, Z.; Zhao, H.; Song, H.; Chou, L. Ordered Mesoporous Zirconium Oxophosphate Supported Tungsten Oxide Solid Acid Catalysts: The Improved Brønsted Acidity for Benzylation of Anisole. *RSC Adv.* **2014**, *4* (43), 22509−22519.
(313) Zhao, Z.; Bababrik, R.; Xue, W.; Li, Y.; Briggs, N. M.; Nguyen, D.-T.; Nguyen, U.; Crossley, S. P.; Wang, S.; Wang, B.; Resasco, D. E. Solvent-Mediated Charge Separation Drives Alternative Hydrogenation Path of Furanics in Liquid Water. *Nat. Catal.* **2019**, *2* (5), 431−436.
(314) Walker, T. W.; Motagamwala, A. H.; Dumesic, J. A.; Huber, G. W. Fundamental Catalytic Challenges to Design Improved Biomass Conversion Technologies. *J. Catal.* **2019**, *369*, 518−525.

(315) Motagamwala, A. H.; Huang, K.; Maravelias, C. T.; Dumesic, J. A. Solvent System for Effective Near-Term Production of Hydroxymethylfurfural (HMF) with Potential for Long-Term Process Improvement. *Energy Environ. Sci.* **2019**, *12* (7), 2212−2222.
(316) Shuai, L.; Luterbacher, J. Organic Solvent Effects in Biomass Conversion Reactions. *ChemSusChem* **2016**, *9* (2), 133−155.
(317) Liu, S.; Lin, Q.; Liu, J.; Xu, S.; Wang, Y.; Xu, H.; Wang, J.; Chen, Y. Enhancement of the Hydrothermal Stability of $WO_3/Ce_{0.68}Zr_{0.32}O_2$ Catalyst by Silica Modification for NH_3-SCR. *ACS Appl. Energy Mater.* **2020**, *3* (1), 1161−1170.

https://doi.org/10.1021/acscatal.1c03326
ACS Catal. 2021, 11, 13603−13648